SYNTHESIS AND RHEOLOGICAL BEHAVIOR OF SHEAR THICKENING FLUIDS (STFs) FOR LIQUID ARMOR APPLICATIONS

A Thesis Submitted to
the Graduate School of Engineering and Sciences of
İzmir Institute of Technology
in Partial Fulfillment of the Requirements for the Degree of

MASTER OF SCIENCE

in Materials Science and Engineering

by
SemaYILDIZ

December 2013
İZMİR

We approve the thesis of **Sema YILDIZ**

Examining Committee Members:

_____

Prof. Dr. Metin TANOĞLU
Department of Mechanical Engineering, İzmir Institute of Technology

_____

Assoc. Prof. Dr. Ekrem ÖZDEMİR
Department of Chemical Engineering, İzmir Institute of Technology

_____

Prof. Dr. Fehime ÖZKAN
Department of Chemical Engineering, İzmir Institute of Technology

_____

Prof. Dr. Selahattin YILMAZ
Department of Chemical Engineering, İzmir Institute of Technology

_____

Prof. Dr. Hürriyet POLAT
Department of Chemistry, İzmir Institute of Technology

16 December 2013

_____

Prof. Dr. Metin TANOĞLU
Supervisor, Department of Mechanical Engineering, İzmir Institute of Technology

_____

Assoc. Prof. Dr. Ekrem ÖZDEMİR
Co-Supervisor, Department of Civil Engineering, İzmir Institute of Technology

_____

Assoc. Prof. Dr. Mustafa M. DEMİR
Head of the Department of Materials Science and Engineering

_____

Prof. Dr. Tuğrul SENGER
Dean of the Graduate School of Engineering and Sciences

ACKNOWLEDGMENTS

I would like to express my deepest gratitude to my advisor, Prof. Dr. Metin Tanoğlu, who gives me the opportunity of working in this area, and patiently guided me throughout the research. My thanks and appreciations also go to Fikret Şenel and Pınar Erbil from BARIŞ Electrical Industry Inc. for their contributions, also Undersecretariat for Defence Industries of Turkey (SSM) for their financial support. Special thanks to my project mate Oylum Çolpankan for her help and sharing difficulties with me.

I would like to thank to Prof. Dr. Hürriyet Polat and Assist. Prof. Dr. Ekrem Özdemir for their help and patience in my analysis. Thanks to the Center for Material Research staff for their friendly cooperation.

I would like to express my endless thanks to my beloved parents Fatma Yıldız and Mehmet Yıldız for their patience, understanding and encouragement throughout my whole life. Finally, i wish to send my special thanks to my sister Leyla Yıldız and Erkan Morateş for their unforgettable and everlasting helps and tenacious support.

ABSTRACT

SYNTHESIS AND RHEOLOGICAL BEHAVIOR OF SHEAR THICKENING FLUIDS (STFs) FOR LIQUID ARMOR APPLICATIONS

Shear thickening is a phenomenon which is generally observed in concentrated colloidal dispersions and defined as the increase in viscosity with increasing shear stress or shear rate. This property brings many drawbacks for general use and restrict their application areas as well as makes them beneficial in protective applications. Liquid armor is the most widely studied field of shear thickening fluids (STFs).

The goal of this study is to produce STFs and measure their rheological behavior as well as preparing STF/aramid fabric composites and testing their mechanical properties in terms of stab, flexibility and ballistic tests.for liquid armor applications. For this purpose, fumed silica and polyethylene glycol (PEG) based dispersions were prepared by sonochemical method. The effect of filler concentration and molecular weight of continuous phase was observed by using 5-30 wt% fumed silica and PEGs having 200, 300, 400 and 600 g/mole molecular weight, respectively. Also, microstructural and thermal characterization of raw materials and STFs were performed.

According to the collected rheological data, viscosity increment of STFs is increased with concentration. The maximum available viscosity was obtained for STF30-PEG 200 as 1622 Pa.s and the lowest critical shear rate was measured for STF30-PEG 300 as 11.1 s^{-1}. Moreover, it was found that the viscous property dominates the elastic property of STFs with greater viscous modulus (G") values than the elastic (G') modulus. Both moduli values were also reflected the thickening property with varying angular frequency and strain %. Stab and ballistic tests showed that STF impregnation enhances the resistance property of neat fabrics. The maximum load was supported by aramid fabric/STF30-PEG200 composite as 137 N whereas the highest stiffness was measured as 9^{o} for aramid fabric/STF30-PEG 600 composite. Also, in ballistic tests, the highest result was obtained as 623m/s for the sample which composed of a configuration of STF impregnated aramid and Ultrahigh molecular weight polyethylene (UHMWPE) fabrics with neat polyethylene (PE) laminae.

ÖZET

SIVI ZIRH UYGULAMALARI İÇİN KESME ile KALINLAŞAN SIVILARIN (KKS) SENTEZLENMESİ ve REOLOJİK DAVRANIŞLARI

Kesme ile kalınlaşma genellikle konsantre kolloidal dağılımlarda gözlenen ve artan kesme gerilmesi ya da kesme hızı altında viskozite artışı olarak tanımlanan bir olaydır. Bu özellik, genel kullanımda birçok dezavantaj getirerek kesme ile kalınlaşan sıvıların (KKS) kullanım alanını sınırlamasının yanında, onları koruyucu uygulamalar için yararlı hale getirmektedir. Koruyucu uygulamalar içerisinde sıvı zırh, KKS lerin literatürde en çok çalışıldığı alanı oluşturmaktadır.

Bu çalışmanın amacı, sıvı zırh uygulamaları için KKS ler üreterek onların reolojik davranışlarını kontrol etmenin yanı sıra, KKS/aramid kumaş kompozitleri hazırlamak ve bu kompozitlerin mekanik özelliklerini delme, esneklik ve balistik yönünden test etmektir. Bu amaçla, fumed silika ve polietilen glikol (PEG) esaslı dağılımlar sonokimyasal method yardımı ile hazırlanmıştır. Dolgu malzemesi konsantrasyonunun ve sıvı fazın molekül ağırlığının etkisi, silika miktarını %5 ila 30 ağırlık konsantrasyonunda değiştirerek ve molekül ağırlığı 200, 300, 400 and 600 g/mole olan PEG'ler kullanarak gözlenmiştir. Ayrıca, ham malzemelerin ve KKS'lerin mikroyapı ve termal karakterizayonu da gerçekleştirilmiştir.

Elde edilen reolojik verilere göre, KKS'lerin viskozitesi fumed silika konsantrasyonu ile artmıştır. Maksimum viskozite değeri, 1622 Pa.s olarak STF30-PEG 200 numunesinde gözlenirken, en düşük kritik kesme değeri 11.1 s^{-1} olarak STF30-PEG 300 numunesi için elde edilmiştir. Ayrıca, KKS'lerin viskoz modül değerlerinin elastik modül değerlerinden yüksek olduğunun gözlenmesi ile, viskoz özelliğinin elastik özelliğine baskın geldiği belirlenmiştir. Her iki modül değeri değişen açısal hız ve % gerinim genliği ile kesme ile kalınlaşma özelliğini yansıtmaktadır. Delme testlerinde en yüksek delme yükü 137 N olarak, aramid kumaş/ STF30-PEG200 kompoziti tarafından gösterilirken en düşük esneklik değeri aramid kumaş/ STF30-PEG600 kompoziti için 9^{o} olarak elde edilmiştir. Balistik testlerde ise en yüksek değer, 623 m/s olarak STF empreyne edilmiş aramid ve Ultrayüksek yoğunluklu polietilen (UHMWPE) kumaşlar ve ham polietilen (PE) tabakalarının konfigürasyonundan oluşan numune için elde edilmiştir

TABLE OF CONTENTS

LIST OF FIGURES

Figure **Page**

LIST OF TABLES

Table **Page**

CHAPTER 1

INTRODUCTION

Personal protection of body from dangers and injuries has always been a need for mankind since the ancient times. This need have lead to the evolution of protective clothing, today which is termed as armor. Therefore, body armors are defined as any defensive coverings worn to protect the body from physical attacks. For this purpose, animal leathers, natural fibers made from thatch, cotton and silk, metal shields such as iron, copper or steel were used as armor materials throughout the history. The natural fibers give their places to synthetic fibers with the innovations in manufacturing technology and materials science during the 20^{th} century (Cavallaro, 2011, Decker et. Al.,2004, Egres et. Al., 2007)

Modern armor materials have been designed not only against puncture which is caused by sharp objects, but also ballistic threats to meet the requirements. They are generally used with the combination of metal, ceramic or hard polymeric plates and many layers of fabrics. The used fabrics are commonly composed of high strength woven polymeric fibers which provide improved protection. They also enhance the mobility of soldiers, police officers and security personnel with reduced weight and flexibility (Cavallaro, 2011).

To improve the flexibility and reduce the weight of these impact resistant and bullet-proof fabrics by using less layers but as strong as current armors, scientists try to develop liquid armors. Liquid armors are created by impregnating these fabrics with shear thickening fluids (STFs).

Shear thickening fluids (STFs) constitutes a sub-group of smart fluids which show non-Newtonian fluid behavior. STFs govern the phenomenon that apparent viscosity increases with increasing stress (Barnes et al., 1989). However, increasing viscosity brings many drawbacks for industrial applications of STFs. This feature makes them ideal for shock-absorbing and damping applications. Considering this ability, STFs are used to improve the impact resistant materials such as sports equipments or liquid armor.

To control and investigate the flow properties of fluids is an important step in terms of industrial applications. Thus, the science of rheology has evolved. Rheological researhes of colloidal dispersions generally consists of steady shear measurements. However, steady shear measurements are not adequately characterize the flow behaviors of non-Newtonian fluids owing to their complex flow behaviors and it becames a requirement to observe their properties in terms of dynamic shear rheology (Barnes et al., 1989; Duvarcı, 2009).

The general objective of this study is to develop silica based shear thickening fluids (STFs) for liquid armor applications and determination of the effect of particle concentration and molecular weight of continuous phase on produced STFs in terms of both steady and dynamic shear properties. Another objective of this thesis is to develop STF impregnated fabrics with different configurations to develop liquid armors instead of conventional soft body armors and measure their mechanical properties by applying stab, ballistic and flexibility tests. Also, characterization of the both STFs and STF impregnated fabrics were conducted.

CHAPTER 2

LITERATURE REVIEW

2.1. Newtonian Fluid Behavior

Isaac Newton mentioned the liquids in his book “Principia” which was published in 1687 and said “ The resistance which arises from the lack of slipperiness of the parts of the liquid, other things being equal, is proportional to the velocity with which the parts of the liquid are separated from one another”. The lack of slipperiness is called as *viscosity* with other words fluids’ resistance to flow. Flow regimes of fluids can generally be classified into two groups as Newtonian and non-Newtonian fluid behaviors(Barnes et al, 1989, Mewis and Wagner 2012).

When a fluid is subjected to a shear stress by a virtue of shear force, a motion is produced until the stress is removed. Let us consider a typical simple flow condition of a fluid seen in Figure 2.1. to clarify the phenomenon. A fluid is contained between two parallel plates with a distance z. When the upper plate slides with the application of a force resulting in a shear stress σ, while the bottom part is stationary, a velocity gradient which is also known as *shear rate*, arises. At sufficiently low velocities to aviod turbulences, the fluid will move parallel in every point between the plates. The local velocities $u_x$vary linearly through the gap. The liquid layers near each plate have the same velocity as that plate in many cases which indicates the lack of slipperiness which was mentioned above. Therefore, shear stress versus shear rate graph of this motion will be linear with the proportionality constant viscosity η (Mewis and Wagner 2012, Goodwin and Hughes 2007, Malkin and Isayev 2012).

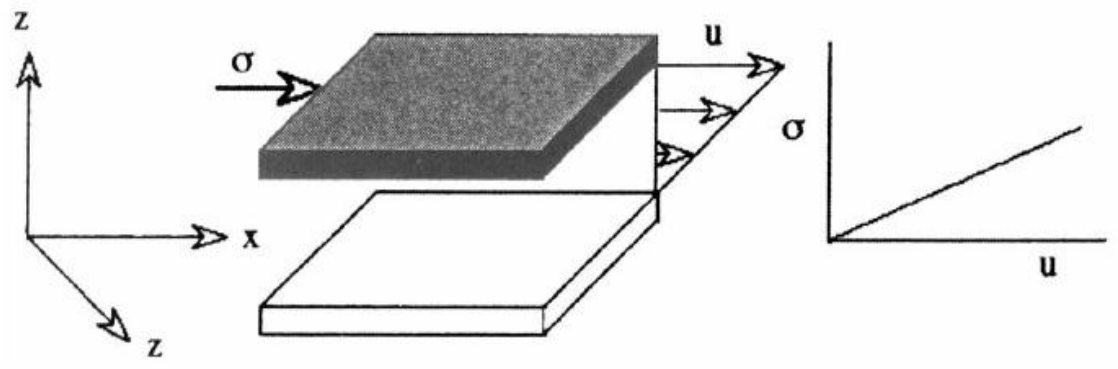

Figure 2.1. A velocity gradient produced when a fluid is sheared
(Source: Goodwin and Hughes 2007)

$$\frac{du}{dz} = \dot{\gamma} \tag{2.1}$$

Where du/dz represents the velocity gradient within the layers. Therefore, $\dot{\gamma}$ is the shear rate (Eqn 2.1). The applied force to the upper plate is transmitted as stress (σ) which is force per unit area. When the stress changes with shear rate linearly, the fluid is a simple Newtonian fluid with the coefficient of viscosity η, being the proportionality constant. Eqn 2.2 indicates the mathematical representation of viscosity coefficient.

$$\sigma = \eta \frac{du}{dz} \tag{2.2}$$

2.2. Non-Newtonian Fluid Behavior

In many suspensions, arising shear stress from a shear flow, is nonlinearly proportional to the shear rate and the resulting behavior deviates from Newton's law. If the shear stress is not linearly proportional to shear rate, the ratiowhich is the viscosity η is not a constant value anymore on the contrary, becomes a function of shear rate and called as *apparent viscosity* and the fluid is *non-Newtonian* fluid. (Mewis and Wagner, 2012; Goodwin and Hughes, 2007; Malkin and Isayev, 2012).

Non-Newtonian fluid behavior can be time-dependent and time-independent. Time-dependency of non-Newtonian fluids are known as *thixotrophy*. On the other hand, time-independent flows can be classified as shear thinning (pseudoplastic), shear thickening and shear independent fluids each with and without yield-stress.Rheograms of time-independent fluids are illustrated in Figure 2.2. (Duvarcı 2009, Sochi 2010).

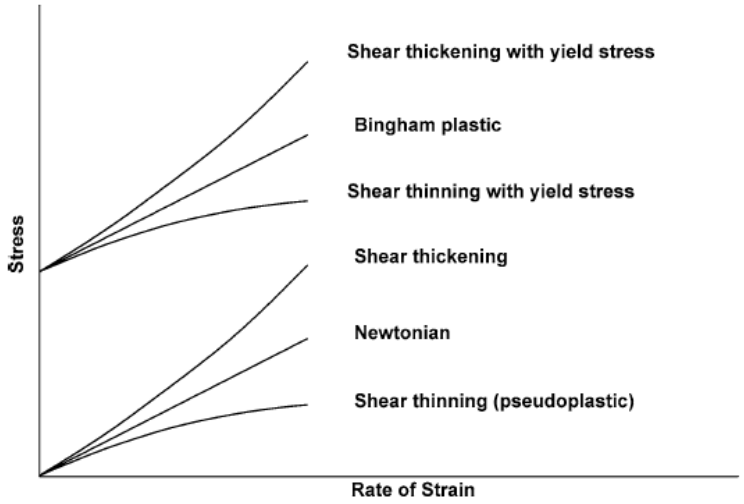

Figure 2.2. The six main classes of the time-independent fluids presented in a generic graph of stress against strain rate in shear flow (Source: Sochi 2010, modified)

2.3. Viscoelasticity

Materials show elastic (solid-like) or viscous (liquid-like) properties or both of them at the same time when they undergo a deformation. The materials that exhibit both type of properties is known as *viscoelastic materials*. When an ideal elastic solid deforms under applied stress, it regains its original form after the removal of the stress. However, if the applied stress exceeds the characteristic yield stress of the material, recovery will not occur completely and *creep* will take place. For an ideal elastic solid, stress in a sheared state is directly proportional to strain which is explained by Hooke's law and the proportionality constant is the shear modulus, *G* (Chabbra, 2008; Malkin and Isayev, 2012; Goodwin and Hughes, 2007);

$$\sigma = G\gamma \tag{2.3}$$

Other phenomenon is for Newtonian fluids which is shear stress is proportional to shear rate. The defining constant is viscosity;

$$\sigma = \eta\dot{\gamma} \tag{2.4}$$

Figure 2.3. (a) Hookean spring with modulus G, (b) a dashpot containing a Newtonian oil with viscosity η (Source: Mewis and Wagner 2012)

2.4. Shear Thickening Fluids (STFs)

Colloidal dispersions have attracted the attention of scienstist and they are under investigation since many decades due to their interesting flow behaviors which make them applicable in various industrial sectors such as ceramics, foodstuffs, paints, mineral slurries, pulp and paper, coatings, reinforced plastics and filled elastomers (Boersma et al. 1990, Carreau et al.1999, Mewis and Wagner, 2012). Also, increasing need of nanotechnological inventions and nanocomposites results in the generation of new areas for use of colloidal suspensions. Colloidusually denotes the dispersed phase of a two-component system in which the elements of the dispersed phase are too small to be easily observed by an optical microscope and whose motion is affected by thermal forces. When the suspending medium is liquid, they do not readily sediment(Mewis and Wagner, 2012). Colloidal solutions are prepared by dipsersion of nano particles into a medium fluid, consolidation, removal of the liquid phase, and densification. They often well suited with optical microscopy and scattering experiments using light, X-rays and neutron. (Duvarcı 2009, Wagner and Brady 2009).

Shear thickening is a time-independent non-Newtonian behavior which is defined as the increase of viscosity with increase in shear rate in the British Standard Rheological Nomenclature (Erdoğan, 2011). It is often observed in concentrated

colloidal dispersions. Shear thickening fluids (STFs) usually display a shear thinning behavior at low shear stresses or shear rate. When shear stress is increased, the viscosity of STFs increase and reach to higher magnitudes by undergoing a transition from shear thinning to shear thickening (Barnes et al., 1989). This increment can be gradually or drastically. The drastic increase in viscosity of STFs is also identified as *discontinuous thickening* (Lee et al., 2002). Another important point that should be keep in mind about STFs is the viscosity increment is reversible, meaning that if the shear stress is withdrawn from the material, its viscosity will begin to decrease immediately (Barnes, 1989).

The dilatancy of concentrated suspensions of solids was firstly discussed by Osborne Reynolds (1885). He stated that the voidage of concentrated suspensions are at a minimal size when they are at rest and the liquid is only sufficient to fill those voids. When low shear rates are applied, the liquid lubricates the motion of one particle past another. At high shear rates the dense packing of the particles is destroyed and the material expands or "dilates" slightly and the voidage increases. In this case, the liquid would not be sufficient anymore to lubricate the flow and allow particles moving passing another. The formation of this new structure results in an increase in viscosity of the material. Regarding to this definition, STFs are termed as "dilatant fluids". However, many of the STFs such as starch pastes do not undergo a volume expansion. Thus, the correct term should be "shear thickening"(Tanner, 2002).

In industrial applications, STFs can limit the formulations in coating and spraying processes and cause damages on mixing blades, mixing motors due to overloading and pumping equipments of concentrated dispersions. Considering these negative circumstances, the use of STFs are avoided or tried to minimize their harmful effects by controlling their flow behavior. The main technique that is used to control the behavior of STFs is performing rheological analyses. Rheological aspects give the opportunity of understanding the microstructural interactions between consisting phases of colloidal dispersions.

However, STFs show some mechanical properties due to their unique rheological responses which make them special for some specific applications. They are used as impact resistant materials and shock absorbers in damping and shielding equipments for protective purposes such as liquid armor, sports equipment (Mewis and Wagner, 2012; Barnes, 1989).

One of the most important future application of STFs may takes place in the field of liquid armor production. Since, the use of fluids instead of layered conventional armors will make them light weight, cost effective, flexibleand wearable so that much beneficial.

Figure 2.4. represents a general curve of STFs that exhibits three characteristic region. In first region, a slight shear thinning occurs until a critical shear rate (γ_c) value, then second region takes place in between critical shear rate and a maxium available viscosity value up to a higher critical rate $\dot{\gamma}$. Following this, a steep shear thinning takes place which covers the reversibility of shear thickening behavior. Overall curves can be defined as follows (Rosales et al., 2011).

$$\eta(\dot{\gamma}) = \begin{cases} \eta_{\mathrm{I}}(\dot{\gamma}) & \text{for } \dot{\gamma} \leq \dot{\gamma}_c\,, \\ \eta_{\mathrm{II}}(\dot{\gamma}) & \text{for } \dot{\gamma}_c < \dot{\gamma} \leq \dot{\gamma}_{max}, \\ \eta_{\mathrm{III}}(\dot{\gamma}) & \text{for } \dot{\gamma}_{max} < \dot{\gamma}, \end{cases} \tag{2.5}$$

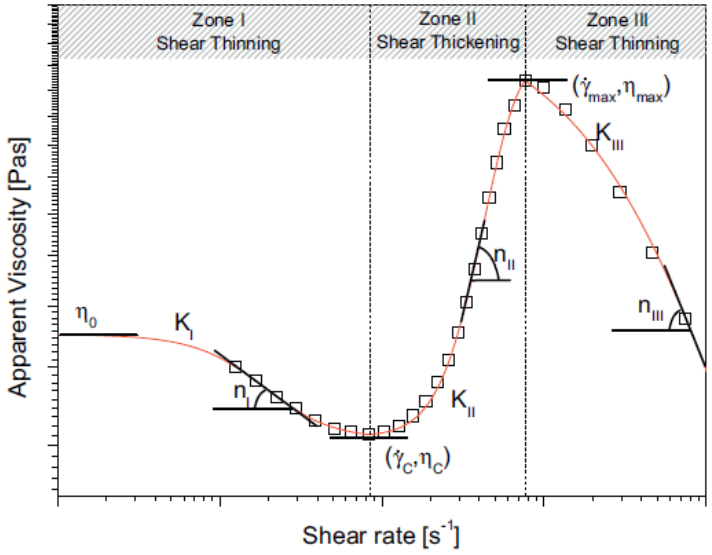

Figure 2.4. Typical viscosity curve of a shear thickening fluid. Experimental data shown is corresponding to a suspension of Aerosil® R816 in polypropylene glycol at 5% (v/v) and 25 ^{o}C(Source: Rosales et al., 2011)

The reasons of shear thickening phenomenon are an important field of research for scientists who mostly deal with its chemical and structural basis. In early studies,

shear thickening is described as ‘‘well-behaved’’ rise in viscosity with increasing shear until Hoffman reported that highly concentrated suspensions of monodisperse particles actually exhibit a discontinuous jump in viscosity at some critical rate of shear. The onset of shear thickening implies the domination of hydrodynamic interactions in the system. However, the microstructural basis of this phenomenon could not been completely revealed yet (Hoffman, 1998; Srinivasa and Khan, 1997).

2.4.1. Reasons of Shear Thickening

2.4.1.1. Order-Disorder Transition (ODT)

Hoffman investigated the concentrated monodisperse suspensions in his researches. Monodisperse suspensions display in situ light diffraction patterns those change with the initiation of shear thickening region. He suggested that at low rates of shear, attraction and repulsion forces between particles interact with the forces of shear field and forms two dimensional hexagonally packed layers (Figure 2.5). These layers are mostly parallel to the constant shear surfaces and one axis is always in the direction of flow. When the applied stress is increased, the excessive stress is transmitted from atoms to the neighbouring ones. Finally, a critical value that causes an instability in flow is reached. Shear stress couples on the layers are sufficient only to overcome the forces between the spheres which hold them together. Due to this instability, the ordered layers of particles are broken down and jam into one another result in a jump in viscosity value of the fluid. Instability is controlled by the balance between the stabilizing forces of repulsion between particles and hydrodynamic forces in concentrated colloidal dispersions. The transition from ordered layers to the broken particles is called as *“order-disorder transition”* (ODT) (Hoffman 1972; Hoffman 1998; Erdoğan 2011).

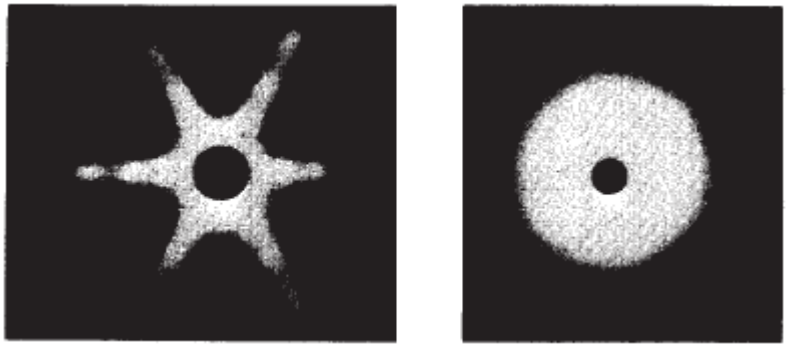

(a) **(b)**

Figure 2.5. Diffraction patterns from monodisperse plastisols sheared in simple shearing flow. (a) Sample sheared below discontinuity shear rate. (b) Sample sheared above discontinuity shear rate (Source: Hoffman, 1972)

2.4.1.2. Hydrocluster Theory

Another theory that has been brought forward to explain the shear thickening behavior is hydrocluster theory. This theory involves with the interparticle interactions and hydrodynamic forces between filling material and continuous phase of STFs. At the equilibrium structure of the STF is only influenced by the stochastic and interparticle forces which are electrostatic and Brownian. However, at low but increasing shear rates both interparticle and hydrodynamic forces effective. Despite the hydrodynamic forces, interparticle interactions enable the particles passing each other easily in this case. As the stress is increased, hydrodynamic lubrication forces dominate all the other forces. When the hydrodynamic and interparticle forces are of the same order of magnitude, the particles in STF ‘Jam‘ into stress bearing clusters which are called as *hydroclusters*. The difficulty of particles flowing around each other leads to a dramatic increase in viscosity and higher rate of energy dissipation. Figure 2.6. illustrates the formation of hydrodynamic clusters under increasing shear stress or shear rates (Bossis and Brady, 1989; Bender and Wagner, 1996; Wagner and Brady, 2009).

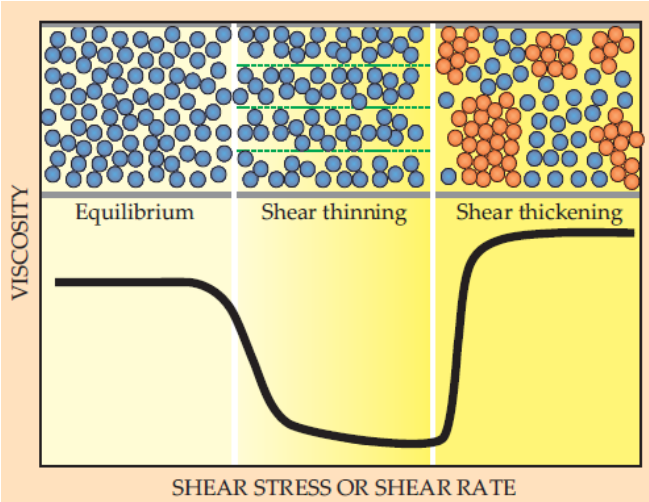

Figure 2.6. The change in microstructure of a colloidal dispersion
(Source: Wagner and Brady, 2009)

2.4.2. Parameters Controlling Shear Thickening Behavior

The suspended phase parameters which have the influence on shear thickening phenomenon was described by Barnes as volume fraction, particle size and shape, dispersity, properties of the continuous medium and interactions between particles and medium (Barnes, 1989).

2.4.2.1. Volume Fraction (Concentration) Dependency

One of the most important parameter that influences the reversible shear thickening is the volume fraction or concentration of filler phase in the suspension. The effect of this parameter is widely studied, especially in the field of liquid armor production. Because, it is important to determine the maximum available volume fraction of a STF to obtain a significant thickening. The older studies pointed that the required volume fraction for the onset of shear thickening is 0.50. However, this is not a rule of thumb and can differ from dispersion to dispersion. The only thing that should be for displaying shear thickening is that particles come into contact with each other, in other words, they should feel each other's presence. When particles packed more closely, neighbouring particles affect force fields of each other's, hence the interactions. Also, the packing cause frictional effects under shear force (Bettin 2002; Kang et al.,

2012). Figures 2.6 and 2.7 clearly indicate the effect of particle volume fraction on the viscosity and critical shear rate at which the onset of shear thickening.

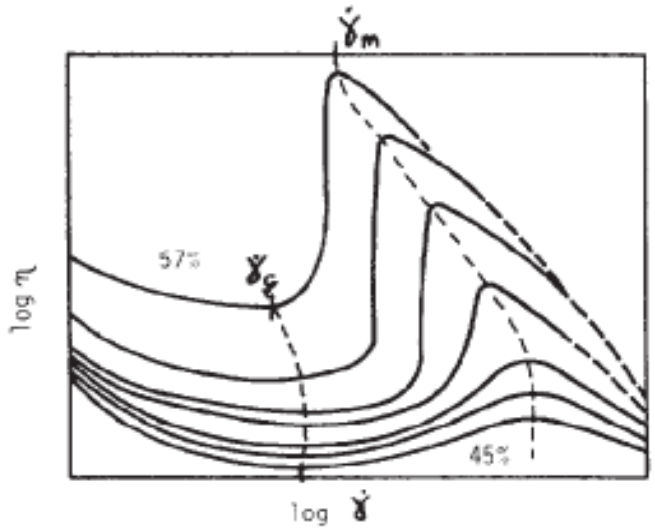

Figure 2.7. Schematic representation of viscosity versus shear rate for shear thickening systems, with approximate phase volume as parameter. Also shown are the loci of $\dot{\gamma}_c$and $\dot{\gamma}_m$ the shear rates at the beginning and end of the shear thickening region (Source: Barnes 1989)

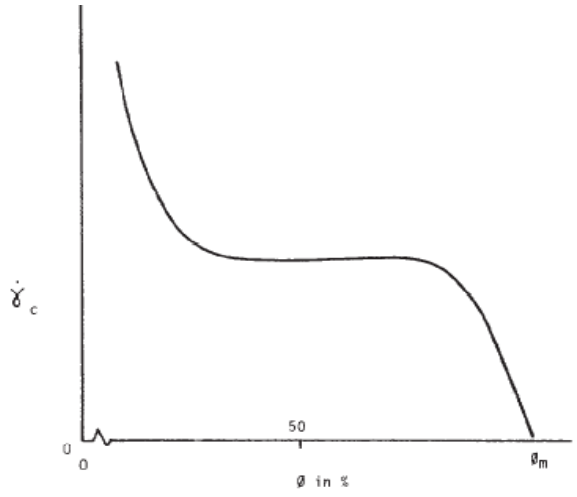

Figure 2.8. Schematic representation of the dependence of the critical shear rate for the onset of shear thickening $\dot{\gamma}_c$, as a function of the phase volume of the dispersed phase ϕ (Source: Barnes 1989)

Kalman et. al. (2007) studied the effect of relatively monodisperse poly-methyl methacrylate (PMMA) volume fraction on the shear thickening behavior. PMMA particles were synthesized by methanol-water synthesis reaction and PEG having 200 g/mole molecular weight (PEG 200) was used as medium fluid. According to the results obtained by the authors, the discontinuous shear thickening was observed below Φ=0.50. In each volume fraction, a shear thinning was observed initially. Then, a thickening was observed at the point of critical shear rate. The magnitude of the viscosity alteration at the shear thickening region increased gradually. Also, the critical shear rate value was reached earlier when particle volume fraction was increased.

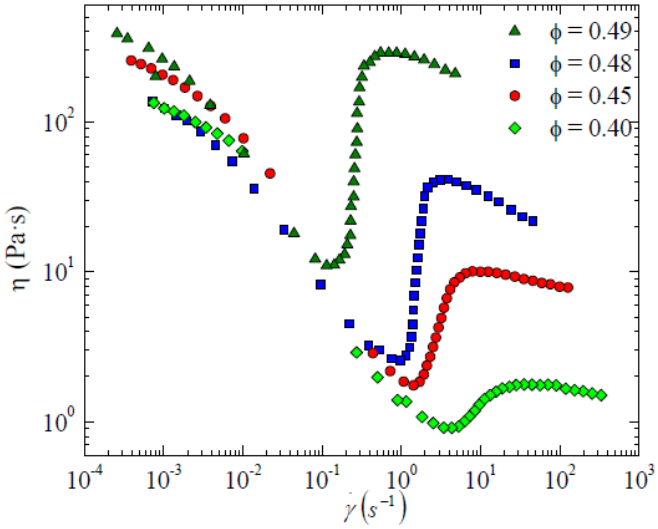

Figure 2.9.Steady-state rheology data of PMMA-PEG STF at multiple volume fractions (Source: Kalman et. al., 2007)

Wetzel et. al. (2004) also demonstrated the enhancement of shear thickening property with increasing particle loading in their experiments. They used spherical silica and PEG 200 at various particle volume fractions. Similar to Kalman et. al., Wetzel and his colleagues also found that as the volume fraction of particles in dispersion is increased, shear thickening effect is observed more strikingly and the onset of shear thickening transition begins earlier. This case is associated with the ease of hydrocluster formation. A remarkable point of this study is that there is no need to very high particle volume fractions close to 50% to observe a shear thickening effect. It was observed at ϕ=0.25 or even below this value. As stated before, the required volume fraction of particles to obtain a shear thickening effect differs from dispersion to dipsersion. Since

volume fraction parameter is also related with other parameters like particle size and size distribution of the filling material. Indeed, each parameter has an individual effect on rheological behavior of STFs. However, combination of all the factors determines the overall behavior.

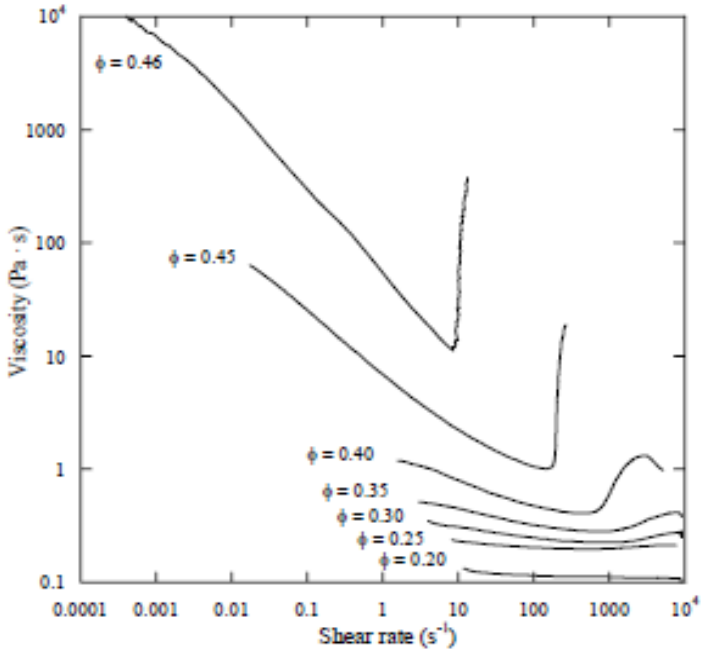

Figure 2.10. Viscosity as a function of shear rate for spherical silica STF at various particle loadings (Source: Wetzel et. al., 2004)

Based on the studies within the literature, it can be concluded that as volume fraction of the filler particles increases shear thickening becomes more pronounced. Overall viscosity of the dispersion increases with a higher jump and the critical shear stress and shear rate on that shear thickening begins to be observed earlier (Bettin 2007, Erdoğan 2011).

2.4.2.2. Particle Size Dependency

Rheological responses of STFs depend strongly on the size of the particles in which shear thickening colloidal dispersions. Barnes and Hoffman stated that the increase in particle size is inversely proportional to the onset of shear thickening and

moves the ciritical shear rate to lower values (Figure 2.11) (Barnes, 1989; Hoffman, 1997).

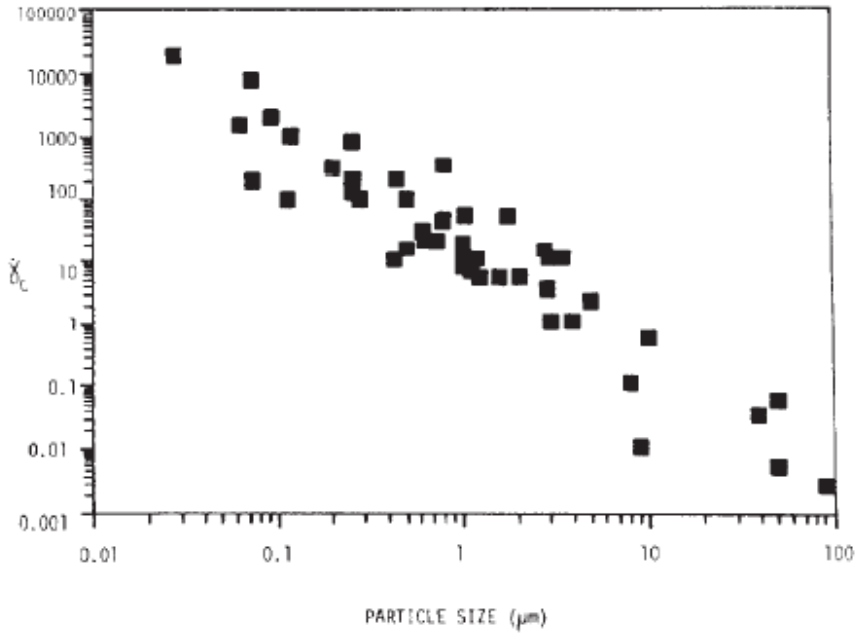

Figure 2.11. Critical shear rate $\dot{\gamma}_c$as a function of average particle size (Source: Barnes,1989)

However, some studies in the literature assert the contrary of that statement which is put forward by Barnes and Hoffman. Zhang et. al. investigated the particle size effect on shear-induced rheological properties of fumed silica (14 nm) and silica particles which are in the size range of 1-5 μm in ethylene glycol at 30%, 40% and 50% volume fractions. STFs were prepared by adding carrier fluid to powders and mixed mechanically during 1 h. The resulting suspensions were placed in a vacuum chamber to eliminate the bubbles. In contrast to the literature obtained data represents that large particles do not exhibit noteworthy thickening effect until 1000 s^{-1} shear rate. As volume fraction increases, the thickening was observed earlier with an abrupt jump in viscosity for small silica particles (Figure 2.11) (Zhang et. al., 2008).

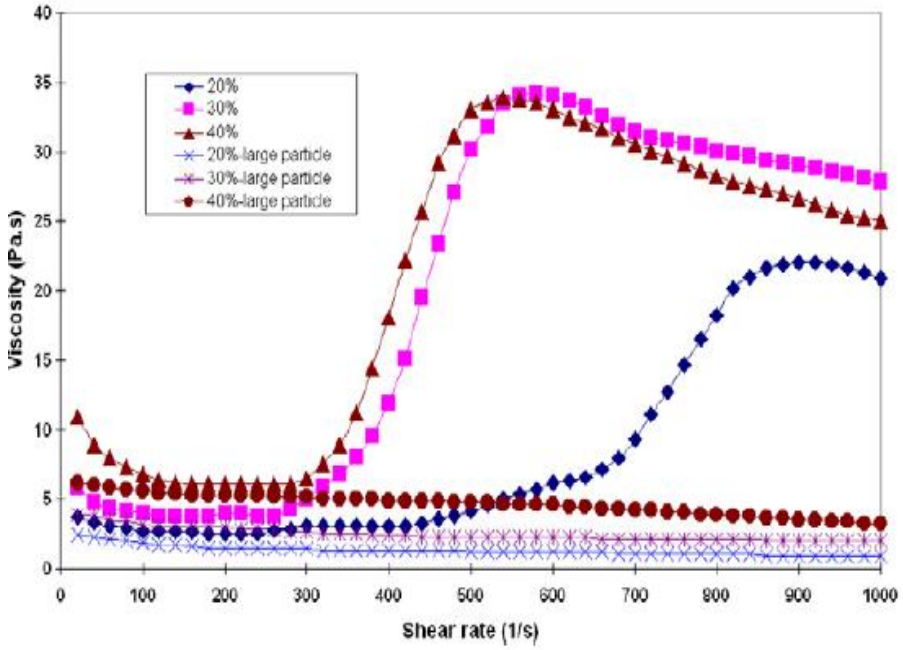

Figure 2.12. Viscosity versus shear rate for big and small particles at three volume fractions (Source: Zhang, 2008)

Hassan et al. observed the effect of particle size on steady state rheological behavior of colloidal and dry powder silica spherical nanoparticles which have the size of 200 and 15 nm, respectively (Hassan et al., 2010). Particles were dispersed in polyethylene glycol having molecular weight of 200 g/mole and excess amount of solvent (ethyl alcohol). For colloidal silica solution no ethyl alcohol was used. Disperisons were synthesized at different weight fractions, 38 wt% for colloidal silica and 52 wt% for powder silica, by sonochemical method with the help of high intensity ultrasonic horn. Then solvent was removed via an evaporation process by heating at about 100 ^{o}C.

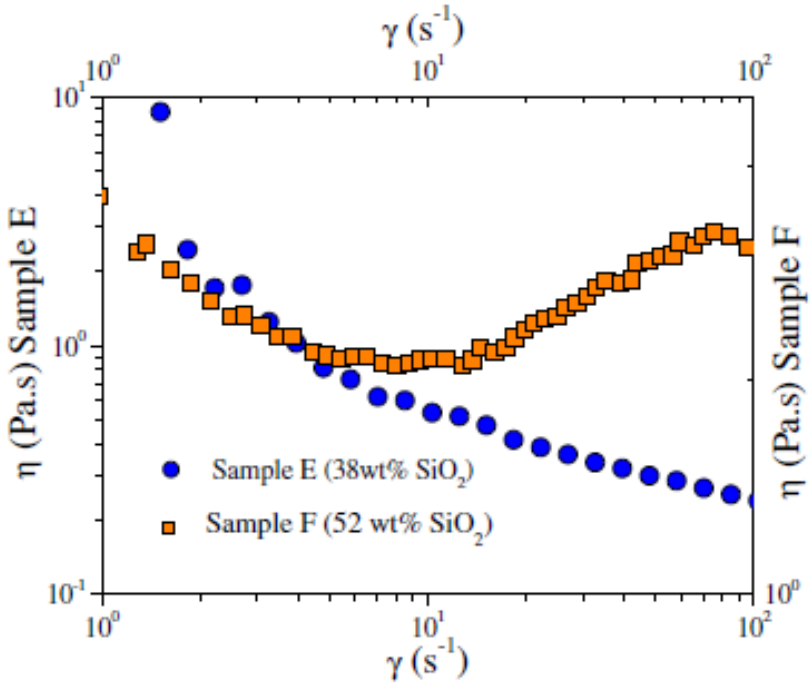

Figure 2.13. Rheology graph of STF Sample E (dry powder silica) and STF Sample F (colloidal silica) (Source: Hassan et al., 2010)

The rheological graph shown in Figure 2.12. sample E which was prepared by using 200 nm sized colloidal silica did not exhibit any shear thickening effect, instead, shear thinning behavior is noticeable at shear rate range of ~2–20/s. On the other hand, smaller sized dry powder silica particles exhibits a shear thickening effect and viscosity changed from 2 to 3.3 Pa s.

2.4.2.3. Particle Size Distribution Dependency

Another parameter that influences the shear thickening is size distribution of particles within the colloidal dispersions. Aggregates composed of various sized particles can pack more effectively. Since smaller particles fill the voids between larger particles and under shear stress, they act as a lubricantfor the flow of the larger particles that results in a reduction in the overall viscosity. To achieve higher viscosities, required particle loading will be higher to obtain a notable thickening. On the other hand, when two dispersions at the same volume fraction, one is polydisperse and the other is monodisperse are compared to each other, monodisperse one exhibit much remarkable shear thickening effect at lower shear rates. As expressed above,

polydisperse particles pack more effectively and at the same volume fraction their particles will be a less connected state (Barnes, 1989;Genovese, 2012; Bettin, 2007).

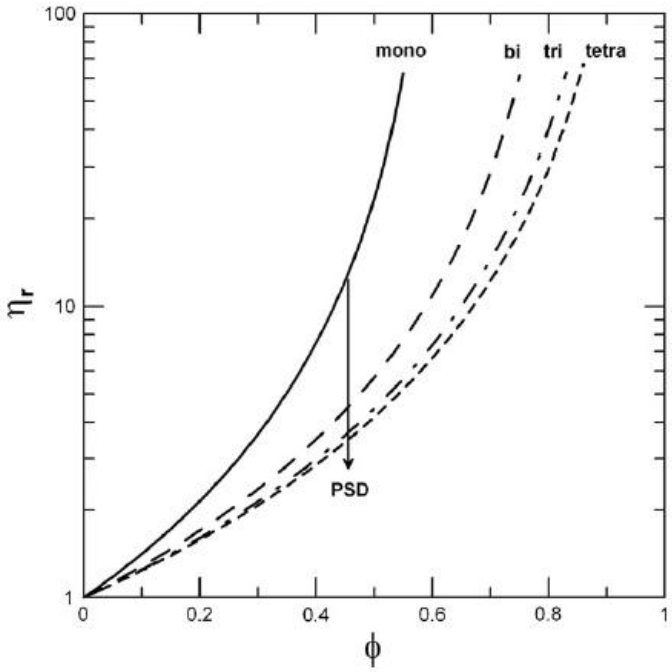

Figure 2.14. Relative viscosity vs. particle volume fraction of suspensions of polydispersed spheres (Source: Genovese, 2012)

The graph in Figure 2.13. explains the effect of particle size distribution (PSD) by means of volume fractionand relative viscosity which is the ratio of suspension viscosity to continuous phase viscosity. Genovese determined that the effective particle volume fraction for monomodal, bimodal, trimodal and tetramodal particles as 0.63, 0.86, 0.95 and 0.98, respectively. Arrow in this Figure indicatesthe effect of increasing particle size distribution for a given particle volume fraction. As a result, for a chosen volume fraction, monomodal particles exhibit higher relative viscosities as compared to bi, tr, and tetramodal particles (Genovese, 2012).

2.4.2.4. Particle Shape Dependency

Shape of the particles in STFs has significant effect on the thickening behavior. Studies show that rod shaped particles are more effective than plate particles. Because rod shaped particles tend to align in the direction of flow and exhibit much greater

elastic behavior. Non-spherical particles dissipate more energy resulting in a greater increase in viscosity. Besides, anisotropic particles verify the non-Newtonian flow with a shear thinning effect at lower volme fractions than spherical particles. Spherical particles show thinning regime above ϕ>0.30. Figure 2.14. shows the shape dependency of STFs at 20% volume fraction (Barnes, 1989; Genovese 2012; Bettin, 2007).

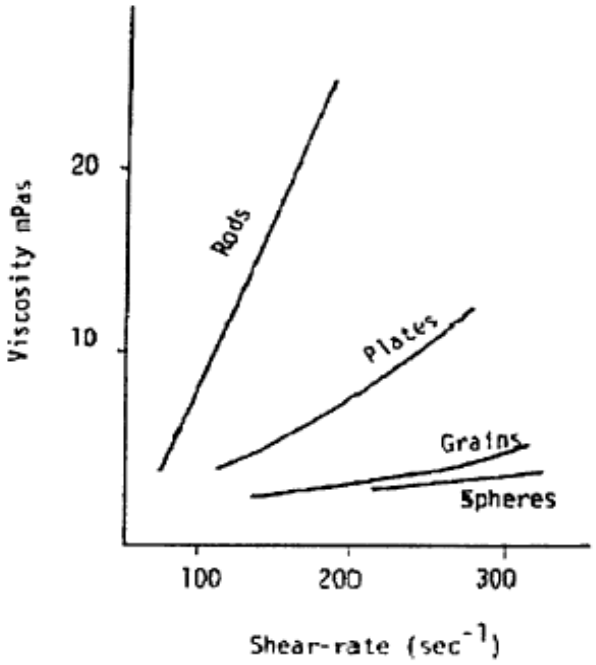

Figure 2.15. The effect of shape on shear thickening at ϕ = 0.2
(Source: Barnes, 1989)

The comparison of spherical silica and fumed silica was done by Kang et. al. (2012). The average particle size of the sphere silica and fumed silica was 120 nm and 300-400 nm, respectively. Also PEG was chosen as the carrier fluid for preparing suspensions. Rheological data indicate that suspension containing sphere silicas exhibit less severe thickening effect than fumed silica. This is due to the fact that fumed silica forms aggregates which makes the hydrocluster formation easier, whereas sphere silica cannot.

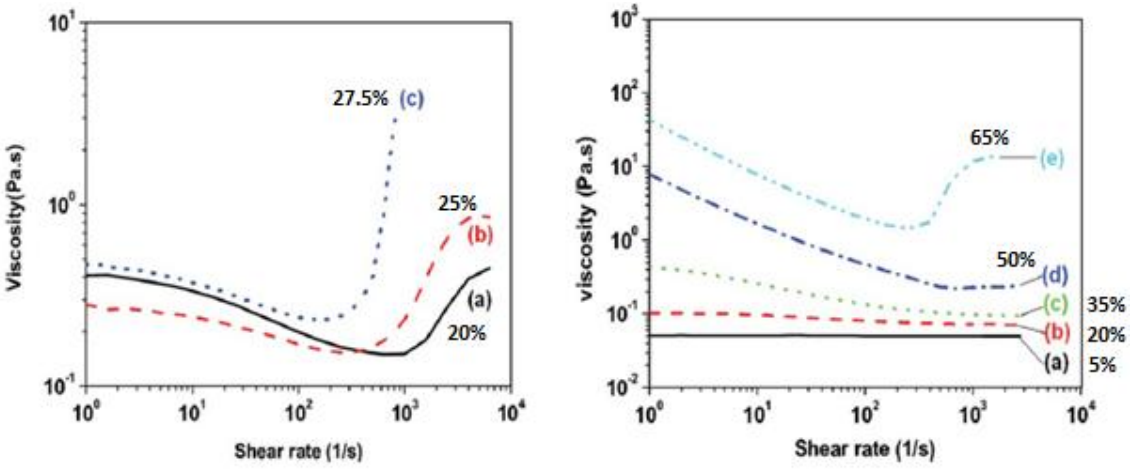

Figure 2.16. Steady-state viscosity curves for (a) fumed silica/PEG, (b) sphere silica/PEG suspensions at various weight fractions (Source: Kang et. al,2012)

2.4.2.5. Effect of Interactions Between Particles

Interactions between particles are very important for colloidal dispersions in terms of predicting their rheological behavior. Stability of colloidal dispersions is governed by the balance of interaction forces between particles. These interactions arise from forces such as van der Waals attractions. They also determine the microstructural behavior of colloidal dispersions. Non-flocculated fluids which means there is no overall attraction between particles, show shear thickening effect, on the contrary flocculated fluids undergo a thinning regime at high shear rates (Figure 2.16). To observe a shear thickening effect particles should be neutral or repel each other electrostatically, entropically or sterically (Barnes, 1989).

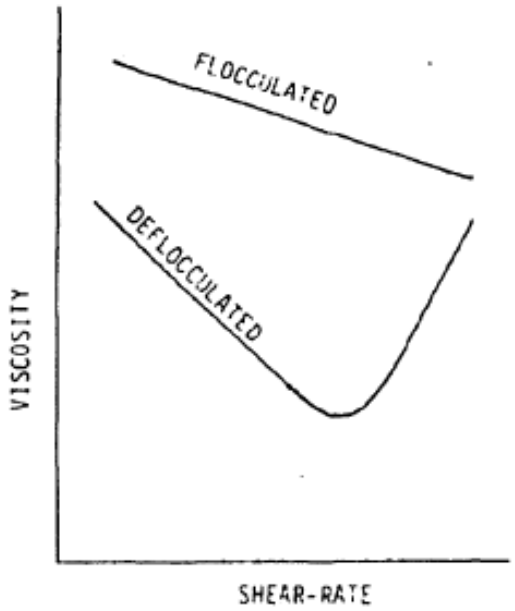

Figure 2.17. Schematic representation of the effect of chemically induced flocculation on shear thickening (Source: Barnes, 1989)

2.4.3. Materials used in STFs

STFs are basically produced by mixing of a nano-sized filling material and a liquid polymer. The materials that are used in the production of STFs in the literature can be examplified as silica species (Hassan et al., 2010), polymethyl methacrylate (PMMA) (Kalman et al., 2007), calcium carbonate (Wetzel et al., 2004), Kaolin clay (Rosen et al., 2007) and corn starch (Crawford et al., 2013). Fumed silica is mostly preferred dry particle for STF preparation due to its greatest response to shear forces. Besides, polyproylene glycol (PPG) (Raghavan et. al., 1997), polyethylene glycol (PEG) (Hassan et. al. 2010, Lomakin et al. 2011, Kalman et. al. 2007), water (Crawford et al. 2013), glycerol (Rosen et. al. 2007) has been used as continuous phase.

2.4.3.1. Fumed silica nanoparticles

Fumed silica particles are used in the industry such as coating, reinforcing and STF production formulations for which impact resistant materials. It is produced by the flame hydrolysis process of silicon tetrachloride in an oxyhydrogen gas flame. With this process silicon tetrachloride fused into branched and chain-like primary particles those

that will agglomerate subsequently. Due to its chain-like morphology and surface chemistry primary particles are linked to each other through hydrogen bonding and results in the formation of a network structure. Untreated fumed silica is anamorphous and hyrodrophilic substance which has high surface area and very low bulk density. Hyrophilicity is provided by the hydroxyl (–OH) gorups which cover approximately 40% of its surface (Cabot Corp.). These groups also give the fumed silica its unique shear thickening property. Remaining groups on the surface of the fumed silica are siloxane and silanol groups (Figure 2.17).

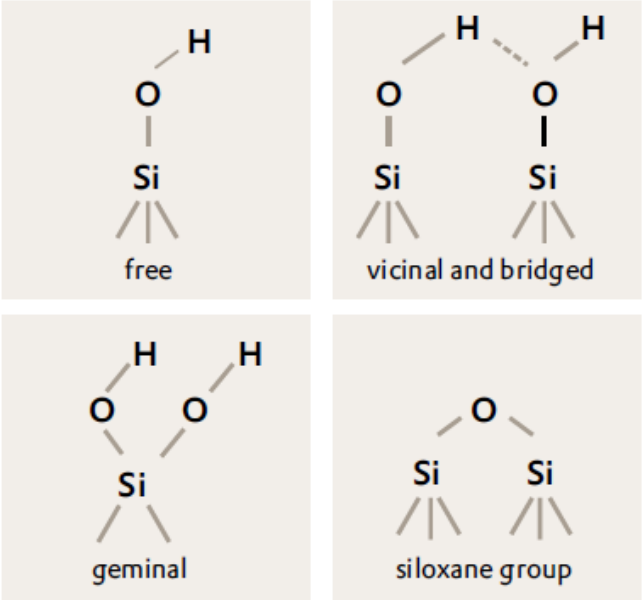

Figure 2.18. Possible surface groups of hydrophilic silicas
(Source: Aerosil®, 2009)

2.4.3.2. Polyethylene Glycol (PEG)

Shear thickening fluids basically consists of a filling material and a carrier fluid. Addition of carrier fluids is an important parameter for controlling the rheological properties of shear thickening fluids. Liquid polymers have the ability of adsorbing onto the surface of filling material. Adsorptions result in the increase of hydrodynamic diameter of the colloids and viscosity of the ultimate suspension, hence they are of the most widely used carrier fluids to ensure the stability of colloidal dispersions. Reversible shear thickening occurs on a critical shear stress value at which the short-range lubrication forces dominates the stabilizing interparticle forces. Polymer coating

of filling material assists to modify the critical shear stress for which initiation of shear thickening by changing the lubrication hydrodynamic forces and repulsive interparticle forces in shear thickening colloidal dispersions (Krishnamurthy and Wagner, 2005). Figure 2.18 indicates the forces between polymer coated particles. The applied shear forcebalances the repulsive force that develops due to the presence of the polymer layer.

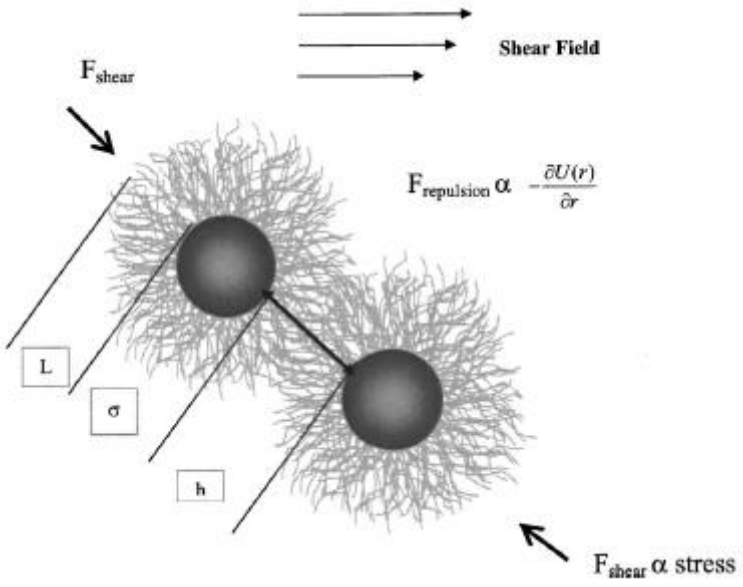

Figure 2.19. Force balance for predicting the shear thickening in polymer coated colloids (Source: Krishnamurthy and Wagner, 2005)

In this study, PEG was selected as carrier fluid. PEG is a water-soluble synthetic polar organic compound which is comercially available in the molecular weight range of 200 to 20 000 g/mole. It is also, non-toxic and easy to handle, thermally stable and easily available in bulk quantities which make it useful for bulk production(Pancera et. al, 2004; Walker, 1999; Hassan et.al., 2010). The molecular formula of PEG is HO–(CH_2–CH_2–O–)$_n$–H.

2.5. Rheology

Rheology is a discipline which is defined as the study of the deformation and flow of matter by American Society of Rheology in 1929 (Barnes, 1989). The term *rheology* comes from Greek words *rheos* (work) and *logos* (science) (Acartürk et al., 2009). All materials display different behaviors relying on their intrinsic micro and

chemical structures. Therefore, controlling the behaviors plays a vital role in industrial applications. The principal theoretical concepts that are underlying the rheology are kinematics, conservation laws and constitutive relations. Kinematics deal with geometrical aspects of deformation and flow, while conservation laws deal with forces, energy interchanges, stresses and constitutive relations special to classes of bodies. Rheology arises from combination of those theoretical concepts and results are used to solve the engineering problems in polymer processing, printing, lubrication, food technology and many other technologies (Tanner, 2000).

The main component of rheological characterization of materials is the *viscometer*. Viscometers are simple devices that measure the flow and viscosity curves via speed. For detailed measurements like torque controlled or step tests, such as creep or relaxation, rheometers are used. Rheometer is an instrument that is used to measure the responses of materials to applied forces. They can be divided into two groups as capillary and rotational rheometers. The most widely used rheometers are rotational rheometers. Rotational rheometers are used with different geometries such as cone and plate, parallel plate, cup and bob and Couette cylinders depending on the required data (Mezger, 2006; Duvarcı, 2009). Figure 2.19 schematically represents a test fluid within a cone and plate geometry.

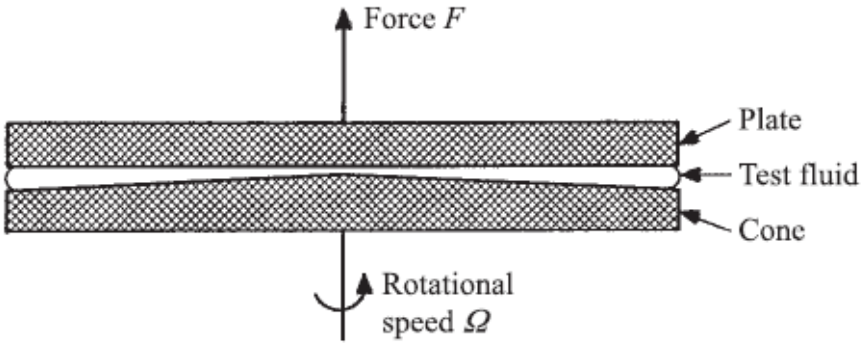

Figure 2.20. Schematic showing the flow of a test fluid placed in the cone-and-plate fixture, where force F perpendicular to the flow direction is measured as a function of rotational speed Ω (Source: Han et. al., 2007)

As described earlier, colloids basically consist of two substances; a filling material and a polymeric dispersant. Shear thickening materials generally cover this definition. The unique property of the STFs is the increment in viscosity with increasing

shear stress. The effect of shear stress on the behavior of STFs can be observed with steady-shear and dynamic shear measurements. In experimental part of my study both steady and dynamic measurements of STFs were performed with a rotational rheometer having cone and plate fixture (Raghavan and Khan, 2007).

2.5.1. Steady Shear Rheology

Steady shear rheological measurements are performed to observe the equilibrium microstructure and bulk viscosity of materials with only minor perturbations. Under steady shearing, there is increasing microstructure distortion with increasing applied shear rate (Mewis and Wagner, 2012; Duvarcı, 2009).

Saito et al. investigated the steady-state rheological properties of silica particles (size of 25 nm) within the 0.5 wt% polyethylene oxide (PEO) and water mixture with 0, 6, 10, 14 and 18% volume fractions (Saito 2011). Results show that the viscosity of silica containing suspensions are highly shear rate dependent. Below 10 vol%, dispersions slightly undergo a shear thinning whereas, with the particle loading shear thickening behavior was observed (Figure 2.20).

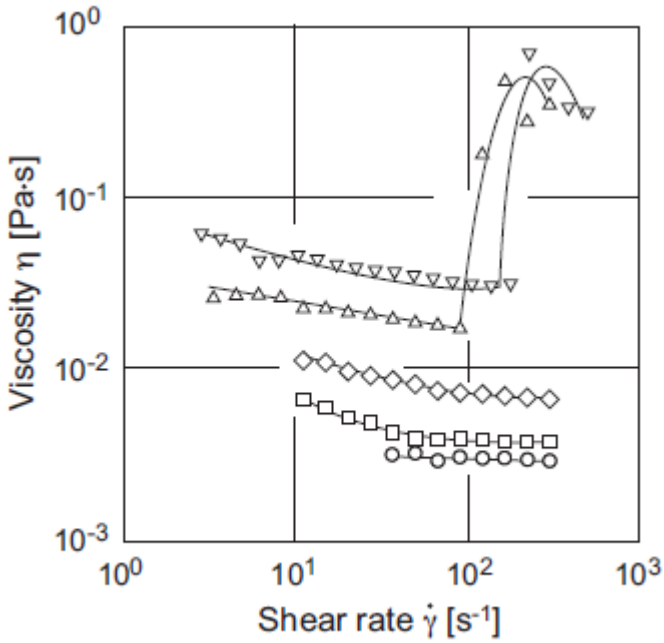

Figure 2.21. Shear rate dependence of viscosity for suspensions in 0.5 wt% PEO solution at different particle concentrations: 0 vol.% (○); 6 vol.% (□); 10 vol.% (□); 14 vol.% (Δ); 18 vol.% (∇) (Source: Saito et. al. 2011)

2.5.2. Dynamic Shear Rheology

Dynamic shear properties of materials enable to observe the viscoelastic properties of materials in terms of complex modulus. In dynamic measurements, a sinusoidal oscillation of stress or strain is applied to the sample. Sample material is being vibrated between two parallel plates or concentric cylinders. Dynamic measurements conducted in different modes such as frequency sweep, strain sweep, time sweep. Complex modulus can be separated into real and imaginary parts which are elastic modulus (G') and viscous modulus (G"). Elastic modulus is also known as storage modulus, because it defines the stored energy by the sample material, whereas viscous modulus (loss modulus) defines the dissipated energy by the material. The shape of the obtained curves are characterized by the suspending medium; the magnitude of the moduli depends on volume fraction (Duvarcı, 2009; Mewis and Wagner, 2012).

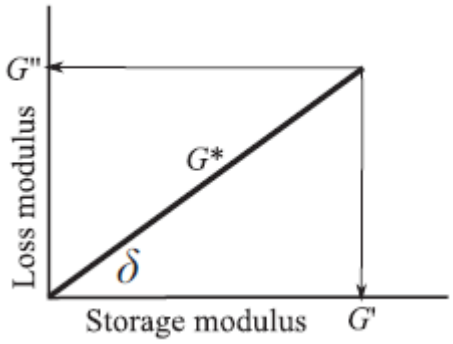

Figure 2.22. Geometric resolution of the complex modulus G*, into its component real (G') and imaginary (G") moduli and δ (Source: Princeton Univeristy press)

Sample material can be thought as Newtonian and Hookean solid to understand the dynamic measurements and their response to to a shear strain which varies sinusoidally with time as

$$\gamma = \gamma_m \sin \omega t \tag{2.6}$$

where γ_m is the amplitude and ω is the frequency of applied strain. For an elastic Hookean solid, the stress is related linearly to strain, i.e.,

$$\sigma = G\gamma = G\gamma_m \sin \omega t \tag{2.7}$$

Thus, in this case, there is no phase shift between shear stress and shear rate. On the other hand, for a Newtonian fluid, the shear stress is related to the shear rate, i.e.,

$$\dot{\gamma} = \frac{d\gamma}{dt} = \gamma_m \omega \cos \omega t = \gamma_m \omega \sin(\frac{\pi}{2} + \omega t) \tag{2.8}$$

and here

$$\eta\dot{\gamma} = \eta\gamma_m \omega \, (\sin \frac{\pi}{2} + \omega t) = \sigma_m \, (\sin \frac{\pi}{2} + \omega t) \tag{2.9}$$

The resulting shear stress is out of phase ($\pi/2$) from the applied strain. Therefore, the measurement of the phase angle δ which can vary between zero (purely elastic response) and ($\pi/2$) (purely viscous response) provides a convenient means of quantifying the level of viscoelasticity of a sample (Chabbra 2008).

The complex viscosity η^* and complex modulus G^* for the linear viscoelastic region can be defined as

$$\eta = \eta' + i\eta" \text{ and } G^* = G'(\omega) + iG"(\omega) \tag{2.10}$$

In Eqn 2.10, η' and $\eta"$ represents the real and imaginary partsare related to the storage (G')and loss (G'') moduli as;

$$\eta^{'} = \frac{G"}{\omega} \text{ and } \eta^{"} = \frac{G'}{\omega} \tag{2.11}$$

The storage and loss moduliG' and G'' are defined as;

$$G' = \frac{\sigma_m}{\gamma_m} \cos \delta \text{ and } G^{"} = \frac{\sigma_m}{\gamma_m} \sin \delta \tag{2.12}$$

Within the scope of this thesis, dynamic properties of STFs were determined as frequency and strain sweep modes. In frequency sweep mode, strain was kept constant while the angular frequency was varied. Likewise, in strain sweep mode angular frequency was kept constant while strain is varying.

Lee and Wagner observed the dynamic shear properties of silica containing colloidal suspensions (Lee and Wagner, 2003). The colloidal silica was obtained commercially as aqueous suspension with aparticle concentration of about 40 wt%. This suspension was centrifugated and the sediment was resuspendedusing a vortex mixer after adding of small amount of the supernatant liquid. This step was repeated four times and in each case the suspending fluid was also replaced with ethylene glycol (EG)gradually so as to keep silica concentration 55 and 60 vol.%.Dynamic and steady measurements were performed in both ascending and descending stress sweeps and steady shear viscosity and the complex viscosity as a function of the steady shear stress or average dynamic shear stress curves were obtained, respectively (Figure 2.22 a and b). Each STF shows a reversible shear thickening under both steady and dynamic shear. Also, It was determined that a critical strain amplitude is required for shear thickening. The complex viscosity decreases with increasing angular frequency at a fixed dynamic shear stress.

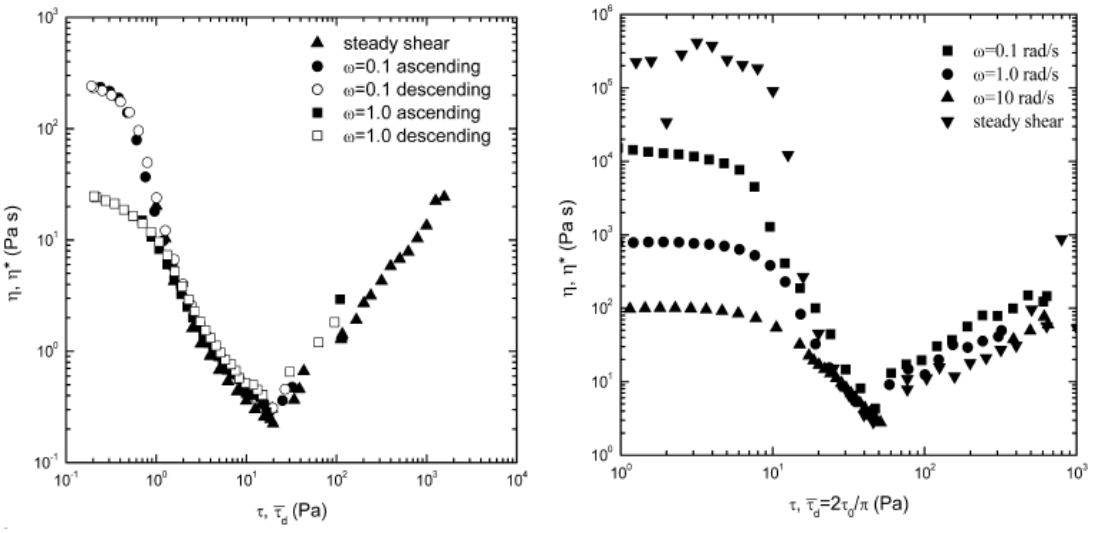

Figure 2.23. Reversible shear thickening behavior of: (a) 55 vol.%; (b) 60 vol.% colloidal silica dispersed in water for both steady and dynamic shearing plotted against the average applied dynamic shear stres (Source: Lee andWagner, 2003)

Raghavan and Khan investigated the viscoleastic behavior of fumed silica/polar PPG and fumed silica/non-polar mineral oil suspensions in strain and frequency modes (Raghavan and Khan, 1997). The average particle size of used fumed silica and molecular weight of used PPG in the experiments was stated as 14 nm and 725 g/mole, respectively. The silica concentration is varied between 3-10 wt%. Each suspension was

prepared by adding the liquid to the silica in a blender and mixing for approximately 1 minute. Figure 2.23 a represents the moduli values of 10 wt% silica and PPG suspension with varying angular frequency while Figure 2.23 b representing the same parameters for 5 wt% silica and mineral oil suspension. It is observed that moduli values of suspension containing PPG depends strongly on the frequency whereas, suspension of mineral oil exhibit a frequency-independent behavior. Frequency dependency indicates that the suspensionin PPG is nonflocculated, with a microstructure composed of discrete units.

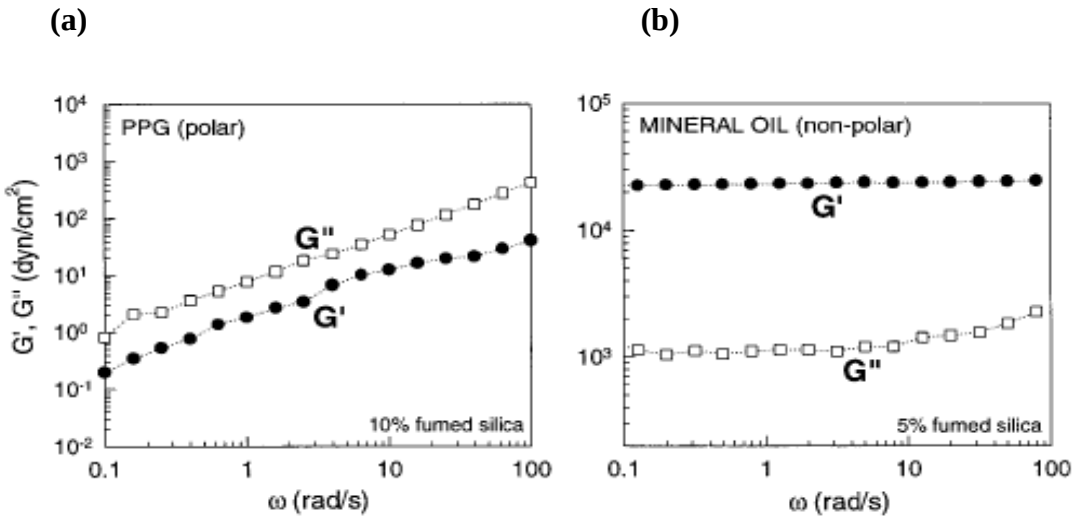

Figure 2.24. Elastic G' and viscous G" moduli as a function of frequency for two dispersions containing fumed silica. (a) suspension of 10% fumed silica in PPG, (b) 5% silica dispersion in non-polar mineral oil(Source: Raghavan and Khan 1997)

Figure 2.24 a and b shows the variation of moduli values of the same systems above, with strain amplitude. In Figure 2.24 a, G" values of the suspension containing PPG is greater than G' values. This situation states that the sample shows the characteristics of a nonflocculated suspension with strain-thickening. At higher strain amplitudes moduli values increases with a drastic jump. On the contrary, the graph in Figure 2.24 b exhibits the the chracateristics of flocculated gels. In this case, G' decreases more rapidly than G" value and ultimately falls below G".

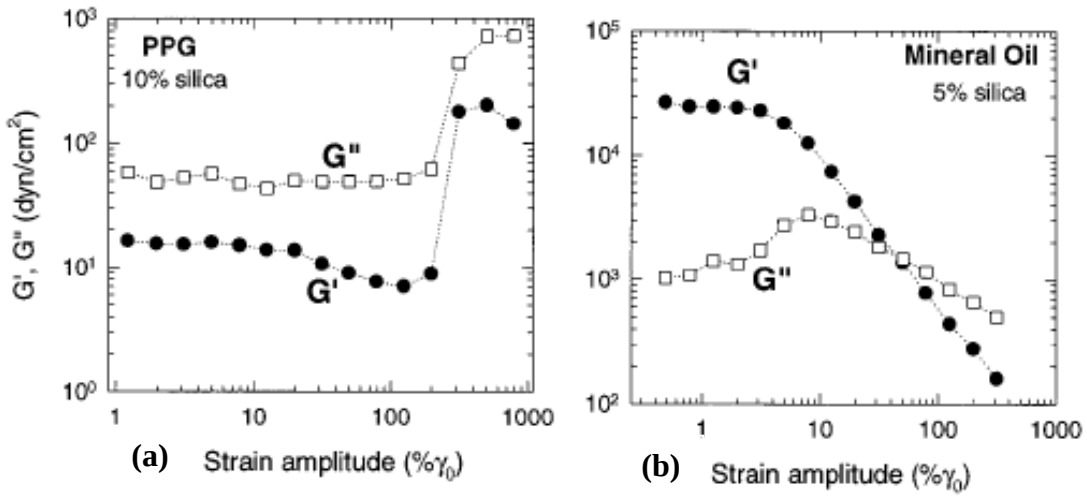

Figure 2.25. Elastic G' and viscous G" moduli as a function of strain amplitude for the same systems (a) 10% silica suspension in PPG, (b) 5% silica dispersion in mineral oil. Both experiments were performed at a frequency of 10 rad/s (Source: Raghavan and Khan 1997)

2.6. Stab Resistance and Flexibility of STFs

STFs are shock absorbing materials due to the ability of abrupt viscosity increase with applied shear stress. This unique feature makes them convenient for protective purposes. They can be used in damping and shielding equipments like sports equipments and body armor. Among them, particularly the armor applications have attracted the attention of scientists. The addition of STFs improves the ballistic and stab resistance of the woven fabrics by absorbing more energy per unit volume (Gopinath et. al., 2012).

Body armors made of woven fabric composites are extensively being used by the military and other law enforcement agencies for personal protection. Conventional body armor consists of 20-40 layers of aramid fabrics such as Kevlar®, Twaron®, Dyneema®. Aramid fabrics are high strength, high modulus and low density para-aramid synthetic fibers. The first invented aramid fabric is Kevlar® which was introduced by the Du Pont de Nemours Inc. In 1971. Besides the aramid fabrics, nylon and ultramolecular weight polyethylene (UHMWPE) fabrics were also used in the literature studies (Decker et. al., 2007; Liang-Sun et.al., 2013).

Conventional body armor is bulky, stiff and heavy. These drawbacks make their use difficult. Therefore, to improve low bulky, much flexible and lightweight armors

which have the same or enhanced protective level, is very important especially for military applications (Dong et. al., 2010; Wetzel 2003).

Decker et. al. have studied the stab resistance of STF impregnated Kevlar fabrics (Decker et. al., 2007). STFs were prepared by mixing of colloidal silica (450 nm sized) with PEG having 200 g/mole molecular weight at a volume fraction of 52%. They emphasized that the rheological results showed the discontinuous shear thickening initiated at 20 s^{-1}. For the aim of producing STF–fabric composites, the STF was solved in ethyl alcohol at a 3:1 volume ratio of ethanol:STF. Then, each fabric in dimensions of 38.1 x 38.1 cm impregnated with the prepared STF/ethyl alcohol solution for 1 min, squeezed to get rid of excess amount of ethyl alcohol and dried during 30 min at 65 ^{0}C. STF add-on was measured between 19.5% and 27% as weight.

Measurements were conducted by spike and knife threats by using drop tower, based on the National Institute of Justice (NIJ) Standard. This standard rules the use of a backing material. The backing material contains 4 layers of neoprene sponge (5.8 mm each), a thick layer of polyethylene foam (31 mm) and a relatively thick layer of rubber (6.4 mm). The threats were adjusted to the crosshead of the drop tower. Also, five witness paper were placed onto the backing material to measure the impact energy more precisely. The drop mass was set as 2.34 kg for knife and 2.33 kg for spike threat and height was varied in the range of 0.1-0.75 m for the first set of experiments. For the second set of experiments, the drop height was fixed at 0.1 m and the drop mass was varied from 2.34 kg to 4.68 kg for the knife and from 2.33 kg to 4.67 kg for the spike. The obtained results which is represented in Figure 2.25 show that the STF addition onto Kevlar slightly enhanced the resistance of fabrics to the knife impactor. Depth of penetration through the witness papers increases with increasing impact energy. At higher impact energy, both targets penetrates the fifth witness paper.

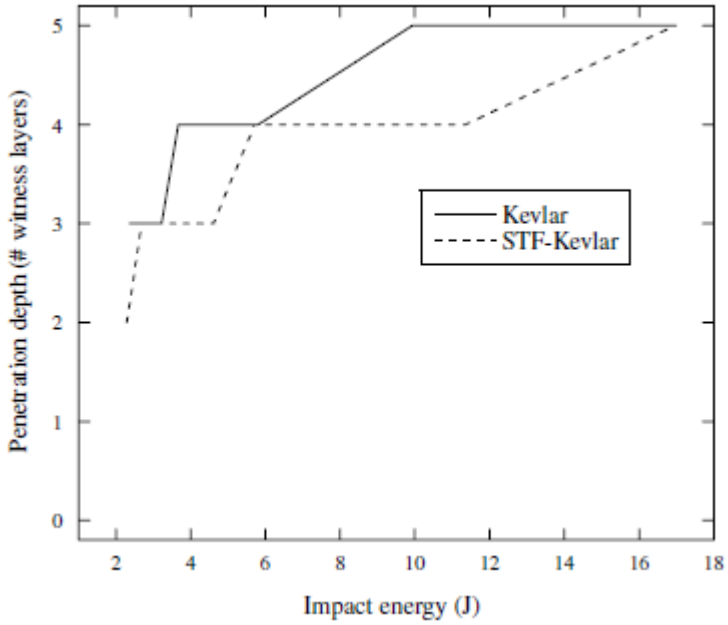

Figure 2.26. Knife drop tower results for Kevlar and STF–Kevlar fabrics
(Source: Decker et.al.,2007)

Penetration depth of drop tower spike threat onto the Kevlar fabrics is seen in Figure 2.26. STF addition improved the neat Kevlar's stab resistance such that at the highest energy level of about 17 J, the STF–Kevlar composite allows penetration through three witness layers.

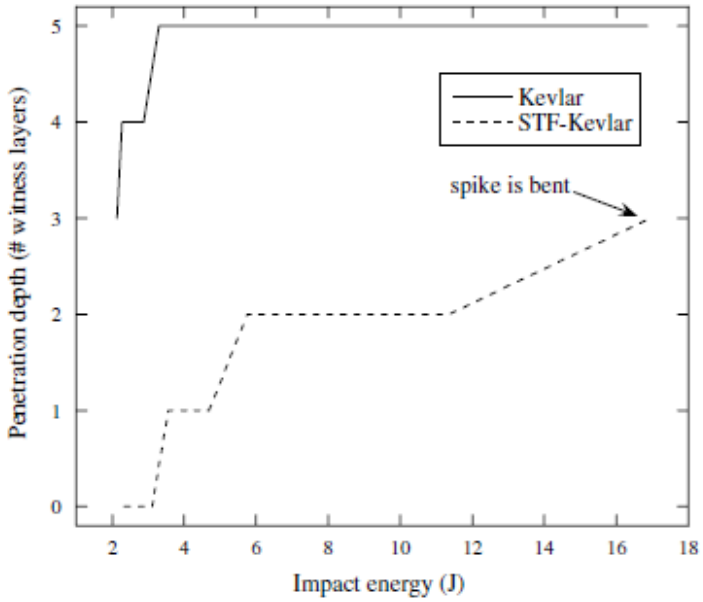

Figure 2.27. Spike drop tower results for Kevlar and STF–Kevlar fabrics
(Source: Decker et.al.,2007)

Besides the drop tower, quasistatic testing of STF impregnated and neat Kevlar fabrics was also performed. The knife and spike threats were adjusted into the upper grip of an MTS Synergie mechanical testing frame which has the 1 kN load cell. The point of zero displacement is defined as the displacement at which the load first exceeds 1.0 N. The threats were approached to the composite samples having the same backing material behind them, at a rate of 500 mm/min to a total displacement of 30 mm. According to the load versus displacement curve in Figure 2.27 both of the threats resist to significantly higher loadings as compared to neat Kevlar composites.

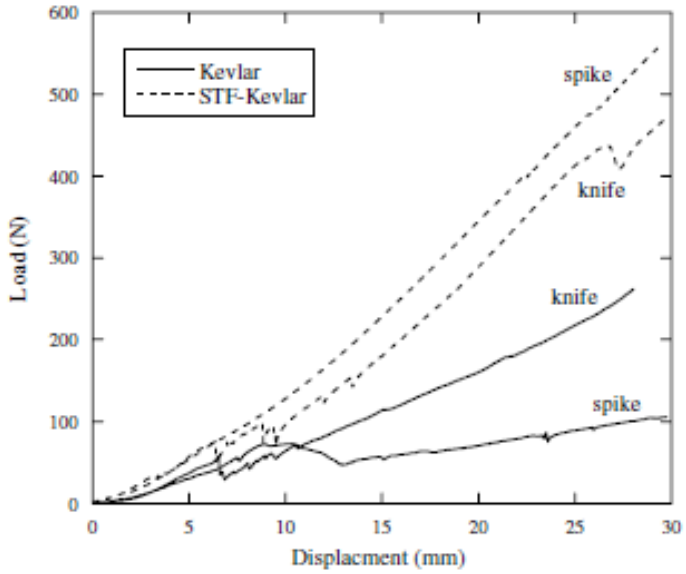

Figure 2.28. Load–displacement curves for quasistatic loading of Kevlar and STF–Kevlar targets, against both spike and knife impactors (Source: Decker et.al., 2007)

Dynamic and quasistatic testing of STF/Kevlar composites with both spike and knife impactors were conducted by Hassan et. al. STFs were synthesized by using silica nanoparticles having the size of 15 nm and PEG with the weight percentages of 40% and 60%, respectively. The average molecular weight of PEG was 200 g/mole. They were ultrasonicated at 50% amplitude during 5h and 10 ^{O}C by adding the excess amount of ethyl alcohol (Hassan et. al. 2010). The obtained STFs were diluted again with ethyl alcohol in the ratio of STF/ethanol (40:60). Each Kevlar fabric (38.1 x 38.1 cm) was soakedin an aluminum containerfilled with STF/ethyl alcohol solution for 1 min and then squeezed usinga steel cylinder to remove the excess amount of the solution. Impregnated fabrics were hanged for 48 h at room temperature for drying. For stab tests

the same backing material as in Decker et. al.'s study, was used again with 5 layers of witness papers.

Figure 2.28 clearly indicates that STF impregnated fabrics exhibits better stab resistance compared to neat Kevlar for low values of impact energy. Approximately 8 J impact energy both of the targets reach maximum penetration depth of 5 witness paper. Quasistatic stab results were shown in Figure 2.29 For spike testing STF/Kevlar composite supports substantially higher loading with 575 N while neat Kevlar supporting 85 N. In knife tests same behavior was observed as 530 N and 286 N for STF/Kevlar composite and neat Kevlar, respectively. It should also be noted that more drastic impact resistance data were collected with spike threat which has sharper tip than knife, for both Decker and Hassan et. al.'s studies.

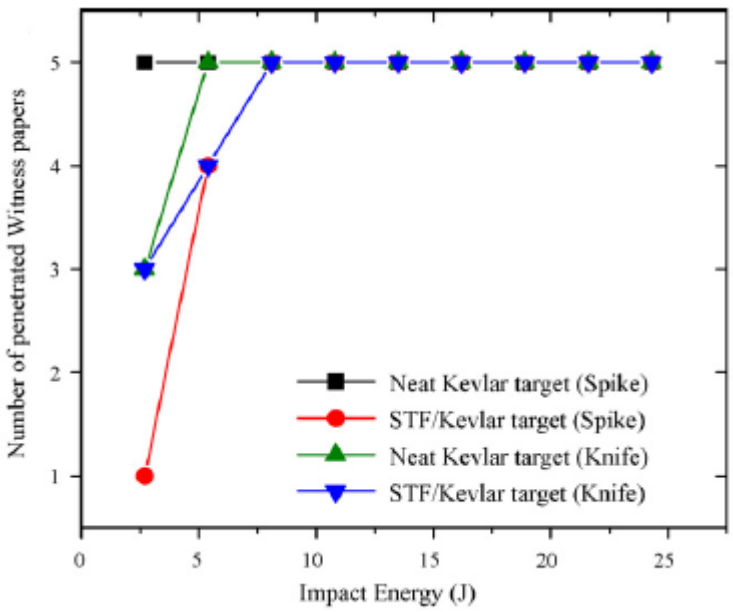

Figure 2.29. Dynamic stab test results for neat Kevlar and STF/Kevlar composite (Source: Hassan et. al., 2010)

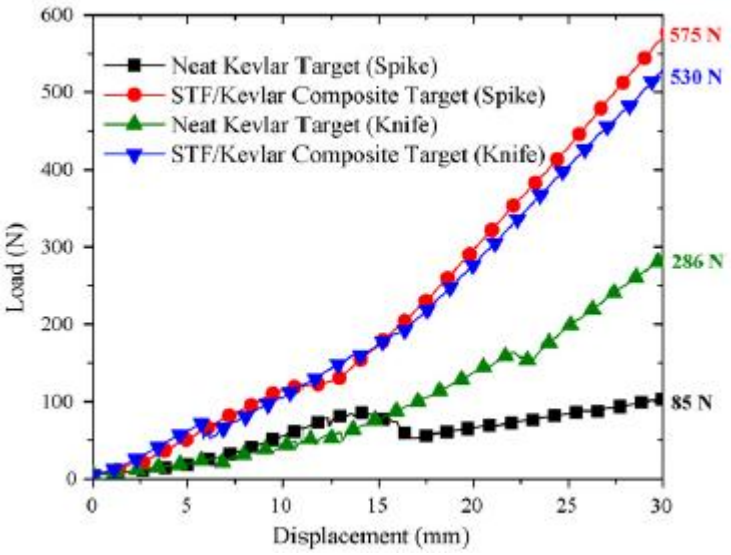

Figure 2.30. Quasistatic stab test results for neat Kevlar and STF/Kevlar composite (Source: Hassan et. al., 2010)

Hassan et. al. also measured the flexibilities of the samples composed of 4 and 10 layers of STF/Kevlar and neat composites. The flexibilit set-up is illustrated in Figure 2.30. To measure the flexibility, neat fabric and STF/fabric were cut into51mm×51mm square layers. A 20 g weight was then attachedto the samples and the bending angle was measured. They found that the flexibilities of the composites are nearly same with the neat samples. For 4 layers STF/Kevlar composite the bending angle is found as 51^{o} whereas it was measured for neat Kevlars as 50^{o}. Likewise, for 10 layers STF/Kevlar composite the bending angle is found as 13^{o} which is the same as neat Kevlars.

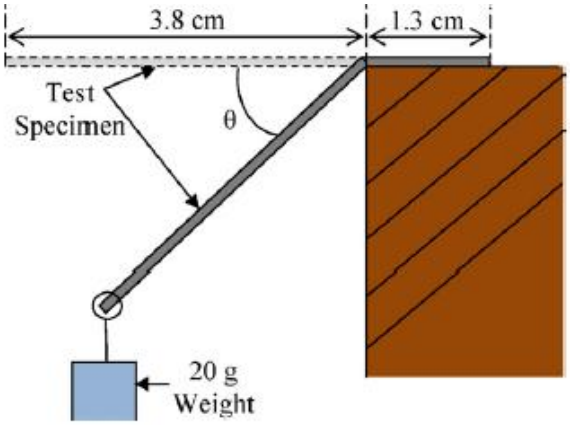

Figure 2.31. Flexibility test geometry (Source: Hassan et. al., 2010)

CHAPTER 3

EXPERIMENTAL STUDY

3.1. Materials

Nano-sized fumed silica particles were used as filling material and purchased from Cabot Corporation, USA. Polyethylene glycol (PEG) having different molecular weights were selected as Newtonian medium fluid (Acros Organics, Belgium). The average molecular weights selected for PEGs were 200, 300, 400 and 600 g/mole and their names were abbreviated as PEG 200, PEG 300, PEG 400 and PEG 600. PEGs mentioned above have increasing viscosities of 60, 85, 120, 160 mPa.s, respectively, due to their molecular weights. Detailed material properties are given in Tables 1 and 2. Another substance that is used in this study is ethyl alcohol. It is used to improve the solubility of fumed silica particles and purchased from Teksol Kimya. Allof the materials used in this study to synthesize STFs were obtained commercially without any further purification.

Table 3.1. Specification of fumed silica nano-particles

Fumed silica	
Avg. Particle size (nm)	40-240
Density (g/cm^3)	2.2 (@ 20^0C)
Bulk Density (kg/m^3)	30-150
Specific gravity	2.2 (@ 20^0C)
Ph (4 % slurry)	3.6-4.5
Surface area (m^2/g)	200

Table 3.2. Physical properties of PEGs used in the thesis

PEG	Molecular weight (g/mole)	Density (g/Ml)	Viscosity at 20°C (mPa.s)	Refractive Index	Melting Point (°C)
PEG 200	200	1,125	60-70	1.4580 to 1.4610	-65
PEG 300	300	1,12	85-100	1.4620 to 1.4650	-15
PEG 400	400	1,1275	120	1.4650 to 1.4680	4 to 8
PEG 600	600	1,1265	160-190	1.4660 to 1.4700	17 to 22

STFs were synthesized with novel techniques developed in this study. The effect of molecular weight of PEG and silica concentration on the rheological behavior of the STF, experiments were performed. To investigate how STFs can improve the stab resistance properties of conventional aramid fabrics which are used in armors, STF/aramid fabric composite materials were prepared as a further stage. The aramid fabrics used were Twaron plain-woven fabrics which have the areal density of 200 g/m^2.

3.2. Synthesis of STFs

Stages of STFs synthesis is illustrated in Figure 3.1, schematically. The first step to synthesize STFs was dispersing fumed silica nanoparticles in ethyl alcohol. Particles were mixed in excessive amount of ethyl alcohol (Ethyl alcohol: fumed silica, 1:5) to obtain well disperse and stable solutions. Also, the use of ethyl alcohol is help of impregnation procedure of STFs by reducing the surface tension of solutions, and provide well impregnated fabrics. The mixing of fumed silica and ethyl alcohol was performed with ultrasonic disperser during 5 hours at 70% amplitude (Hielscher UP400S Ultrasound Technology, 24kHz, $75W/cm^2$). This sonochemical method provides better homogenous solutions as compared to those obtained with mechanical

mixing or magnetic stirrer. Following this, PEGs were added to the solutions at various weight fractions so as to fix the fumed silica/ PEG concentration in between 5-30% w/w and ultrasonic disperser was applied for an additional 3 hour. The obtained solution was poured into the petri dishes and dried in an air-circulating oven at 79 ^{0}C until removal of all Ethyl alcohol in the solution. Temperature was fixed at 79 ^{0}C which is the boiling point of Ethyl alcohol to ensure a quasi-static drying and avoid the distortions in the microstructural system of the STFs. Petri dishes were used to reduce evaporation time by increasing the surface area. After drying, obtained materials were grinded with the help of an agate mortar and the obtained fluids were keep under vacuum to remove the air-bubbles which can influence the rheological analyses adversely. Schematic representation and illustrations of homogenization and grinding process were given in Figures 3.1. to 3.3, respectively. Names of STFs were abbreviated according to their fumed silica concentrations and type of the polymer in the thesis for the sake of easiness. As an example, Table 3 represents those concentrations and abbreviations of STFs which contain PEG 200. The same nomenclature was used also for other STFs those composed of PEG 300, PEG 400 and PEG 600 such as STF5-PEG 300, STF5-PEG 400 etc.

Table 3.3. The weight fraction specifications and Sample Ids of the STF samples

Sample ID	**Weight fraction of Fumed SiO_2 (%)**
STF5-PEG 200	5
STF10-PEG 200	10
STF15-PEG 200	15
STF20-PEG 200	20
STF25-PEG 200	25
STF30-PEG 200	30

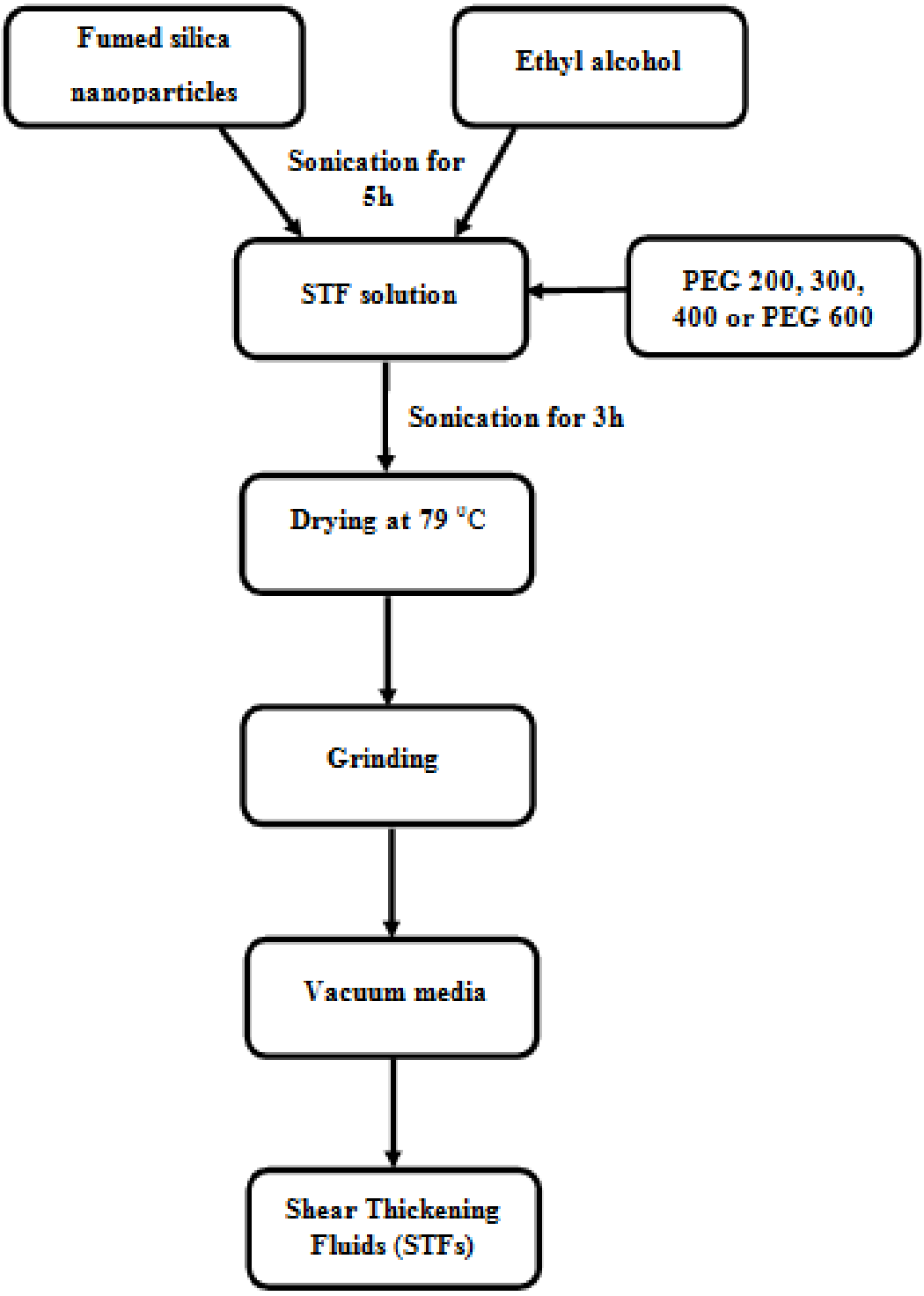

Figure 3.1. Schematic representation of STF production procedure

Figure 3.2. Photo showing the homogenization step of STF production process

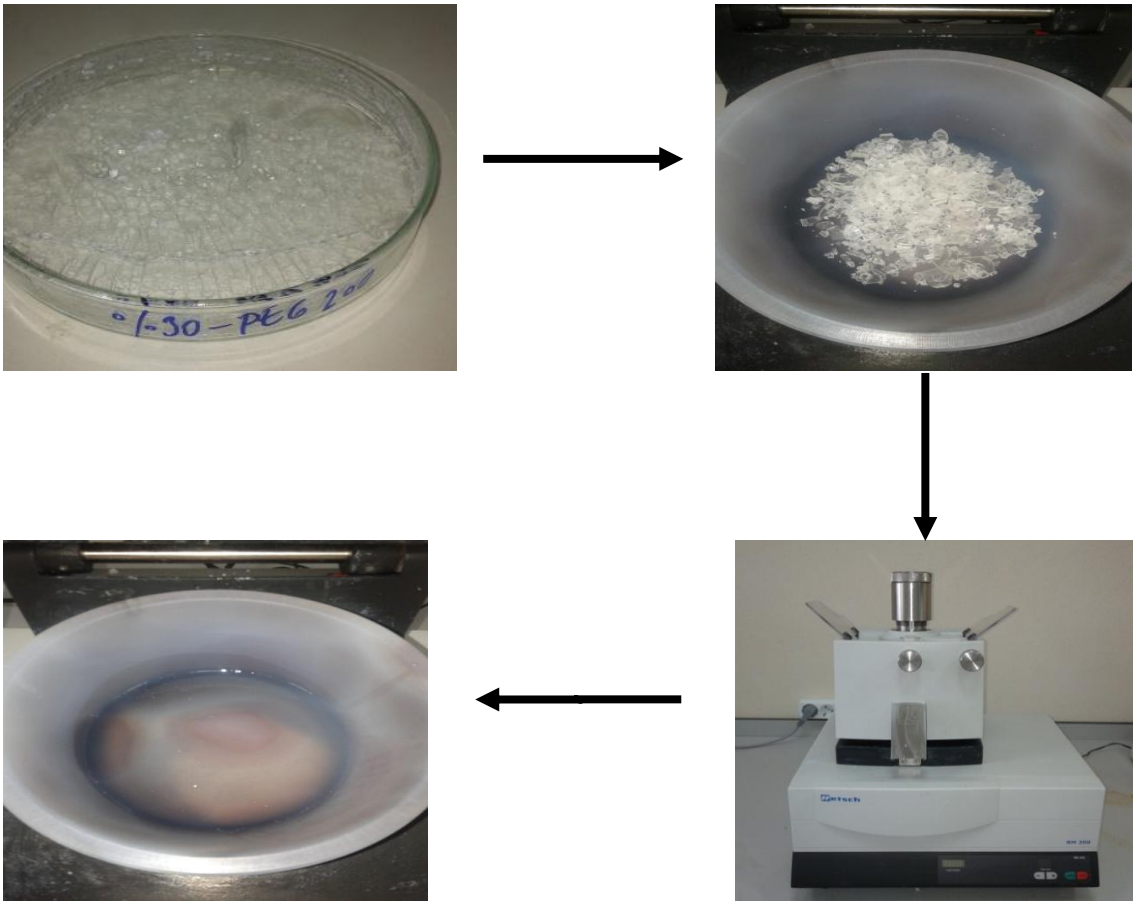

Figure 3.3. Photos illustrating the grinding step in STF production process, (a) and (b) appearance of STF solution after drying, (c) Photograph of agate mortar which was used in experiments. (d) STF after grinding

3.3. Preparation of Aramid fabric/ STF Composites

To investigate the potential of STFs on fabrication of liquid armors, aramid fabric/STF composites were prepared. To begin, STFs were diluted in ethyl alcohol to ensure better coating of fabrics. According to the rheological results, the use of STFs containing 30% w/w silica concentration was determined to obtain the best impact resistant properties. Twaron aramid fabrics were cut into 20 cm x 20 cm pieces. For every stab test, 10 layers of fabrics were used and each layer was impregnated by soaking them into the diluted STF solution for several minutes. Then, fabrics were dried in the air-circulating oven. Stages of aramid fabric/STF composite production is illustrated in Figure 3.4. Also some photographs which were taken during the process can be seen in Figure 3.5.

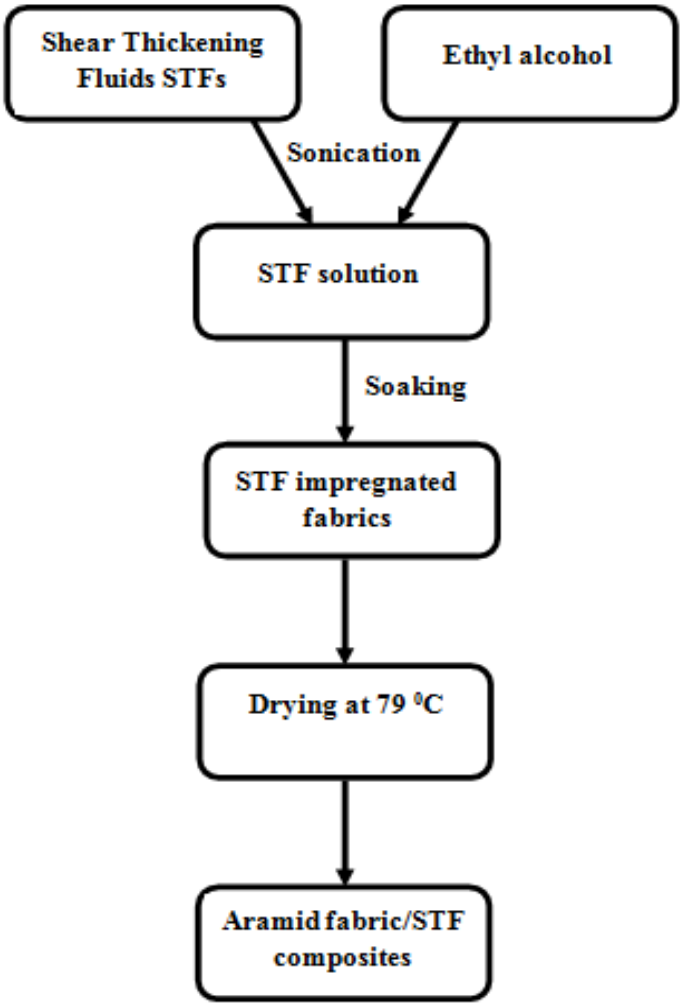

Figure 3.4. Schematic representation of impregnation procedure

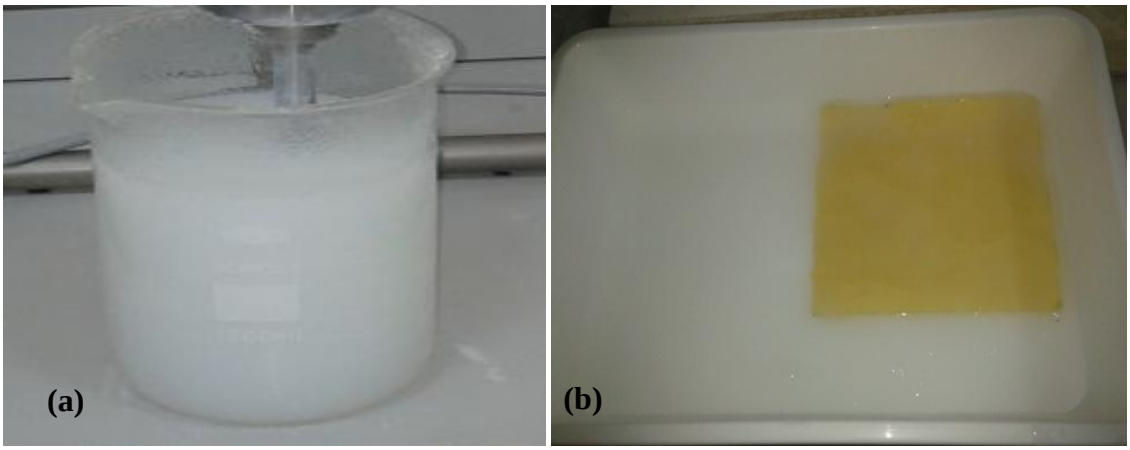

Figure 3.5. Photographs from aramid fabric/STF production procedure. (a) Diluted STF solution, (b) Appearance of STF solution impregnated fabric

3.4. Characterization of Nano-Sized Particles and STFs

3.4.1. Size Distribution of Particles by Dynamic Light Scattering (DLS)

Toinvestigate the average particle sizes of the used fumed silica nano particles, Malvern Mastersizer 2000 which operates with the principle of Dynamic Light Scattering (DLS) technique was used. Particle size versus volume percentage data was obtained by this method. Analyses were carried out in two stages. The first stage consists of the measurements of nanoparticles that were dissolved in ethyl alcohol. The second one consists of addition of liquid polymer into the silica solution to observe the effect of polymer-silica interactions on the size and determine the final average size. Before first analysis, dry fumed silica particles were dispersed in ethyl alcohol medium for 5 hours with the help of an ultrasonic disperser (Hielscher UP400S Ultrasound Technology, 24kHz, 75W/cm^2) at 70% amplitude to enhance the particle solubility. As a part of the second stage, liquid polymer was added into the silica/ethyl alcohol solution and dispersed with ultrasonic disperser for extra 3 hours. Samples were taken from both stages to perform the analyses.

3.4.2. Microstructural Evaluation

3.4.2.1. X-Ray Diffraction

X-Ray diffraction (XRD) analysis was performed to evaluate the crystalline structure of the fumed silica nanoparticles. In this analysis, Cu-Kα technique with wave length of 0.1541nm was used in the range of $5\text{-}80^0$ by Phillips™ Xpertdiffractometer which were operating at 40 Kv and 40 Ma. The datas were collected in 2θ range of $5\text{-}70^0$ with a scanning speed of10^0/ min.

3.4.2.2. Scanning Electron Microscopy (SEM)

The microstructure of silica particles suspended in ethly alcohol and silica particles suspended in ethyl alcohol/liquid polymer mixture (STF solution) was evaluated by using Phillips™ XL-30S FEG Scanning Electron Microscopy (SEM). All samples suspensions were dried at 79 ^oC before analyses to evaporate ethyl alcohol. Also, gold sputtering technique was applied before analyses to have a thin gold layers on the samples in order to prevent electron charge accumulation on samples by having conductive surfaces.

3.4.3. Thermal Evaluation

3.4.3.1. Thermogravimetric Analysis (TGA)

The weight changes as a function of temperature of STFs and pure liquid polymers weremeasured using a Perkin Elmer Diamond Thermo Gravimetric Analyzer. A temperature ramp of 10^oC/ min from 30 to 800^oC was selected for TGA analysis.It gives us ideas about the thermal stability, the decomposition trend and the amount of volatiles such as moisture or any impurities of STFs and pure liquid polymers. The operating athmosphere for TGA was selected as nitrogenat a flow rate of 50 mL/ min.

3.4.4. Rheological Characterization

The steady and dynamic shear rheological characterizations of STFs were performed at room temperature (25 ^{o}C) by rotational TA Instruments 2000ex (Figure 3.6) rheometer with the cone and plate fixture having a diameter of 25 mm and cone angle of 0.1 radian. Steady shear measurements were conducted to observe the change in viscosity and stress values of STFs with shear rate. Dynamic data were collected in terms of frequency and strain sweep modes under sinusoidal oscillation. In frequency sweep mode, elastic and viscous moduli values were measured with varying angular frequency by keeping strain amplitudes constant. Moreover, in strain sweep mode, angular frequencies were held fixed and moduli values were observed with varying strain amplitudes. A pre-shear of 1 s^{-1} was applied during 1 minute prior to each rheological measurement for removal of the sample loading effects and wall-slip history to ensure the confidence. Also, equilibration step was applied during 2 minutes.

Figure 3.6. TA Instruments AR2000ex Rheometer

3.4.5. Mechanical Characterization

3.4.5.1. Stab Tests

Investigation of the impact properties of STFs impregnated fabrics are important for liquid armor applications. Tests were performed with Schimadzu AGI Universal test machine with a 5 kN load cell by following the procedure of NIJ 0115.0 standard which decribes the stab testing conditions. During the tests an engineered spike that was prepared according to the technical drawing given in the standard (Figure 3.7) was attached to the mouth of load cell and also a slab of backing material (Figure 3.8) was prepared. Backing material consists of four layers of neoprene sponge (5.8 mm), one layer of polyethylene foam (31 mm) and two layers of rubber (6.4 mm) and they were arrayed from strike face down, respectively. Targets were located below the spike impactor. The impactor was pushed onto the target surface at a rate of 500 mm/min through the distance of 30 mm.

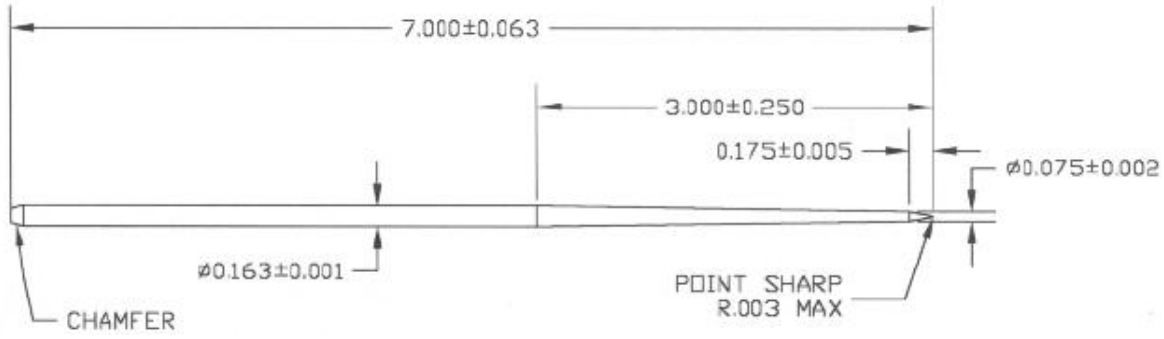

Figure 3.7. Engineered spike
(Source: NIJ 0115.0 standard, 2000)

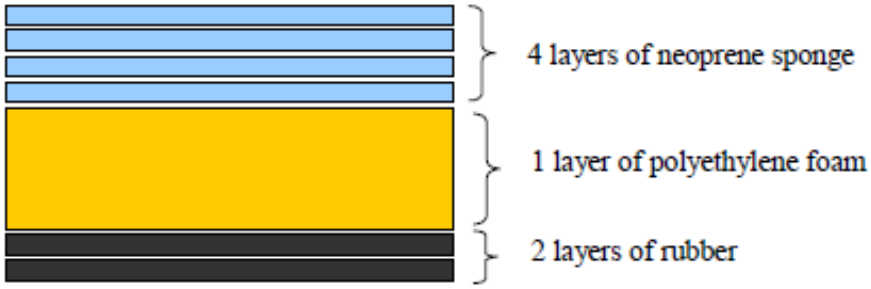

Figure 3.8. Composite backing material
(Source: NIJ 0115.0 standard, 2000)

Figure 3.9. Stab test set-up

3.4.5.2. Flexibility Tests

Flexibility of the prepared STF/fabric composite samples was measured through flexibilty tests. 10 layers of fabrics was measured with flexibility tests for wearing applications. Flexibility set up was prepared by mounting one end of a wire to the edge of the composite bag and the other end to the mouth of the load cell at which is used in

Schimadzu AGI Universal test machine. Edge of the samples was forced to bend by applying a tensile force onto the wire attached to the sample. A maximum force of 6N was applied to samples. The displacement of the sample edge was measured and the angle occured to the wire was calculated.

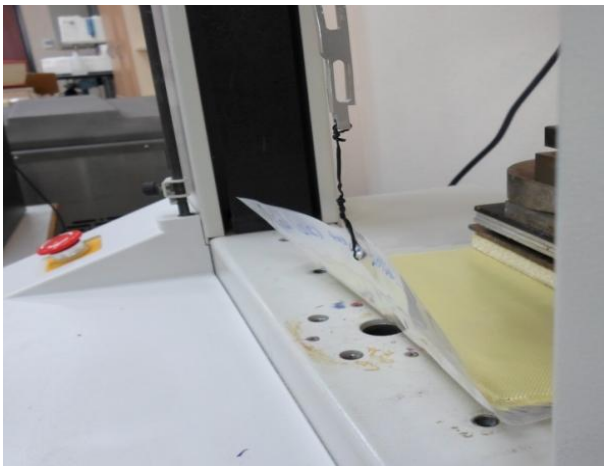

Figure 3.10. Flexibility test set-up

3.4.5.3. Ballistic Tests

Ballistic tests were performed for STF impregnated aramid and UHMWPE fabrics with the combination of PE laminae based on the NIJ ballistic test standard of 0101.04 at 8th Major Maintenance Center Command, Afyon. Different configurations of materials with the size of 30x40 cm were tested by putting into a camouflage (Figure 3.12) in the set up which is given in Figure 3.13. The tests were performed with fragment- simulating projectiles (FSPs).of each has 1.1 g of weight (Figure 3.11). FSPs were evaluated in terms of V_{50} tests which is a measure of the ballistic limit. Ballistic limit is defined as the The minimum velocity at which a particular projectile is expected to completely penetrate armor of given thickness and physical properties at a specified angle of obliquity(MIL-STD-662F, 1997).

Figure 3.11 shows the parts of the test set-up. The chronographs which were adjusted to the stop and start triggers determine the impact velocity. The deformation of the fabric targets was measured from he glass cement backing material.

Figure 3.11. 1,1 ± 0,03 gram (17grain) FSP

Figure 3.12. Image of the camouflage used in the ballistic tests

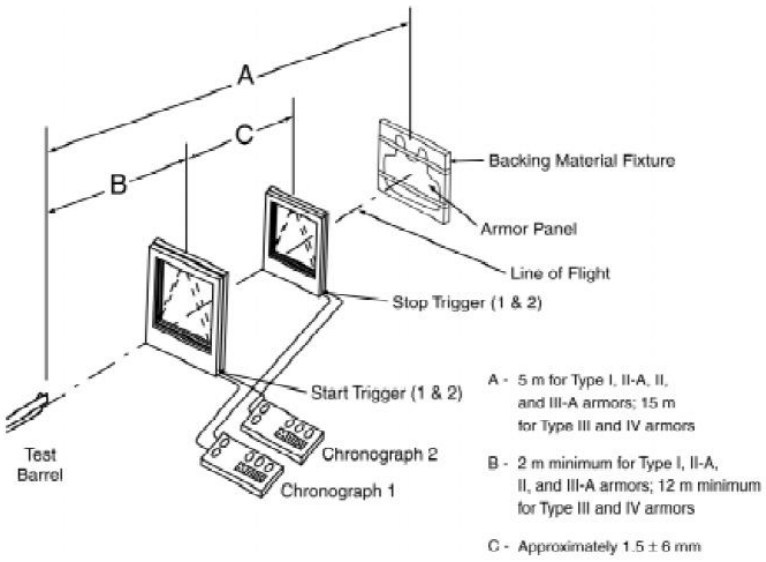

Figure 3.13. Ballistic test set-up
(Source: NIJ 0101.04, 2000)

CHAPTER 4

RESULTS AND DISCUSSION

Production of STFs and preparation of aramid-UHMWPE fabrics/STFs composites for liquid armor applications were explained in experimental part of this study. This chapter covers the outcomes of obtained STFs in terms of microstructural, thermal and rheological characterization as comprehensive as possible. The results were reported to understand the nature of the STFs. Also, their effect on mechanical properties of fabrics was measured by stab, flexibility and ballistic test, and results were discussed.

4.1. Properties of Nano Particles and STFs

4.1.1. Dynamic Light Scattering (DLS) Analysis

Size distribution of the fumed silica nanoparticles and STF30- PEG 300 solution was given in Figure 4.1. The experiments were carried out with DLS technique by providing homogenity with the ultrasonic horn of the Malvern Matersizer 2000 in ethyl alcohol medium. The output data was obtained in terms of volume amount of silica within a specific size. As it is seen in the Figure . the size of the fumed silica particles ranges between 40 and 240 nm with the average value of 137 nm. The polydispersity of the particles may caused by the commercial production techniques or aggregation. Similarly, the size range of STF30-PEG 300 solution was determined as 46-275 nm with the average size of 185 nm. The slight increase in average particle size may be due to the adsorption of the PEG on to the silica surface.

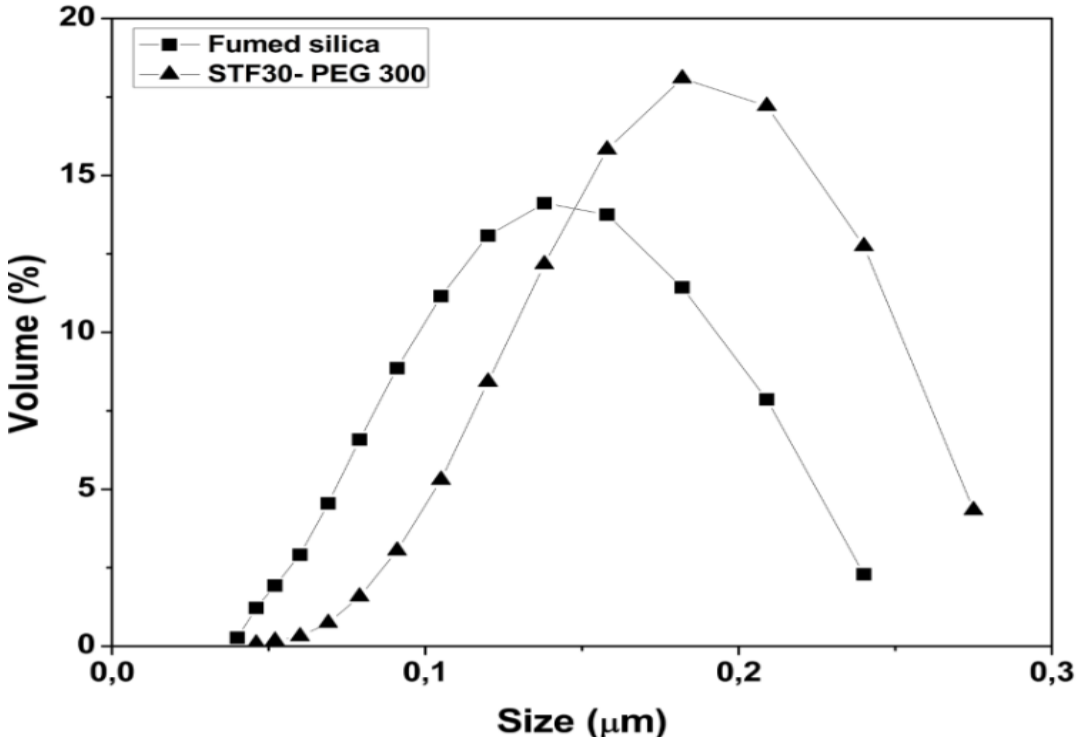

Figure 4.1. Particle size distribution of fumed silica and STF30-PEG 300 solution

4.1.2. X-Ray Diffraction (XRD) Analysis

The crystallinity of the pristine fumed silica nano particles was observed with XRD analysis in 2θ range of 5-80^{o}. Many noisy-like peaks can be seen in the XRD pattern which is given in Figure 4.2. revealing that the amorphous structure of the particles. The broad peak centered at about 22^{o} indicates the existence of the elemental silicon.

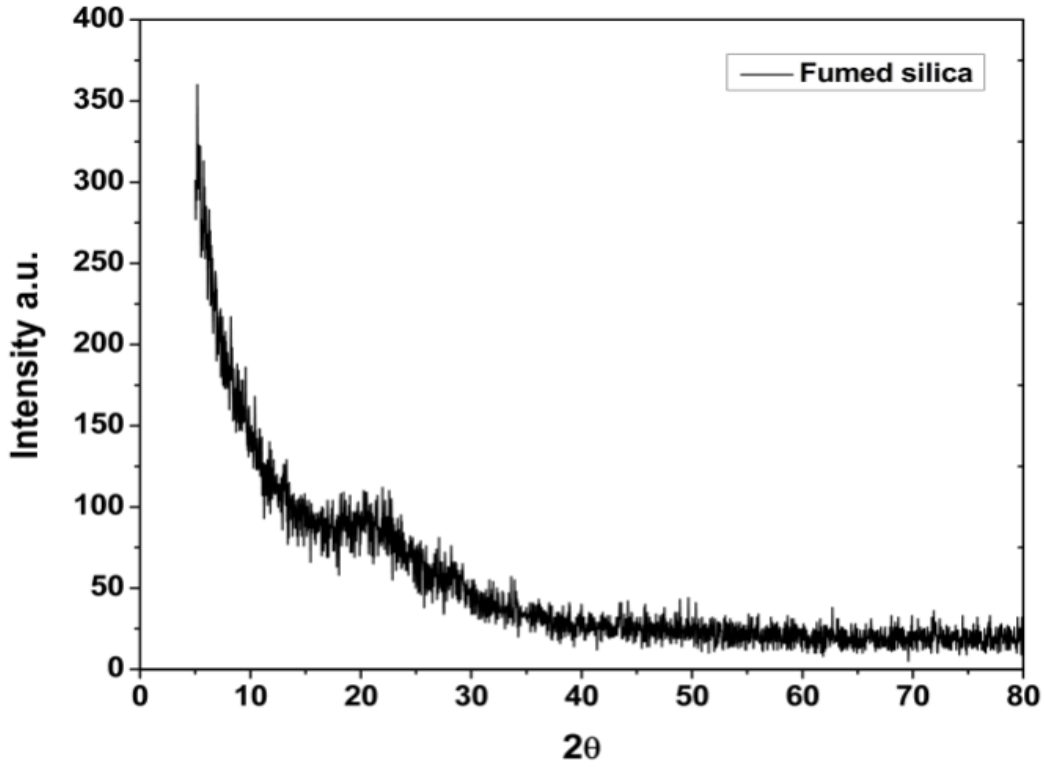

Figure 4.2. XRD Pattern of the fumed silica nanoparticles

4.1.3. Microstructural Characterization by SEM

Microstructures and surface morphology of the fumed silica and STF solutions which were dried to remove ethyl alcohol, were investigated with SEM. Figures 4.3 to 4.7. show the SEM micrographs of the fumed silica, STF30-PEG 200, PEG 300, PEG 400 and PEG 600 at various magnifications, respectively. The branched like aggregates showing fractal nature of the silica particles can be seen in Figure . The rest of the micrographs which belongs to the STFs reveals that the fumed silica particles were coated with PEG and have blend structure. The formation of the blend structure denotes the well dispersion of silica particles in PEG and homogenity of the STFs.

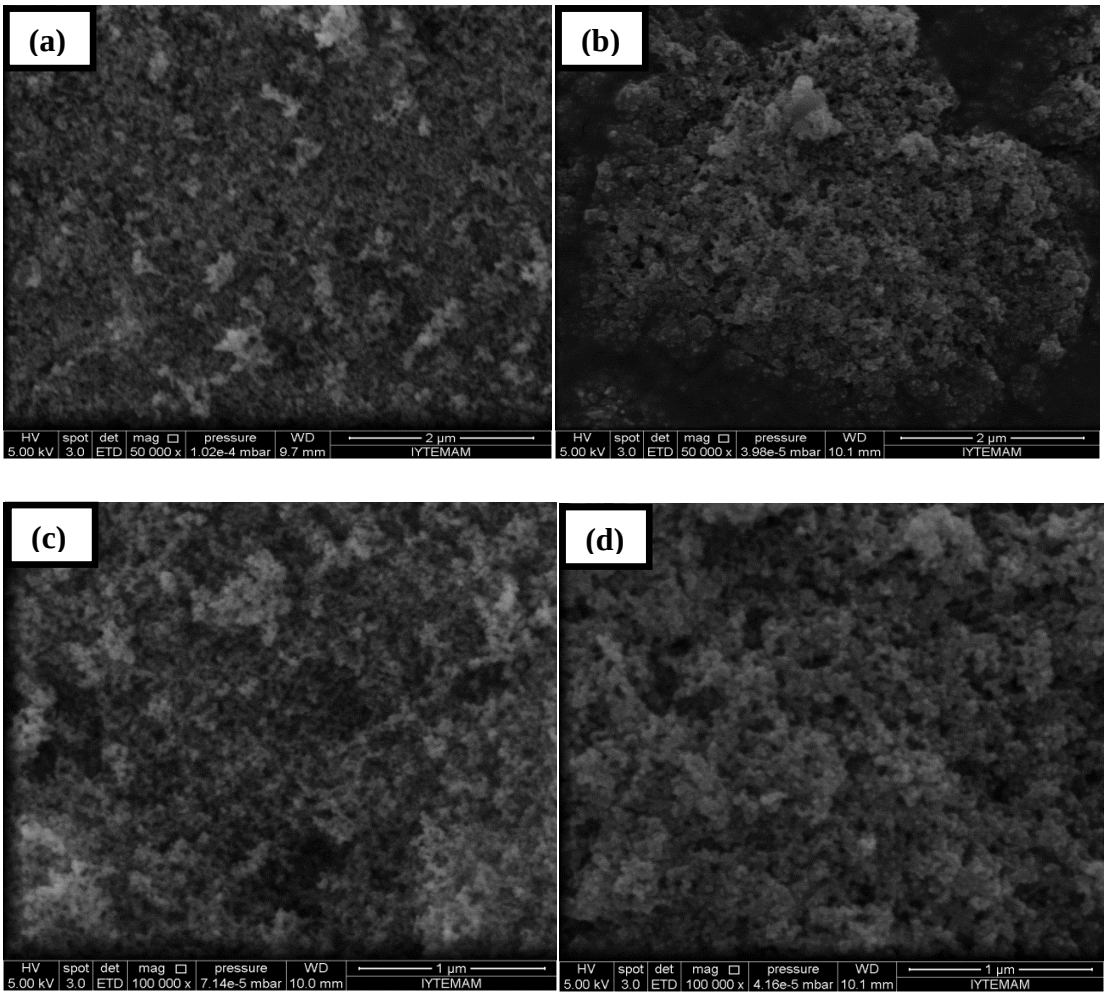

Figure 4.3. SEM images of fumed silica nanoparticles (a) and (b) at 50000x, (c) and (d) at 100000x magnifications

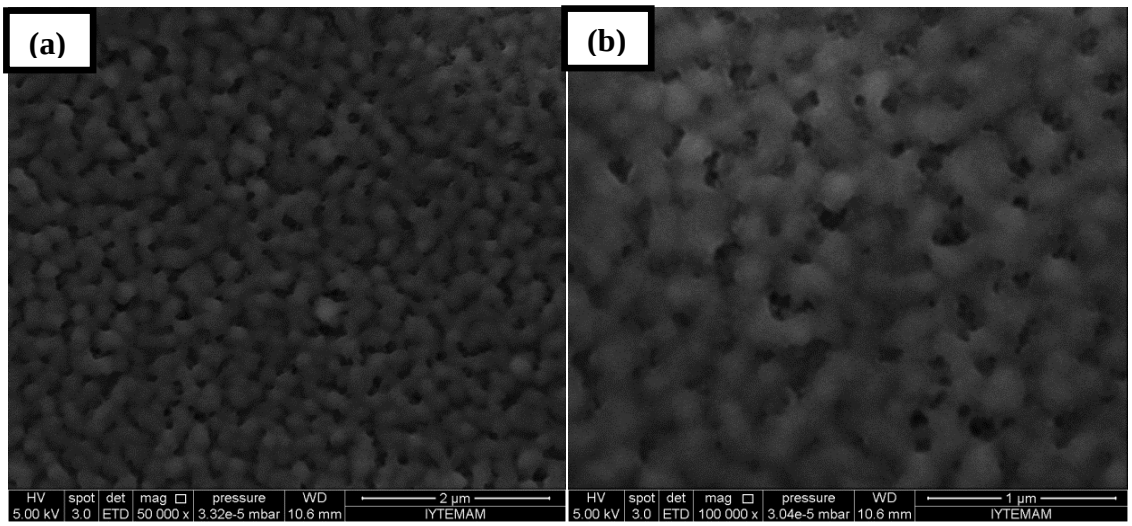

Figure 4.4. SEM images of STF30-PEG 200 (a) at 50000x, (b) at 100000x magnifications

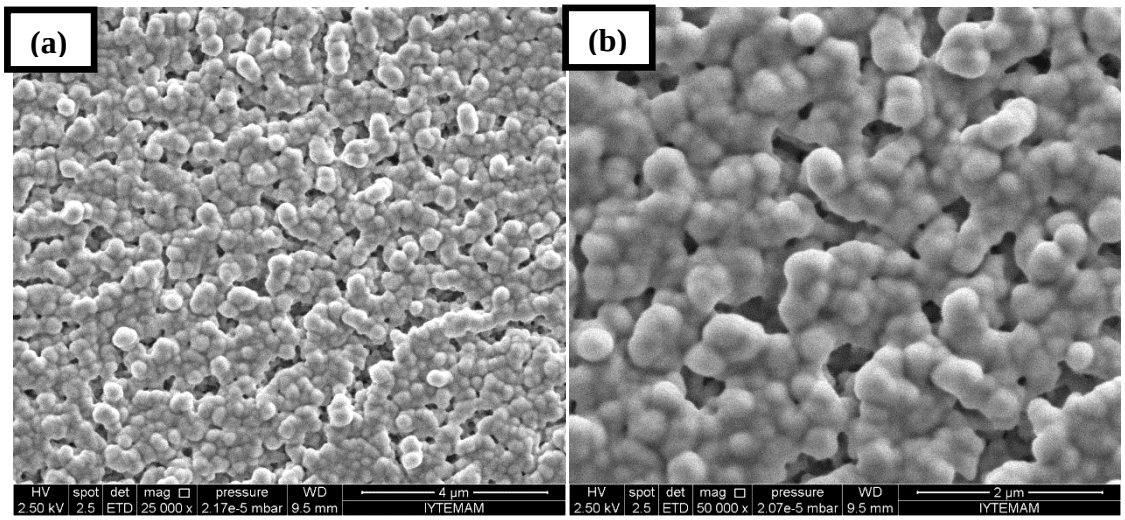

Figure 4.5. SEM images of STF30-PEG 300 (a) at 25000x, (b) at 50000x magnifications

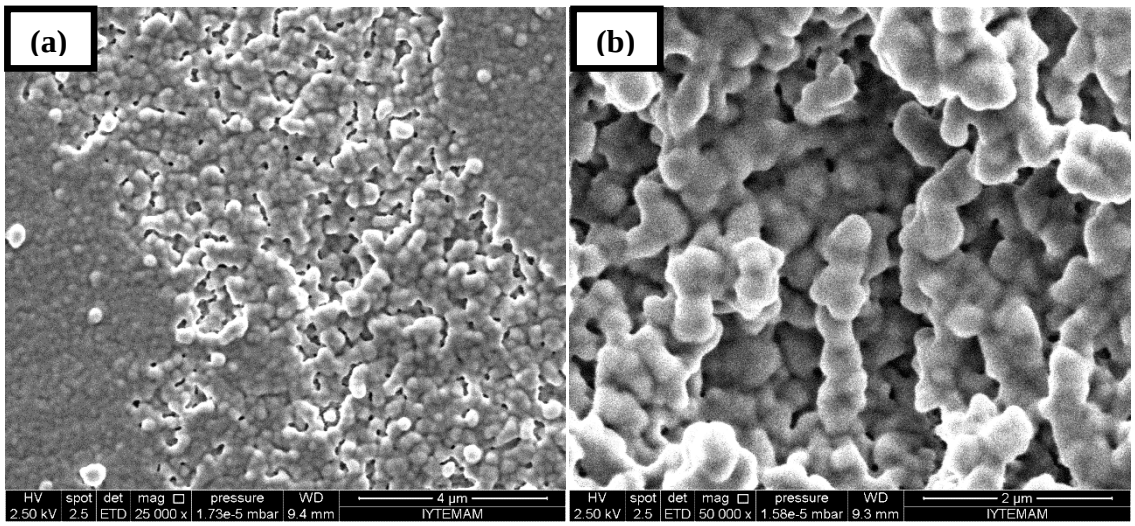

Figure 4.6. SEM images of STF30-PEG 400 (a) at 25000x, (b) at 50000x magnifications

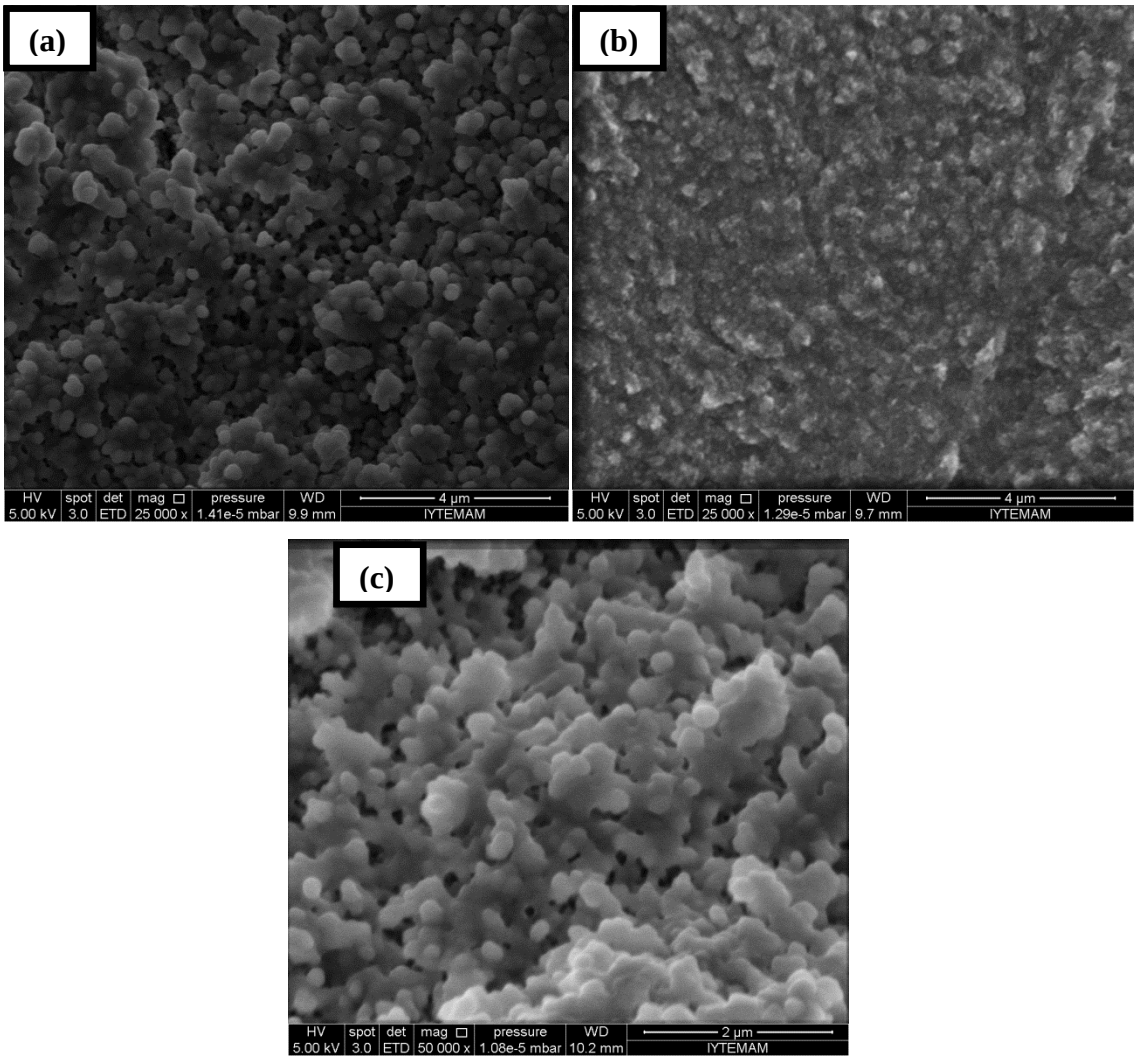

Figure 4.7. SEM images of STF30-PEG 600 (a) and (b) at 25000x, (c) at 50000x magnifications

4.1.4. Thermal Characterization by TGA

The weight losses of the STFs produced by using PEG 300, with increasing temperature (30-800 ^{0}C) was evaluated by TGA. The measurements were performed to determine the real silica amount in the STFs. Due to the Figure 4.8. the first weight loss occurs at about 160 ^{0}C which indicates the evaporation of PEG 300, and the following huge weight loss represents the total decomposition of the polymer. The remaining is residue silica. The ultimate weight percentages of the silica represents that there is no loss during synthesis except for STF20 and STF30- PEG 300 samples. There exists a difference approximately 2 wt% in silica amount for both of them. This can be

attributed to the loss of particles during production or experimental error of TGA. This slight difference lies within the error margin of the tool.

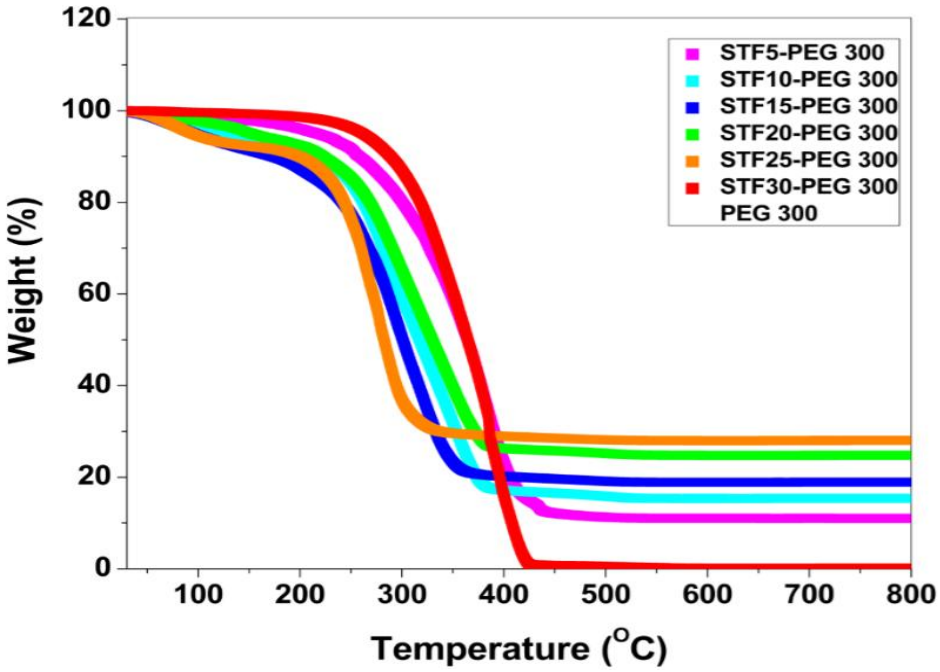

Figure 4.8. TGA curves of neat PEG 300 and STFs prepared with PEG 300 revealing weight change of the samples as a function of temperature

4.2. Rheological Characterization

4.2.1. Steady-Shear Rheology

The rheological properties of STFs which were synthesized with different fumed silica concentrations and PEGs having various molecular weights, were investigated. Fumed silica concentration was ranged in between 5-30% w/w, whereas the used PEGs have the molecular weights of 200, 300, 400 and 600 g/mole. The prepared STFs were abbreviated as it was stated in chapter 3. Measurements were performed with the help of TA AR2000ex stress-controlled rotational rheometer. The geometry which was used in the experiments is cone and plate fixture with plate diameter of 25 mm and spindle angle of 0.1 rad. Before each measurement, a pre-shear of 1 s^{-1} was applied during 1 minute to remove the sample loading effects.

Results of the steady-state measurements help to observe the effect of fumed silica concentration, likewise molecular weight of polymeric medium. Viscosities of PEGs reveal an increasing trend with molecular weight. Viscosity variations of all STF series those have filler concentration of 5-30% w/w are categorized and graphed according to the PEGs used in STFs. The curves of pure PEGs does not show a change in their viscosities with the applied shear rate. This situation confirms their Newtonian flow nature. On the contrary, viscosity curves of STFs show the characteristic shear thickening behavior due to the addition of fumed silica nanoparticles as filler. At low rates of shear, STFs exhibit a shear thinning which is followed by a transition to shear thickening through reaching the critical shear rate value. The onset of the shear thickening zone is characterized by the critical shear rate.

Figure 4.9 illustrates the viscosity behavior of STFs prepared with PEG 200 within the concentration range of 5 to 30 wt% and neat PEG 200. Based on the data, it was demonstrated that the PEG 200 is a Newtonian fluid with no effective change in viscosity with applied shear rate. For STF5-PEG 200 sample also does not exhibit a thickening until 1000 s^{-1} shear rate which is the measurement limit of this study, but a slight decrease is observed within the first part of the shear rate range indicating the shear thinning region of the fluid. However, the addition of silica from 5 to 30 wt% makes the system gradually more realistic in the sense of shear thickening phenomenon. Remarkable thickening effects first begin to be observable with STF10-PEG 200 sample. It can be obviously seen from the curves, when fumed silica particle loading increases, viscosity increases steeply. Fumed silica is a fine grained material that has high surface area which is produced by flame hydrolysis process. Pristine fumed silica consists of branched shaped aggregates as it was seen in SEM images before (Figure 4.3 a to d). The open structure of these aggregates allows them to absorb considerable amounts of liquid and lead to the formation of hydroclusters resulting in rapid increments in viscosity of the STFs which was prepared by fumed silica. As silica concentration increased, the interparticle forces increased, so the friction between particles increased, causing an enhanced shear thickening feature. The maximum available viscosity and low critical shear rate data were acquired at the highest silica concentration of STF30-PEG 200, expectedly. Besides, the addition of silica particles shifts the onset of shear thickening regime to the left hand side, thereby the critical shear rate is observed earlier. The determination of critical shear rate which indicates

the onset of the thickening effect is an important parameter for liquid armor applications in order to predict operating range. Furthermore, the maximum available viscosity was obtained for STF30-PEG 200 as 1622 Pa.s at the critical shear rate value of 14.4 s^{-1}.The abrupt increase in viscosity of this STF within the shear thickening region is nearly on two order of magnitude from 13.8 to 1622 Pa.s. Critical shear rates, viscoities at critical shear rates and maximum viscosities of all STFs synthesized by PEG 200 is listed in Table 4.1. The sharp viscosity increase is followed by a second shear-thinning region which proves the reversible thickening behavior of the STFs. As stated in chapter 2, there are two important mechanism that explains the shear thickening behavior which are ODT and hydrocluster theory. In ODT theory, it was assumed that an ordered arrangement of particles occurs at low shear rates. This is a result of repulsive forces which exist between particles causing reduction in viscosity at low shear rates. At high shear rates, the hydrodynamic forces govern the flow behavior by breaking the layered arrangement and increase the viscosity. It is possible the formation of ordered layers in monodisperse particles having regular shapes. However, in this case, the primary flow units are polydisperse fumed silica aggregates which have irregular shapes and anisotropic structure. So, it seems that STFs in this study, obey the hydrocluster theory (Raghavan et. al. 1997, Qui-mei et. al. 2006).

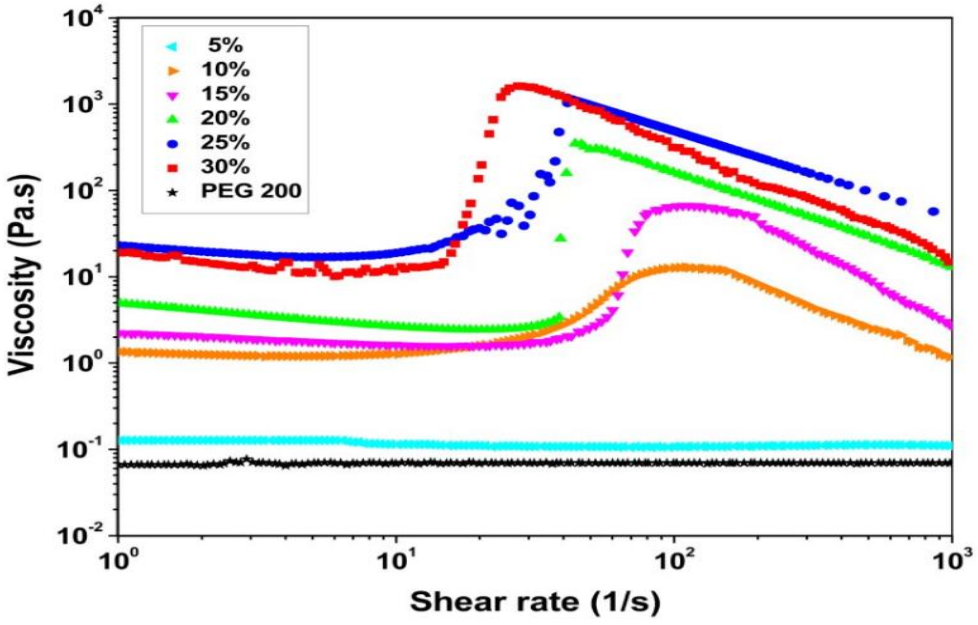

Figure 4.9. Steady shear viscosity curves of STFs containing PEG 200 at varying concentrations (STF5 to STF30-PEG 200)

Table 4.1. Steady rheological specifications of STFs prepared with PEG 200

Sample ID	Critical shear rate (s^{-1})	Viscosity at critical shear rate (Pa.s)	Max. Viscosity (Pa.s)
STF5-PEG 200	271.3	0.11	0.1107
STF10-PEG 200	38.3	2.65	12.9
STF15-PEG 200	37.8	1.90	66.81
STF20-PEG 200	33.65	2.8	350.3
STF25-PEG 200	15.20	25.4	1185
STF30-PEG 200	14.4	13.8	1622

Steady rheological behavior of STFs produced by PEG 300 is seen in Figure 4.10. All of the dispersions exhibit shear thickening effect at high shear rates. At lower shear rates, the medium fluid dominates the behavior, because it has the opportunity of filling voids between silica nanoparticles. When shear rates increases, fluid can no longer keep up with silica particles by filling the voids and particles rub each other resulting in a friction force between them. Increasing the silica concentration causes not only an abrupt increase in viscosity, but also a reduction in crtitical shear rate values. However, as compared to the rheological behavior of STFs-PEG 300 with each of the equivalent concentration of STFs-PEG 200, the onset of shear thickening was observed earlier. Also, the increase in viscosity within the thickening range is less steeper than STF series of PEG 200 in accordance with the literature (Raghavan et al., 2000). The highest viscosity rise up is observed again as two order of magnitudes for the STF having the highest silica weight fraction which is STF30-PEG 300. The critical shear rate and maximum viscosity of STF30-PEG 300 sample is determined as 11.1 s^{-1} and 1241 Pa.s, respectively. The specific rheological properties of other concentrations is also listed in Table 4.2. In contrast to the STF5-PEG 200, STF5-PEG 300 shows thickening effect within the shear rate range of the graph in Figure 4.10. This may be caused by the shifting of critical shear rate to lower values with the addition of polymer which has higher molecular weight (Raghavan et. al., 2000).

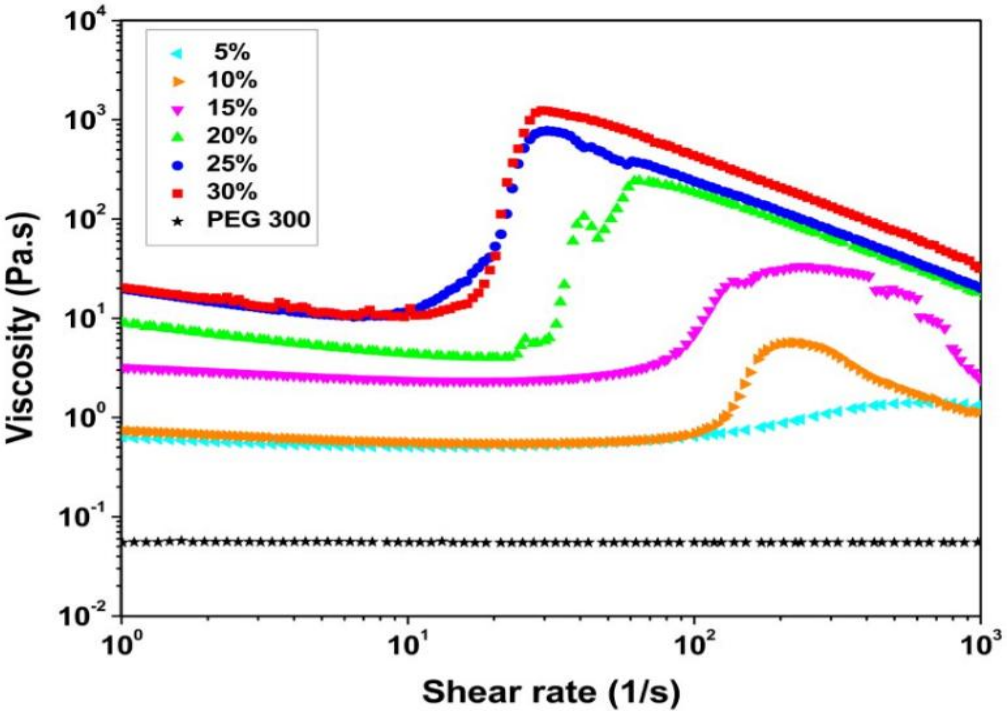

Figure 4.10. Steady shear viscosity curves of STFs containing PEG 300 at varying concentrations (STF5 to STF30-PEG 300)

Table 4.2. Steady rheological specifications of STFs prepared with PEG 300

Sample ID	Critical shear rate (s–1)	Viscosity at critical shear rate (Pa.s)	Max. Viscosity (Pa.s)
STF5-PEG 300	151.2	0.75	2.1
STF10-PEG 300	105.3	0.72	5.7
STF15-PEG 300	68	3.2	33.4
STF20-PEG 300	28.25	5.66	243.6
STF25-PEG 300	15.3	22.7	774
STF30-PEG 300	11.1	10.75	1241

As it can be represented in Figure 4.11 and 4.12 all of the STFs prepared with PEG 400 and PEG 600 show also shear thickening behavior same as previous STFs.

The onset of critical shear rates decreases regularly with increasing silica weight fraction in each of the PEG series. The critical shear rates for STF30-PEG 400 and PEG 600 was recorded as 30.4 and 57.4, respectively. The viscosity of the STF30-PEG 400 increased from 37.25 to 588.3 Pa.s within the thickening region. Similarly, viscosity increased from 4 to about 350 Pa.s for STF30-PEG 600. According to the literature, the onset of shear thickening decreases with increasing molecular weight of the continuous phase and the viscosity rise up is smaller (Raghavan et al., 2000). In this study, the viscosity increments at the shear thickening region for the STFs prepared with higher molecular weighted polymers is less steeper as consistent with the literature. However, unexpectedly, the critical shear rate values of STFs-PEG 400 and PEG 600 are not low adequately. The detailed rheological data of PEG 400 and 600 including STFs at moderate concentrations are given in Table 4.3 and 4.4. Among all of the dispersions the most effective rheological properties were obtained for 30 wt% silica concentration. Also, within the STF30s, the most sharp viscosity increase is observed for PEG 200 whereas the lowest critical shear rate is obtained for STF30-PEG 300.

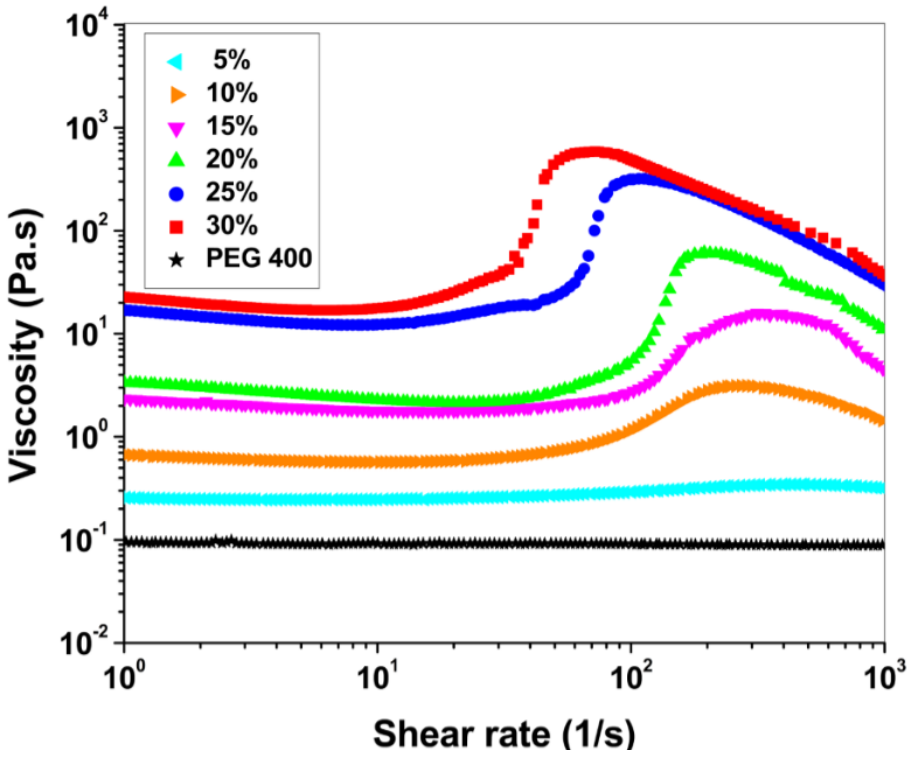

Figure 4.11. Steady shear viscosity curves of STFs containing PEG 400 at varying concentrations (STF5 to STF30-PEG 400)

Table 4.3. Steady rheological specifications of STFs prepared with PEG 400

Sample ID	Critical shear rate (s–1)	Viscosity at critical shear rate (Pa.s)	Max. Viscosity (Pa.s)
STF5-PEG 400	219.4	0.33	0.69
STF10-PEG 400	96.3	1.1	3.2
STF15-PEG 400	86.25	2.45	15.94
STF20-PEG 400	80.8	4.04	61.6
STF25-PEG 400	52	24.2	320.6
STF30-PEG 400	30.4	37.25	588.3

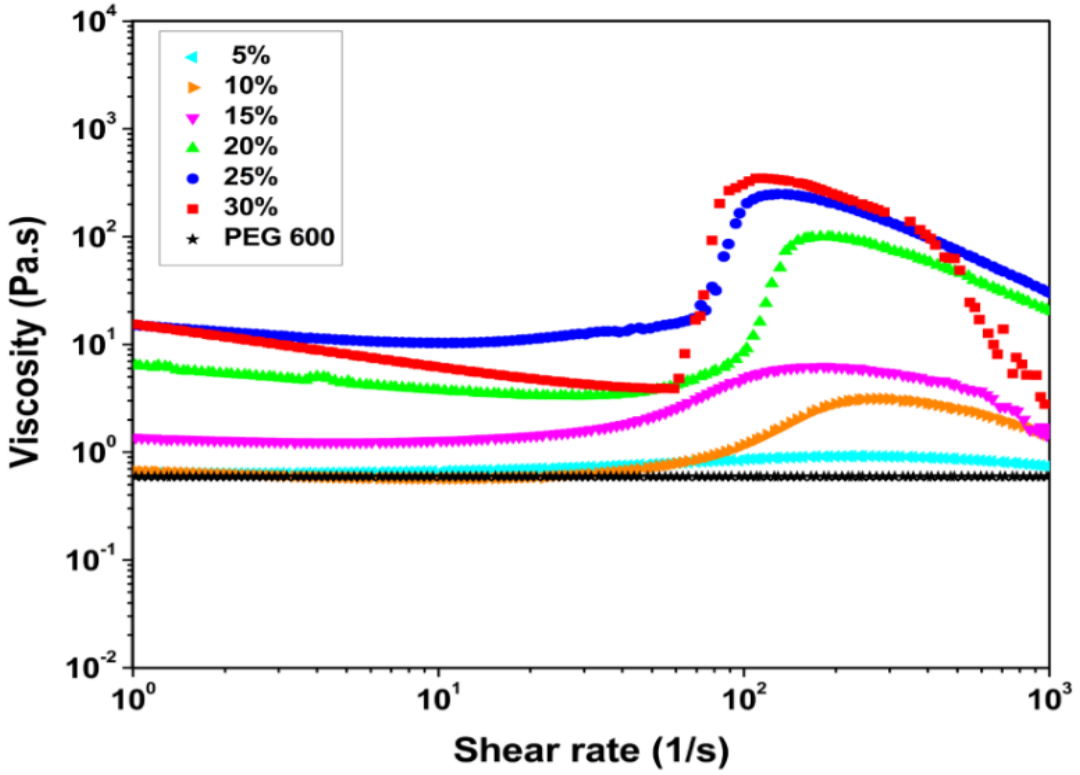

Figure 4.12. Steady shear viscosity curves of STFs containing PEG 600 at varying concentrations (STF5 to STF30-PEG 600)

Table 4.4. Steady rheological specifications of STFs prepared with PEG 600

Sample ID	Critical shear rate (s–1)	Viscosity at critical shear rate (Pa.s)	Max. Viscosity (Pa.s)
STF5-PEG 600	79.6	0.83	0.92
STF10-PEG 600	72.9	0.88	3.13
STF15-PEG 600	45.6	1.98	6.24
STF20-PEG 600	72	5.1	100
STF25-PEG 600	63.7	16.2	248.6
STF30-PEG 600	57.4	4	350

4.2.2. Dynamic Shear Rheology

4.2.2.1. Frequency sweep

Dynamic shear measurements of the prepared STFs were conducted with frequency and strain sweep modes by oscillation. The viscoelastic properties of STF20,25 and 30 of PEG 200, 300, 400 and 600 were investigated by keeping strain amplitude constant at 100, 500 and 1000% under varying angular frequency. According to the Figure 4.13 to 4.15 the elastic (G') and viscous (G") moduli curves of STFs-PEG 200 depend strongly on the angular frequency. Also, G" values are greater than the G' as much as one order of magnitude. This situation obviously indicates the STF dispersions of PEG 200 is nonflocculated. Flocculation is prevented owing to the adsorption of PEG chains on the fumed silica aggregates via hydrogen bonding between hydroxyl end groups of the PEG and hydoxyls on the silica surface. The microstructure of the nonflocculated STFs are composed of discrete units. The difference between G" and G' gets considerably greater when strain is increased from 100 to 1000% strain. However, both G" and G' curves intercept with their correlate at high frequencies, and G" ultimately fall below G'. This behavior shows that materials are strongly viscous until very high frequencies. However, after the interception point, which is termed as

the critical deformation point, precise physical interpretation of G' and G" becomes unclear(Raghavan et al., 1997; Boersma et al., 1991). On the other hand, the frequency sweep graphs reflects the shear thickening behavior of the STFs with a thickening at critical frequency. As strain amplitude increases the thickening effect begins earlier. Also, increase in silica concentration shifts the curves of G' and G" slightly to above and thickening is observed more strongly.

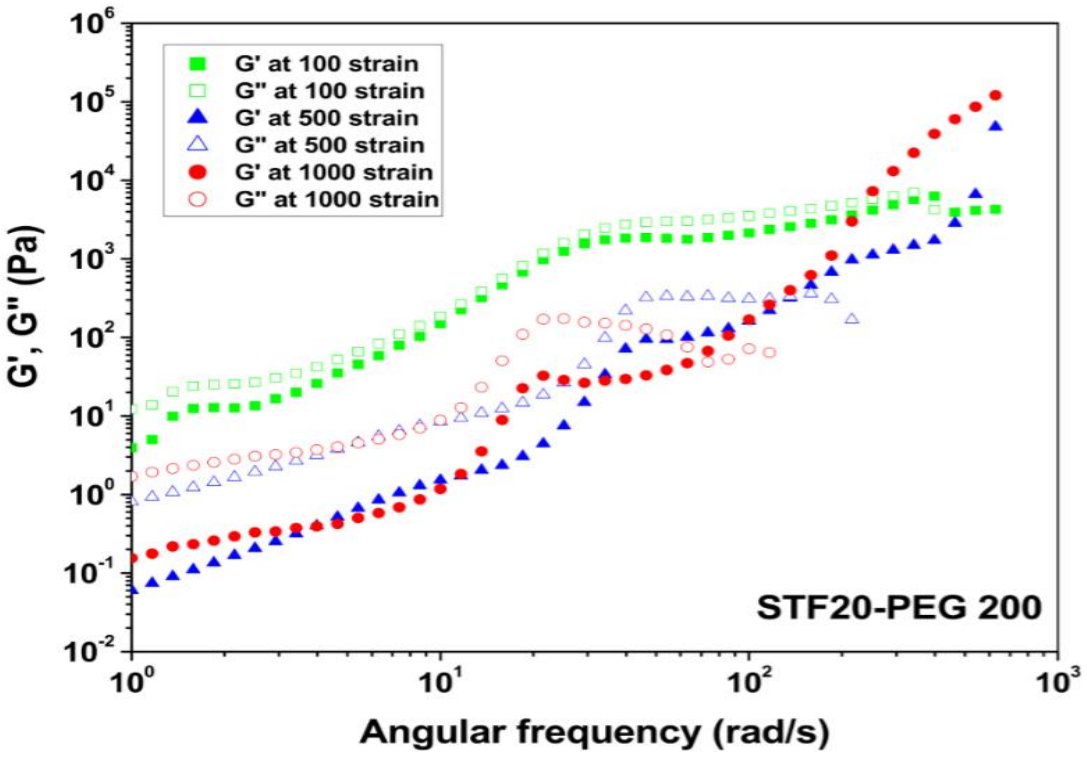

Figure 4.13. Elastic G' and viscous G" modulus curves of STF20-PEG 200 as a function of angular frequency

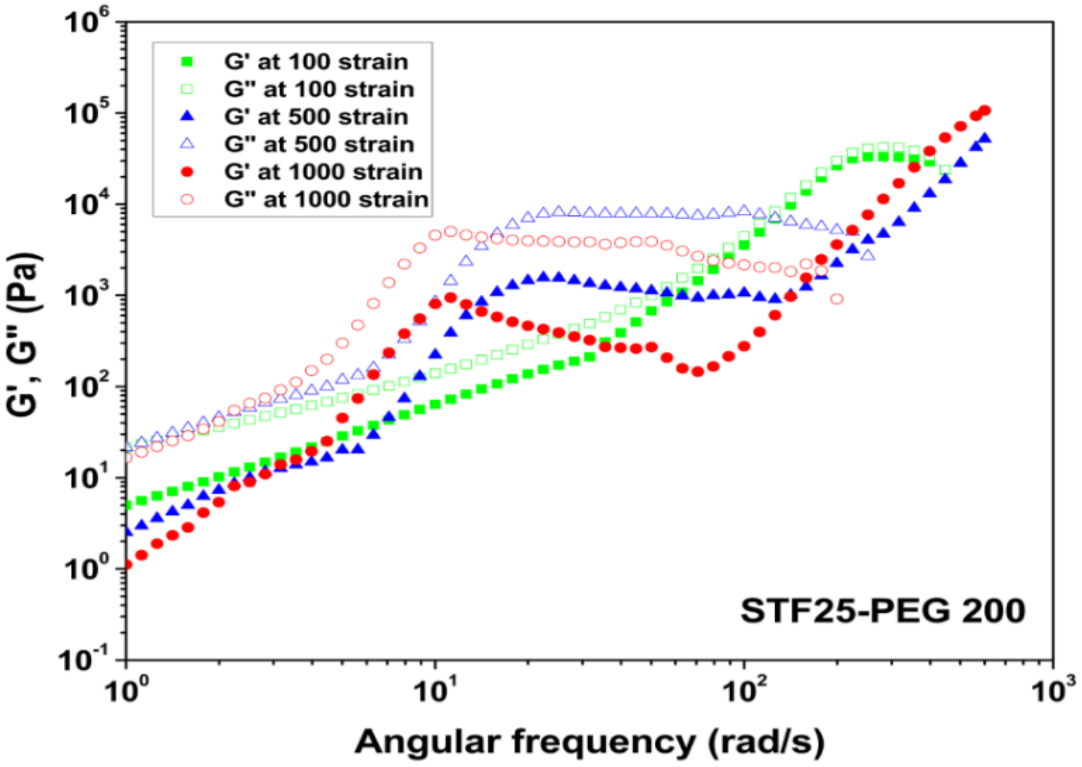

Figure 4.14. Elastic G' and viscous G" modulus curves of STF25-PEG 200 as a function of angular frequency

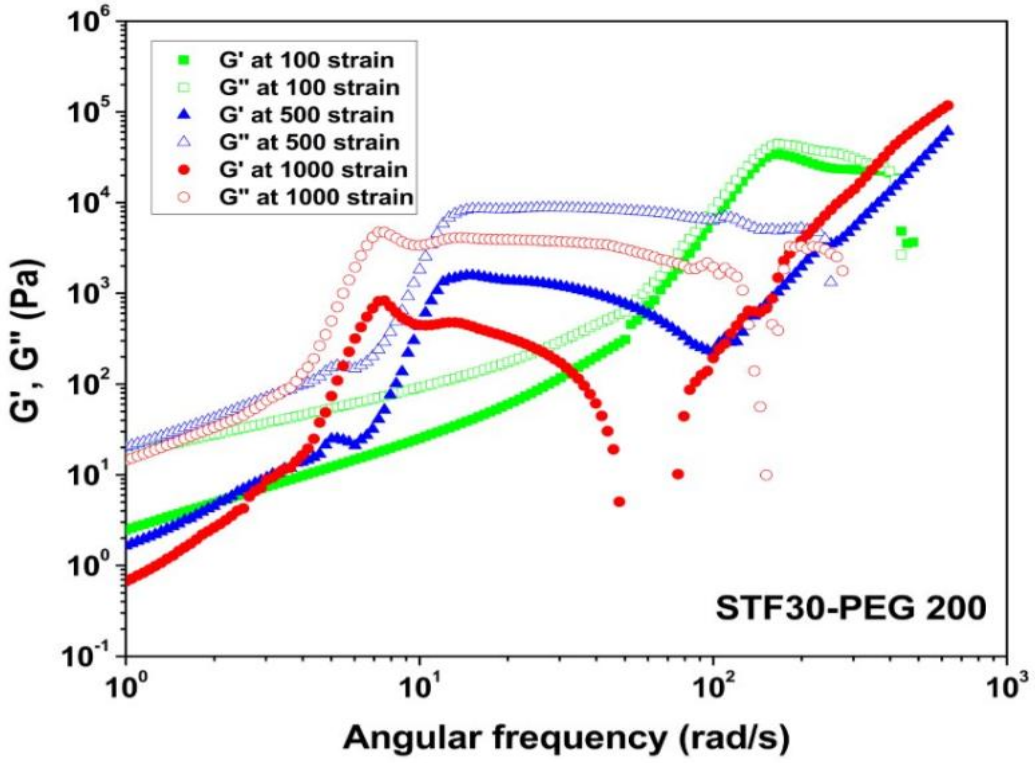

Figure 4.15. Elastic G' and viscous G" modulus curves of STF30-PEG 200 as a function of angular frequency

G’ and G” values of the STFs which was prepared with PEG 200 at all produced weight fractions (STF5-STF30) are seen in Figure 4.16. and 4.17. Moduli values were measured at varying angular frequency and constant deformation of 100% strain amplitude. For STFs having low silica loading, the difference between G’ and G” values is less than the more concentrated samples. This indicates that samples display both solid and liquid-like properties. As stated before, increase in concentration increases the moduli values with an abrupt rise at the critical frequency. The magnitude of the rise at this point gets steeper with concentration.

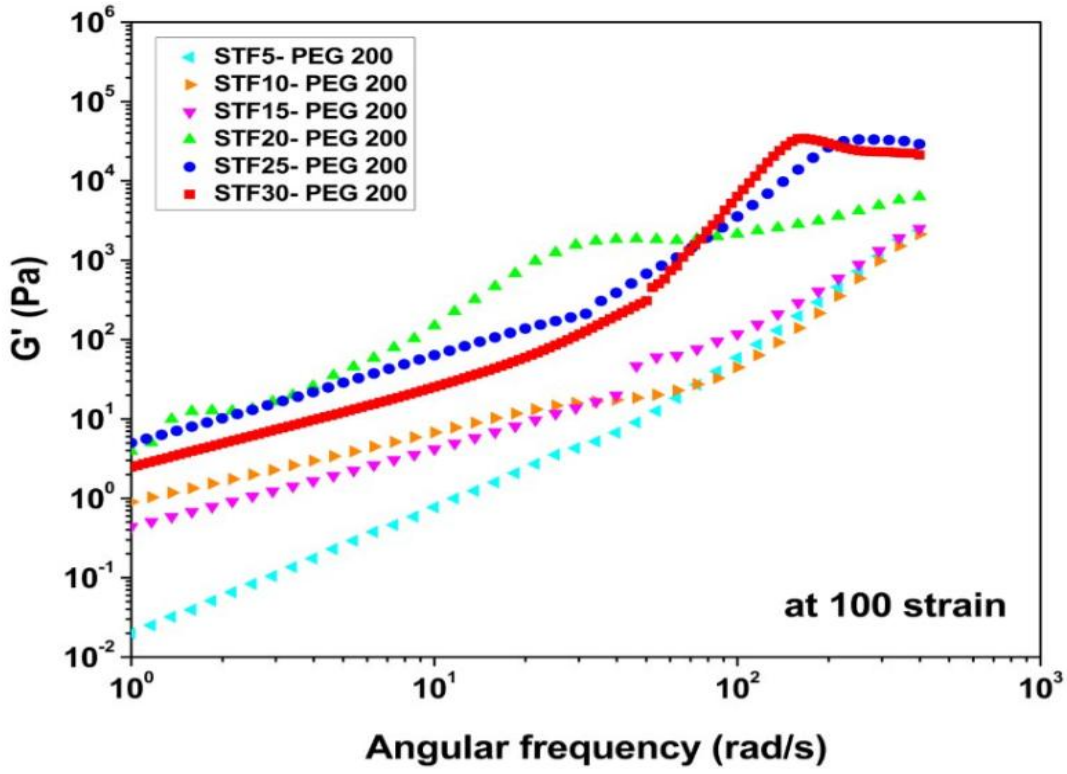

Figure 4.16. Elastic G’ modulus curves of STF5 to STF30-PEG 200 as a function of angular frequency at 100 strain amplitude

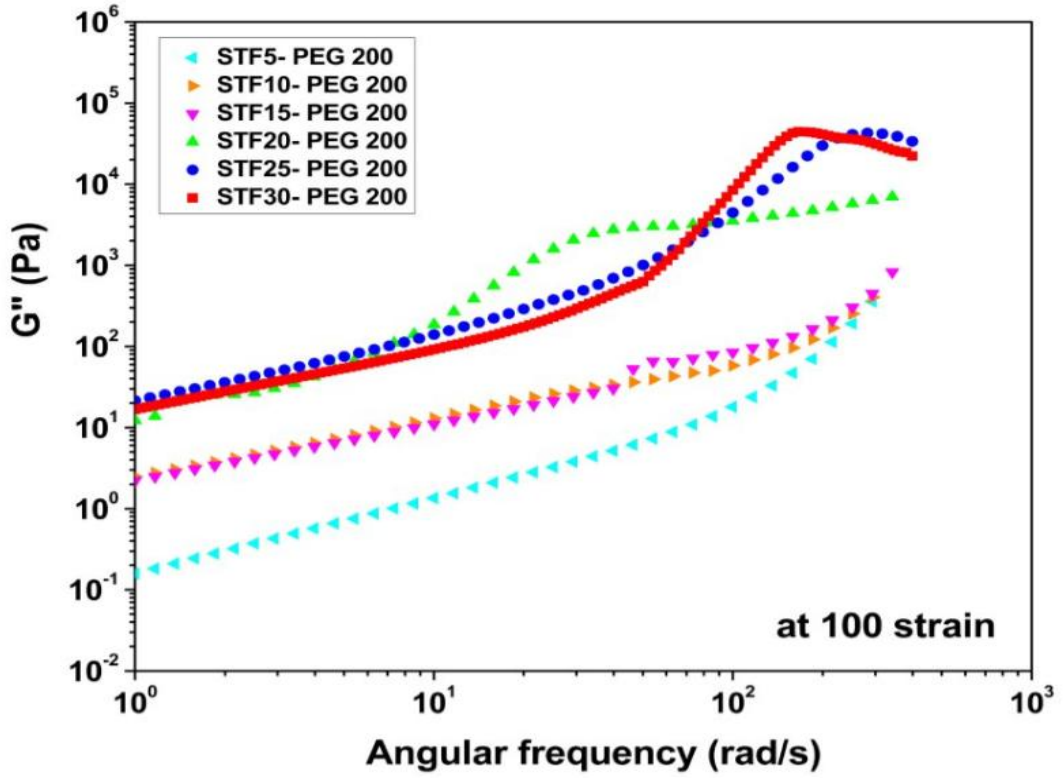

Figure 4.17. Elastic G" modulus curves of STF5 to STF30-PEG 200 as a function of angular frequency at 100 strain amplitude

Figure 4.18 to 4.20, Figure 4.23 to 4.25 and Figure 4.28 to 4.30 clearly indicates that the viscous modulus values are higher than the elastic modulus for STF20,25 and 30-PEG 300,400 and 600 until a critical deformation point. This indicates that the amount of the energy that will be dissipated by the viscous forces is greater than the stored energy in the material's structure. After the deformation point G' exceeds the G". This situation is observed only when the dispersion is subjected to high frequencies or deformations. According to the literature when this situation occurs, the shape of the reponse curve is no longer sinusoidal and creates confusion about the physical meaning of the both moduli. The dynamic rheological properties of the samples change with frequency which indicates the nonflocculated nature of them. Also the discrete nature of the particles means that the dispersions are well-stabilized (Boersma et al., 1991;Raghavan et. al., 1997; Qui-mei et. al., 2006). As silica concentration increases the critical frequency point are observed at lower values. The same effect was also created by increasing the % strain amplitude from 100 to 1000% with a stronger jump in the moduli values. Generally, all of the STFs prepared with PEGs those have different molecular weights behave similarly with increasing angular frequency at constant

deformation rates. However, the increase in molecular weight changes the magnitudes and values of these important dynamic parameters by shifting the moduli curves. The use of PEG 300 increases the power of the thickening effectas compared to PEG 200. However, for PEG 400 and 600, some fluctuations happen at different concentrations. For instance, the power of the thickening effect in STF20-PEG 400 is less than PEG 300. Likewise, the thickening effect of STF25-PEG 600 is greater than STF30-PEG 600. These may be caused by experimental errors.

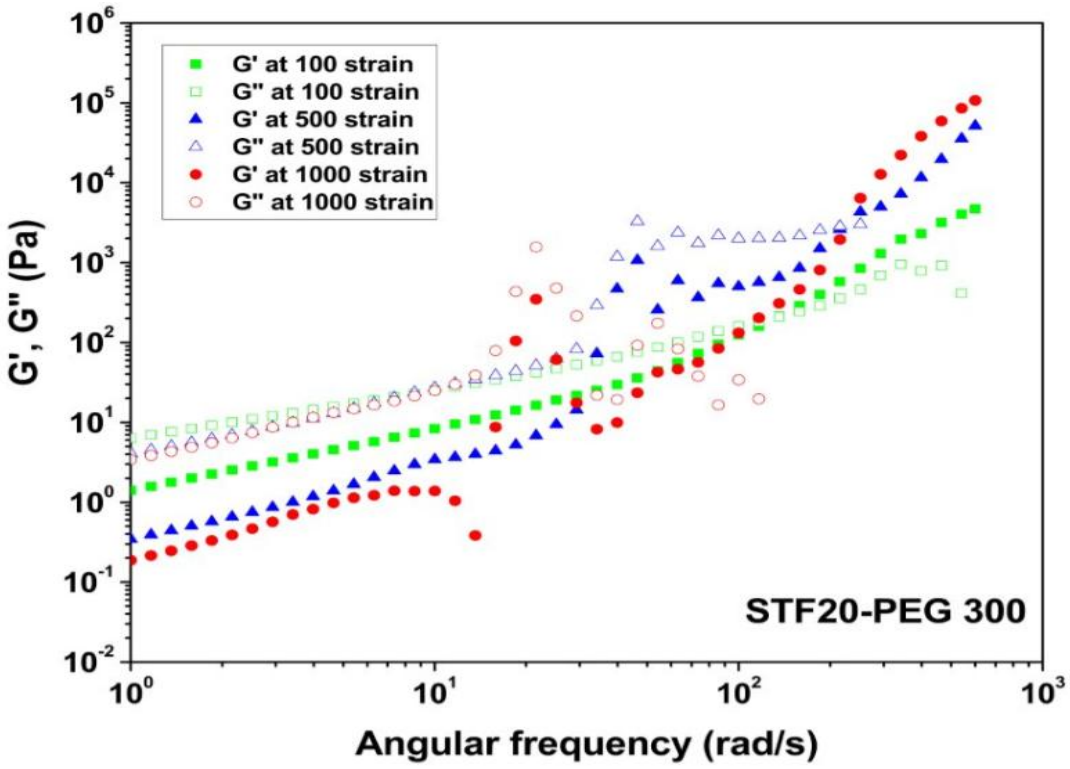

Figure 4.18. Elastic G' and viscous G" modulus curves of STF20-PEG 300 as a function of angular frequency

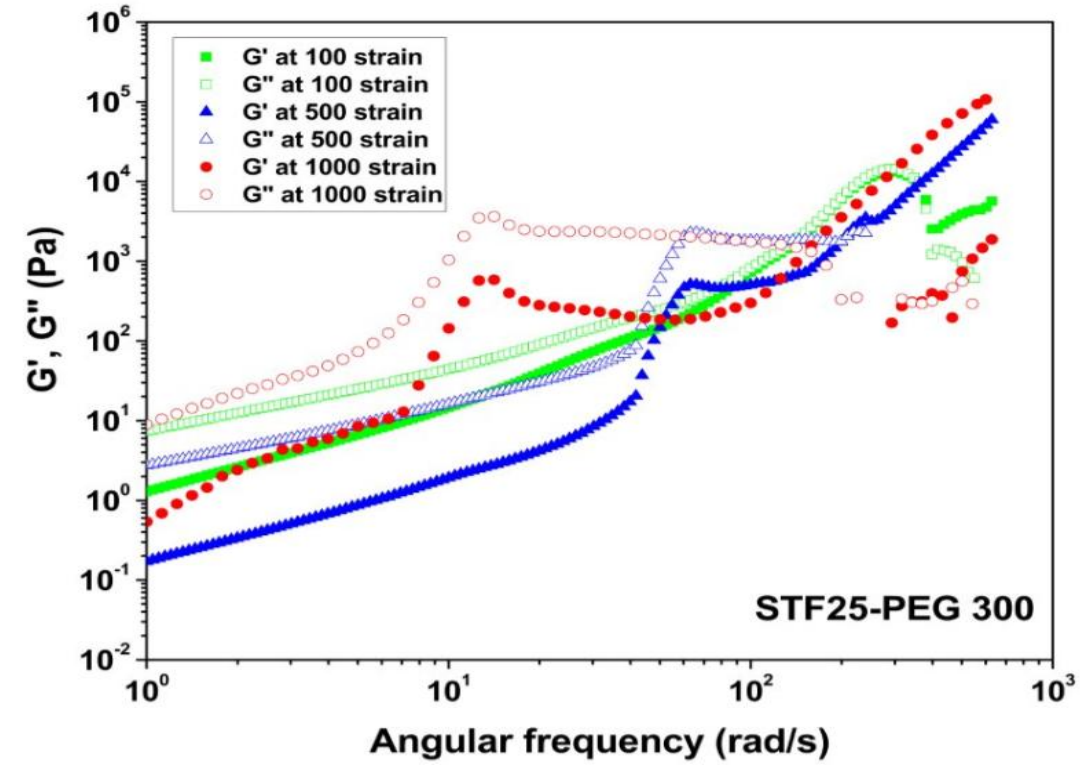

Figure 4.19. Elastic G' and viscous G" modulus curves of STF25-PEG 300 as a function of angular frequency

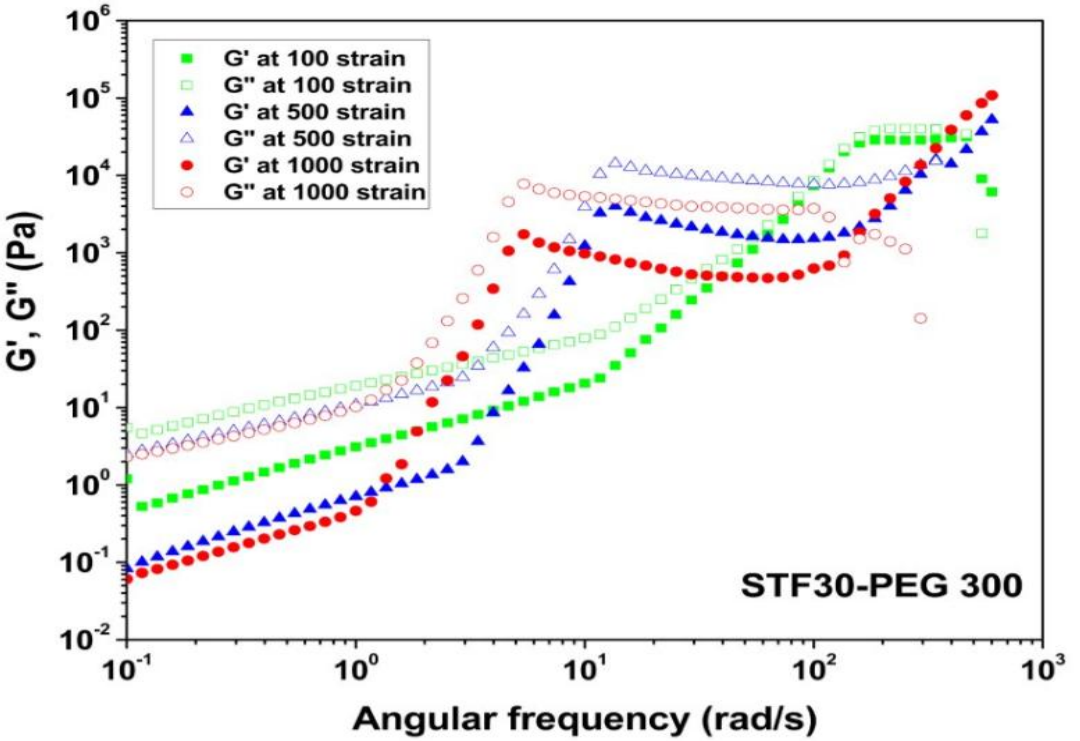

Figure 4.20. Elastic G' and viscous G" modulus curves of STF30-PEG 300 as a function of angular frequency

Effect of concentration on the viscoelastic properties of the STFs- PEG 300, 400 and 600 with increasing frequency is observed in Figure 21-22, 26-27 and 31-32. The strain amplitude was fixed constant at 100 strain. The same effect of concentration is observed in all of the STFs. As a general trend, critical angular frequency at which the flow blockage occurs is shifted to the lower frequencies. Some fluctuations can be observed as in STF10-PEG 300, and they are attributed to the experimental errors. G' and G" values is increased with the increase in silica amount in STFs with a general trend of G" > G'. Raghavan et. al. prepared a STF with 10 wt% fumed silica and PEG 300 in their study which is similar to in this study and measure the viscoelastic properties within the angular frequency range of 0.1-100 rad/s (Raghavan et. al., 2000). They found that G" > G' and describe the material as purely viscous, structureless sols. In the context of the colloidal dispersions, the behavior of the STFs can be divided into two groups as sols and gels. In our case, the same behavior was observed within the same frequency range. However, It is a controversy to describe all of the STFs in this study as sols or gels. Since, Raghavan et al. stated that stable silica sols show low viscosity under steady shear and viscous response under dynamic shear. In the same way, gels exhibit extremely high viscosity, but greater frequency-independent elastic behavior. It can be concluded that, for only low concentrated STFs, it is possible to define the structure as sol. Because viscous modulus is also greater than elastic modulus for highly concentrated dispersions in our study.

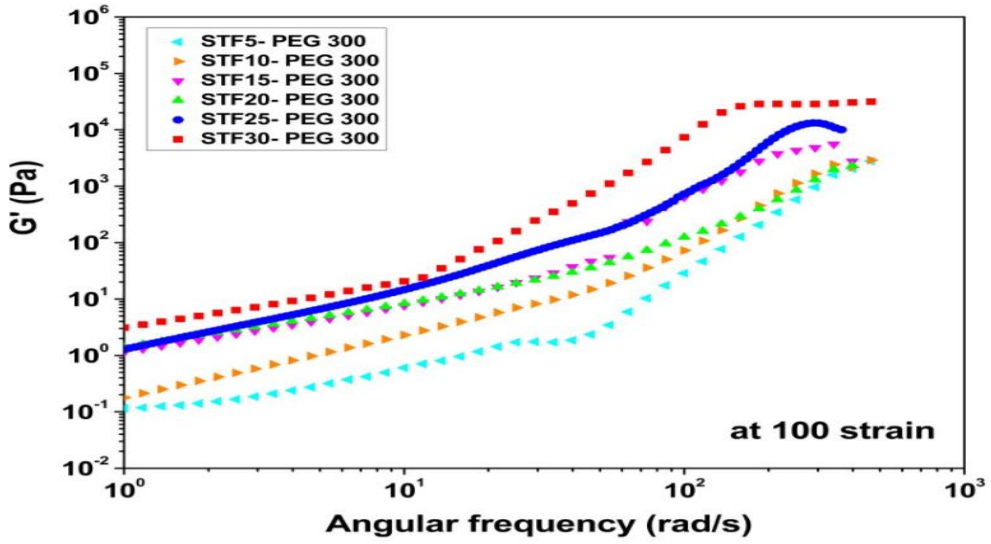

Figure 4.21. Elastic G' modulus curves of STF5 to STF30-PEG 300 as a function of angular frequency at 100 strain amplitude

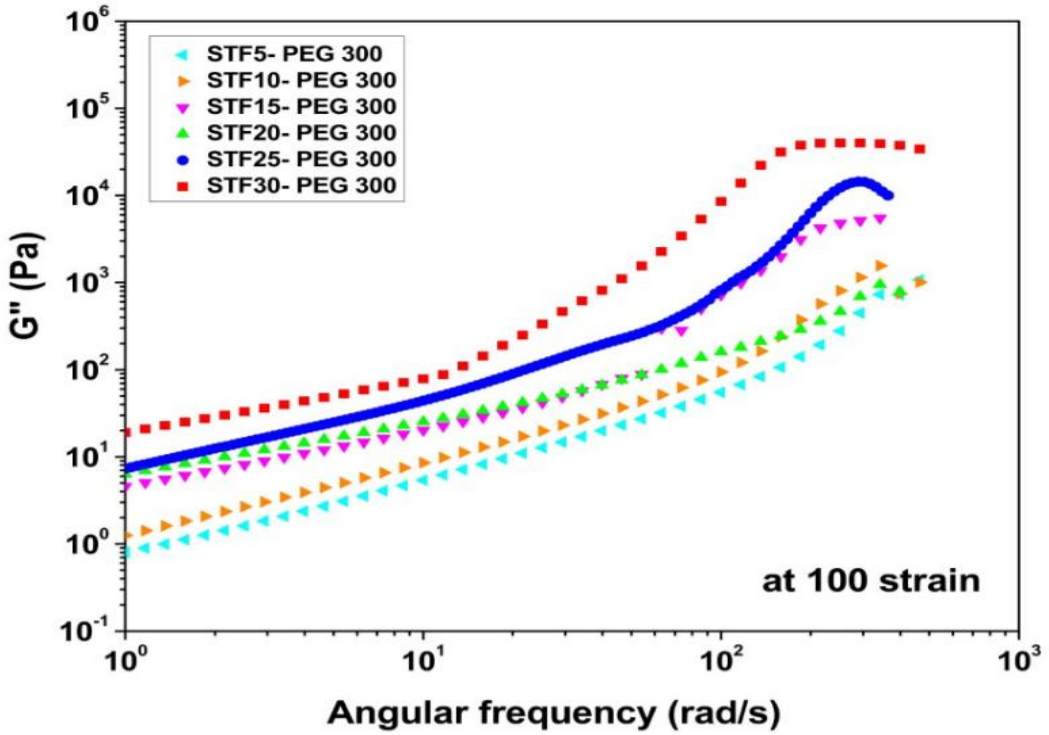

Figure 4.22. Elastic G" modulus curves of STF5 to STF30-PEG 300 as a function of angular frequency at 100 strain amplitude

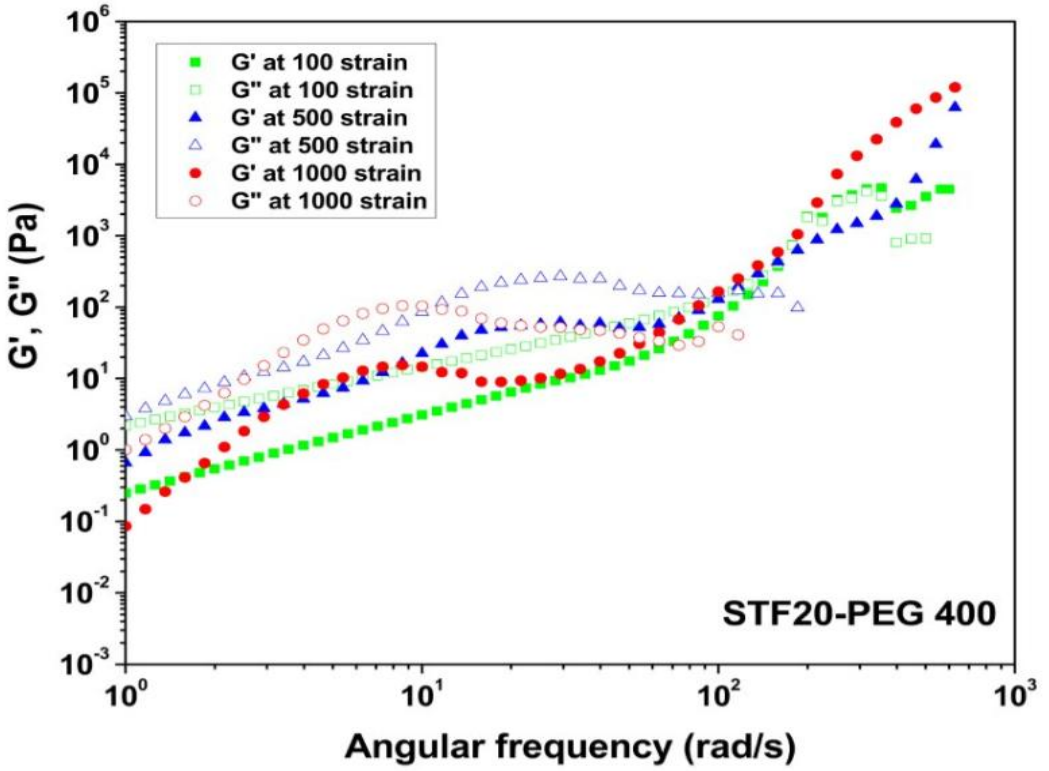

Figure 4.23. Elastic G' and viscous G" modulus curves of STF20-PEG 400 as a function of angular frequency

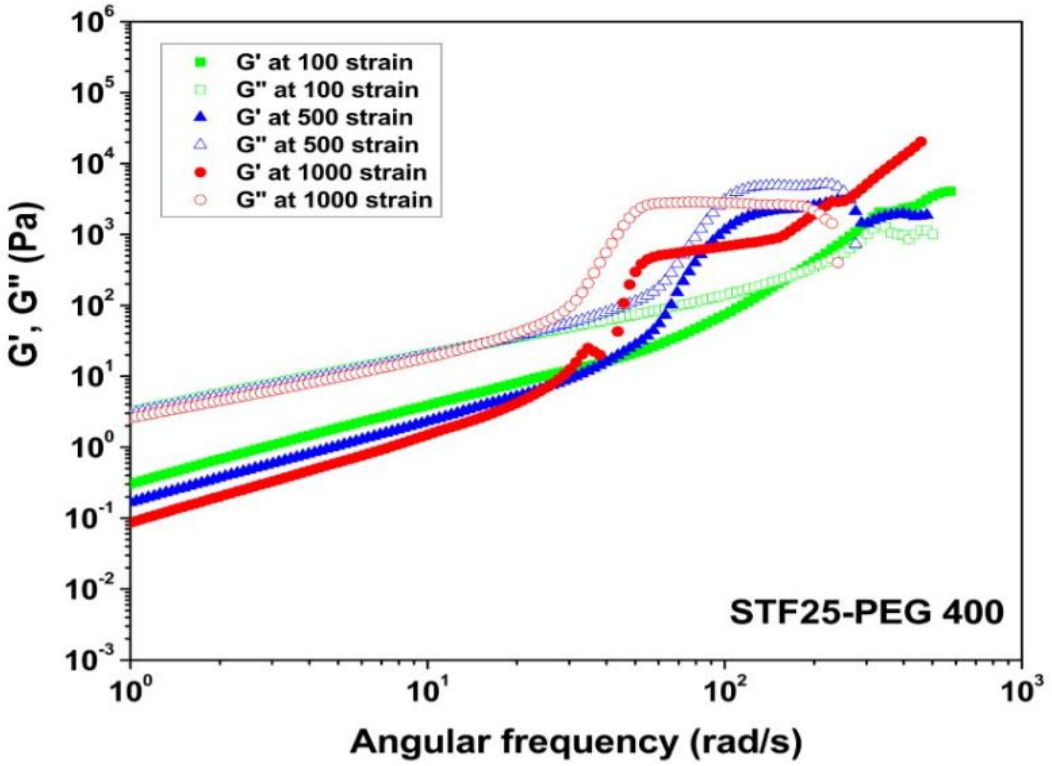

Figure 4.24. Elastic G' and viscous G" modulus curves of STF25-PEG 400 as a function of angular frequency

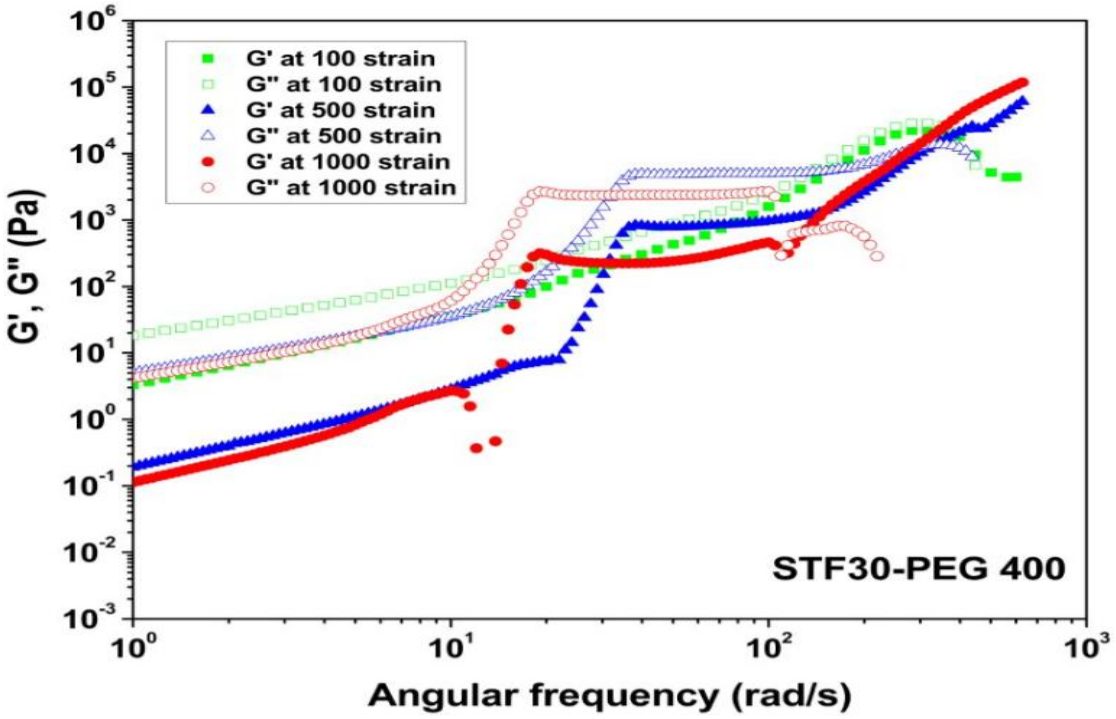

Figure 4.25. Elastic G' and viscous G" modulus curves of STF30-PEG 400 as a function of angular frequency

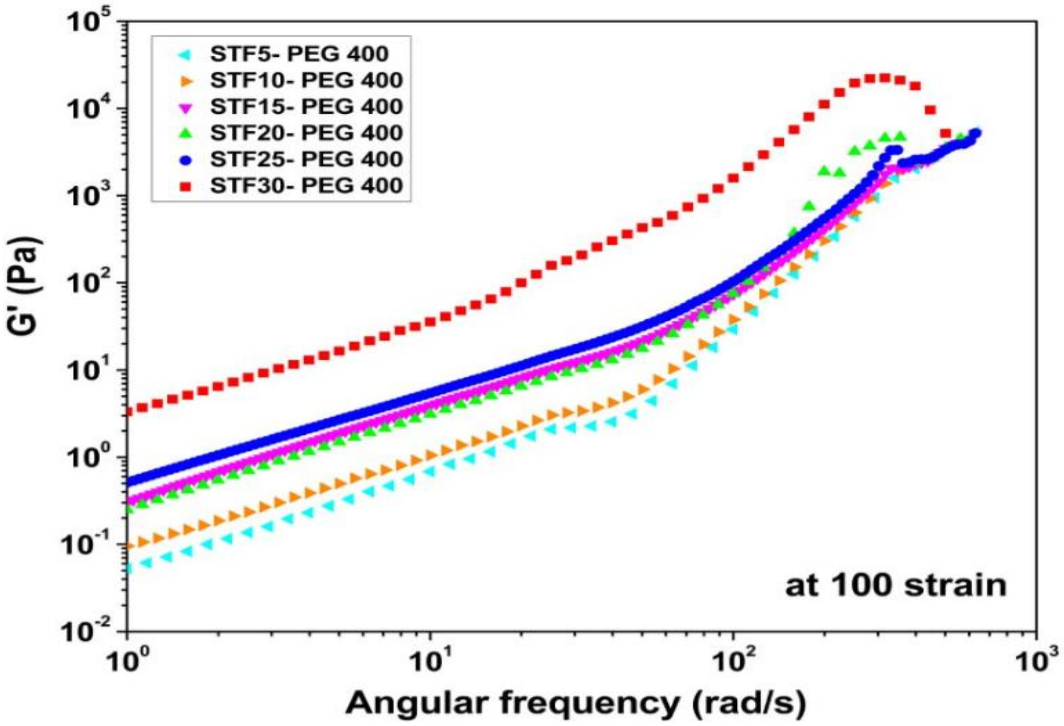

Figure 4.26. Elastic G' modulus curves of STF5 to STF30-PEG 400 as a function of angular frequency at 100 strain amplitude

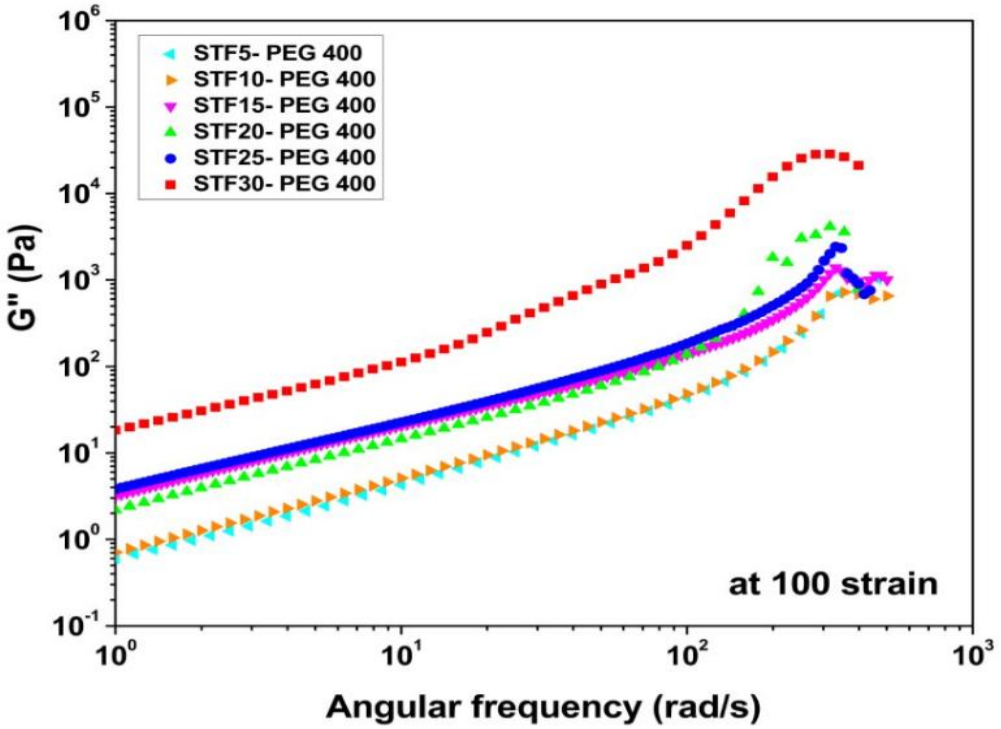

Figure 4.27. Elastic G" modulus curves of STF5 to STF30-PEG 400 as a function of angular frequency at 100 strain amplitude

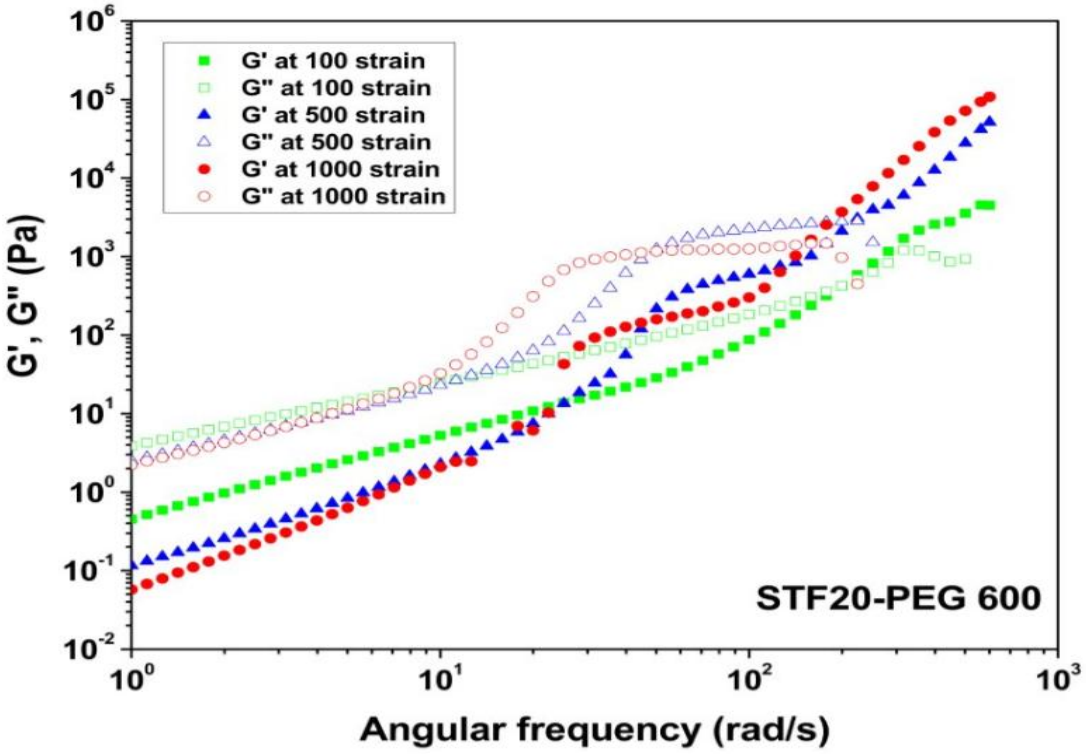

Figure 4.28. Elastic G' and viscous G" modulus curves of STF20-PEG 600 as a function of angular frequency

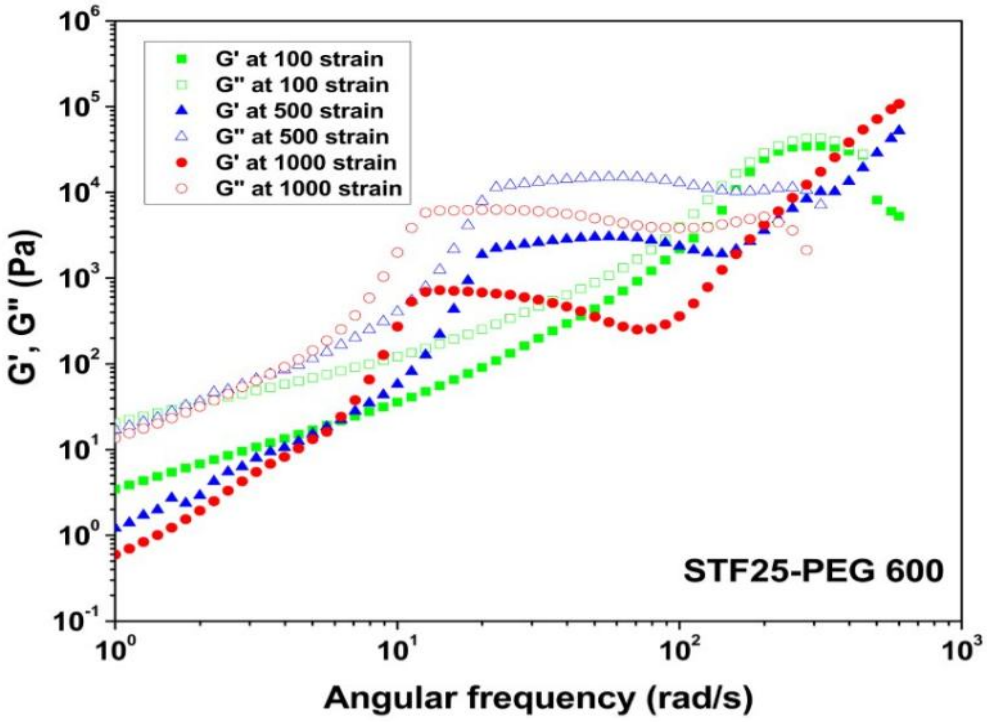

Figure 4.29. Elastic G' and viscous G" modulus curves of STF25-PEG 600 as a function of angular frequency

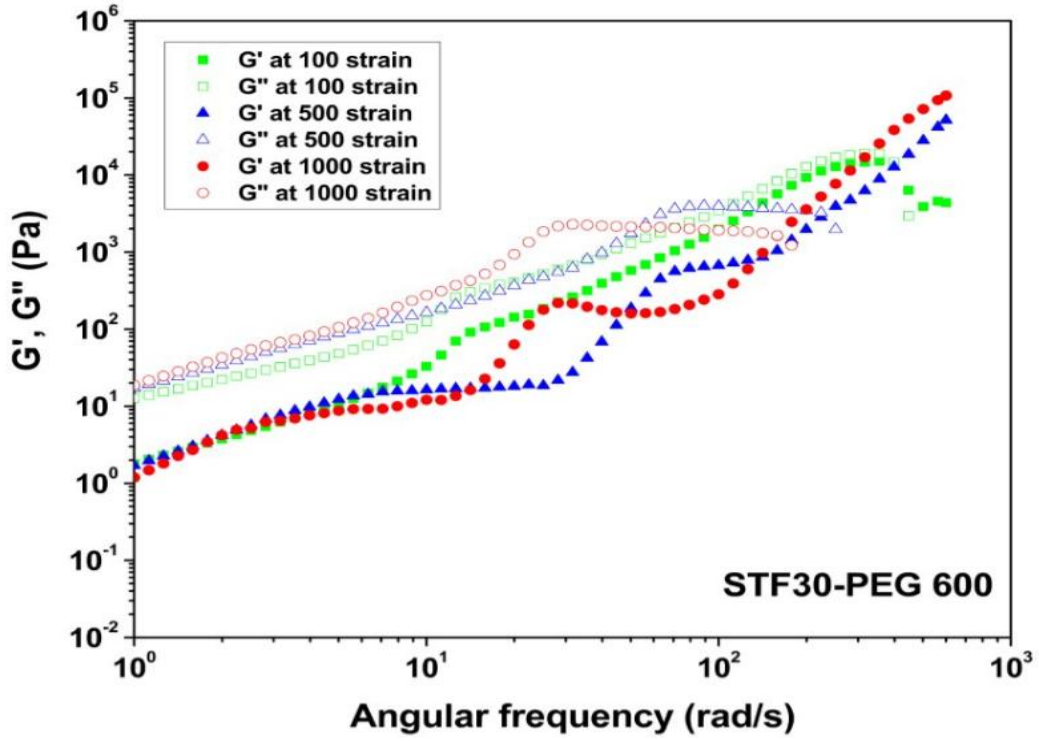

Figure 4.30. Elastic G' and viscous G" modulus curves of STF30-PEG 600 as a function of angular frequency

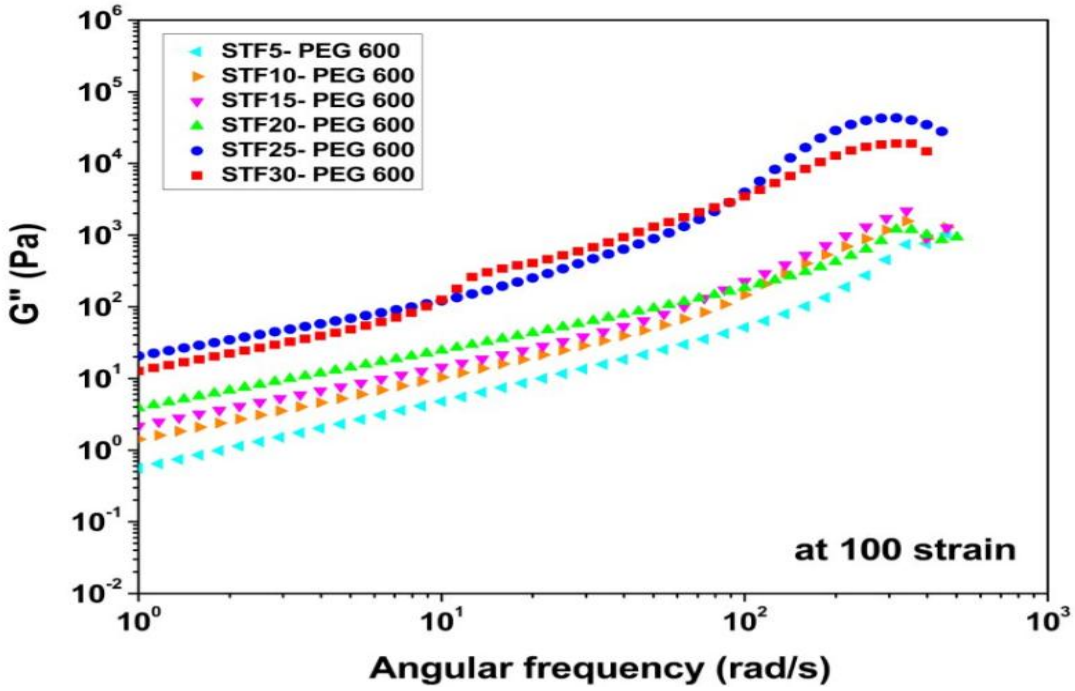

Figure 4.31. Elastic G' modulus curves of STF5 to STF30-PEG 600 as a function of angular frequency at 100 strain amplitude

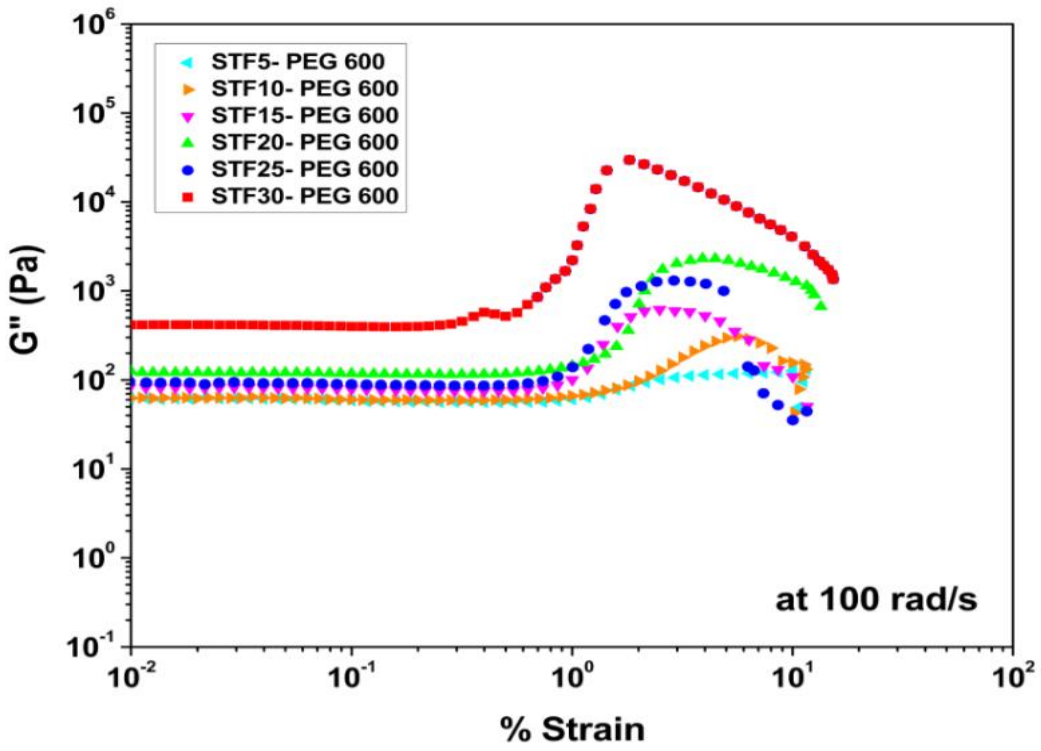

Figure 4.32. Elastic G" modulus curves of STF5 to STF30 – PEG 400 as a function of angular frequency at 100 strain amplitude

4.2.2.2. Strain sweep

The effect of deformation on the viscoelastic properties of STFs were investigated with strain sweep mode under constant angular frequencies of 10,50 and 100 rad/s with increasing strain amplitude. Figures 33 to 52 illustrates the changes in G' and G" moduli values of the STFs synthesized with PEG 200,300,400 and 600. The appearance of the curves in the graphs which was obtained from strain sweep mode is quite similar to steady rheological curves of the STFs. The nonflocculated suspensions exhibit strain-thickening at high strain% values by blockage of the flow with showing an abrupt jump to higher levels. Laun et al. stated that the strain thickening occurs at critical amplitude value at which the fluid becomes highly viscous (Laun et al., 1991). Usually, in all of the curves obtained in this study, G" is greater than G' which denotes the domination of viscous properties to elastic properties. However, some fluctuations occur at the initial portion of the applied strain amplitudes until the critical amplitude as in STF20-PEG 200. After this point, G" absolutely exceeds G' in accordance with the Laun et. al's statement. Altough the incipience of the strain thickening is usually

observed earlier with the increasing constant angular frequency, the steepness of the strain thickening behavior differs not so much. The effect of the molecular weight of the medium fluid is also observed under increasing strain amplitudes. Results show that the highest moduli values were obtained for STFs-PEG 200 and PEG 300 with a slight difference. In contrast, STF systems which was produced with PEG 400 and 600 exhibits lower moduli values. Therefore, it can be concluded that increasing the molecular weight of the medium fluid decreases the moduli values of the STFs.

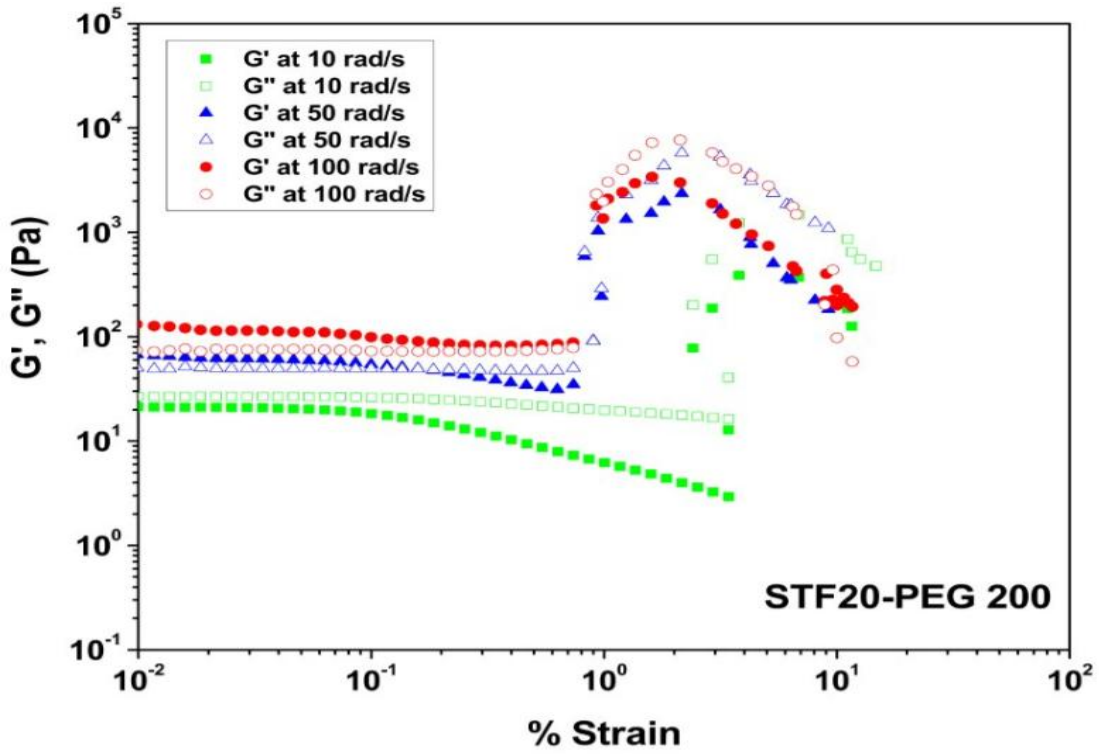

Figure 4.33. Elastic G' and viscous G" modulus curves of STF20-PEG 200 as a function of strain amplitude

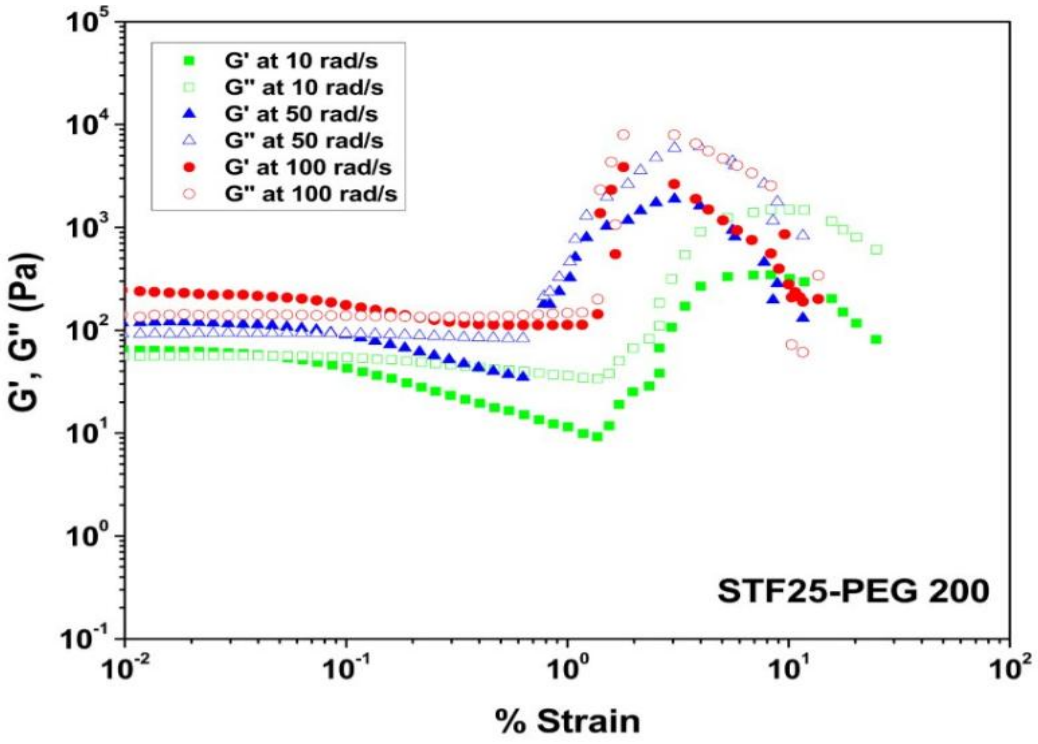

Figure 4.34. Elastic G' and viscous G" modulus curves of STF25-PEG 200 as a function of strain amplitude

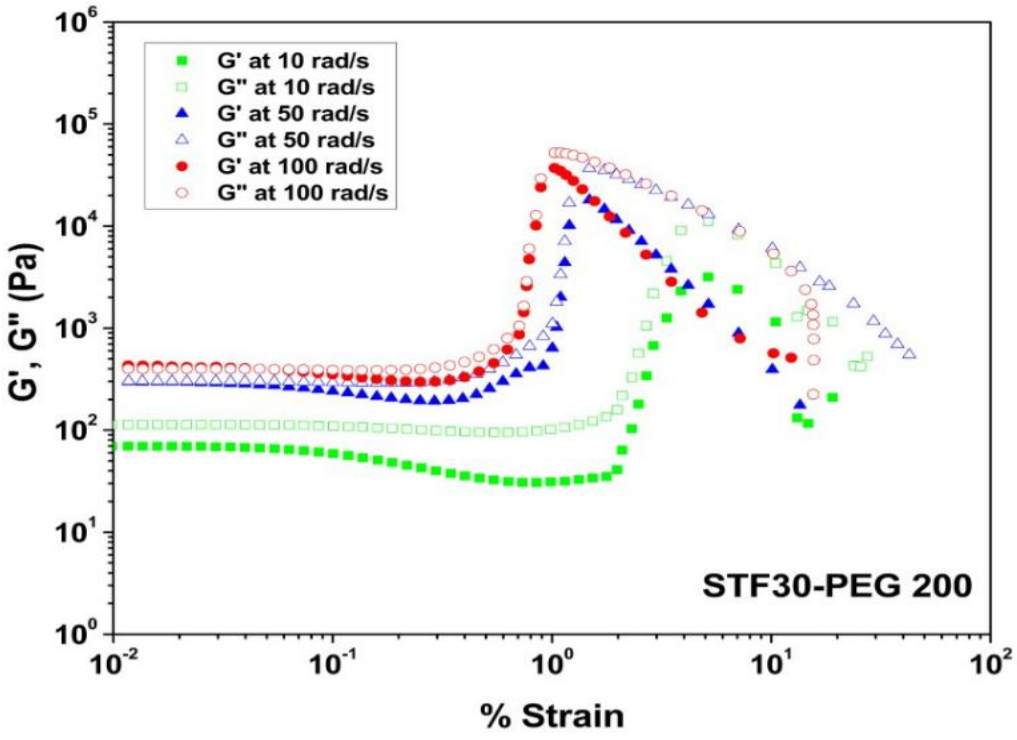

Figure 4.35. Elastic G' and viscous G" modulus curves of STF25-PEG 200 as a function of strain amplitude

The effect of fumed silica concentration on the moduli values of the STFs under varying strain amplitude at 100 rad/s is ivestigated for all of PEG systems. As it can be clearly seen in Figures 36-37, 41-42, 46-47, 51-52, elastic and viscous moduli values gradually increases with silica weight fraction. The obtained curves are similar with the curves of viscosity as a function of shear rate. The general increasing concentration behavior is also valid for strain sweep results. As silica loading increases, the onset of strain thickening is observed at lower values with a gradually increasing abrupt jump in moduli values. Among all of the concentrations STF30 for all PEGs shows the most strong thickening value.

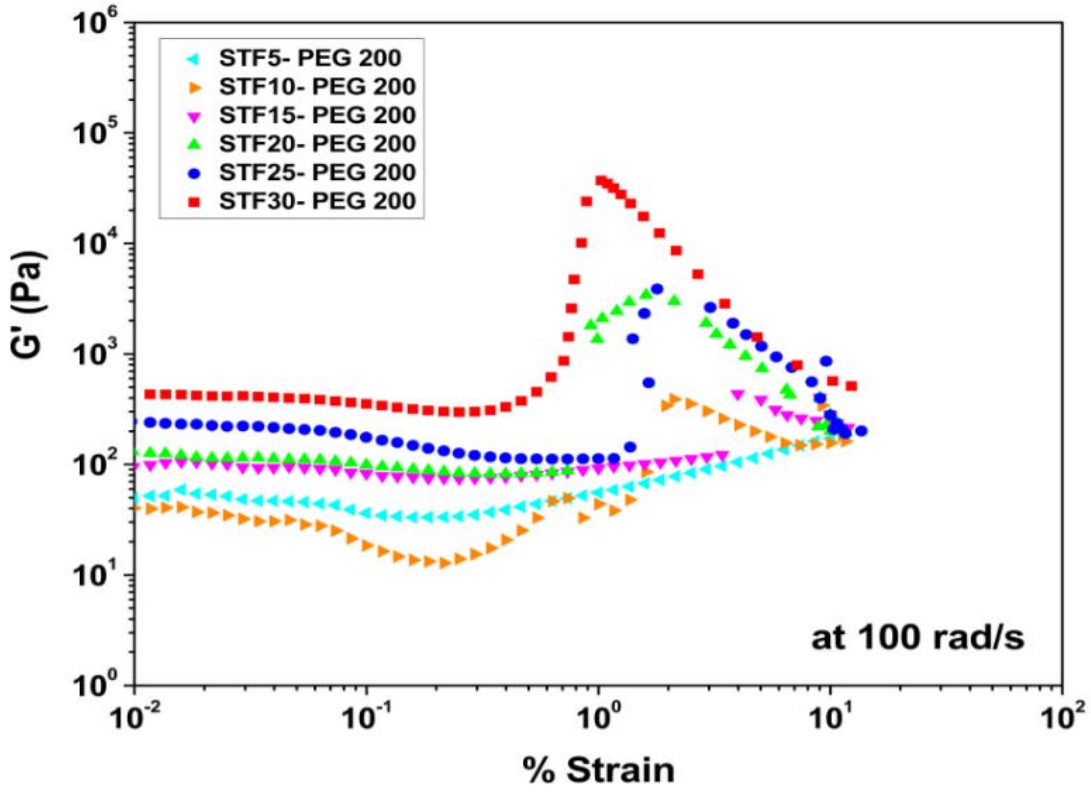

Figure 4.36. Elastic G' modulus curves of STF5 to STF30-PEG 200 as a function of angular frequency at 100 rad/s

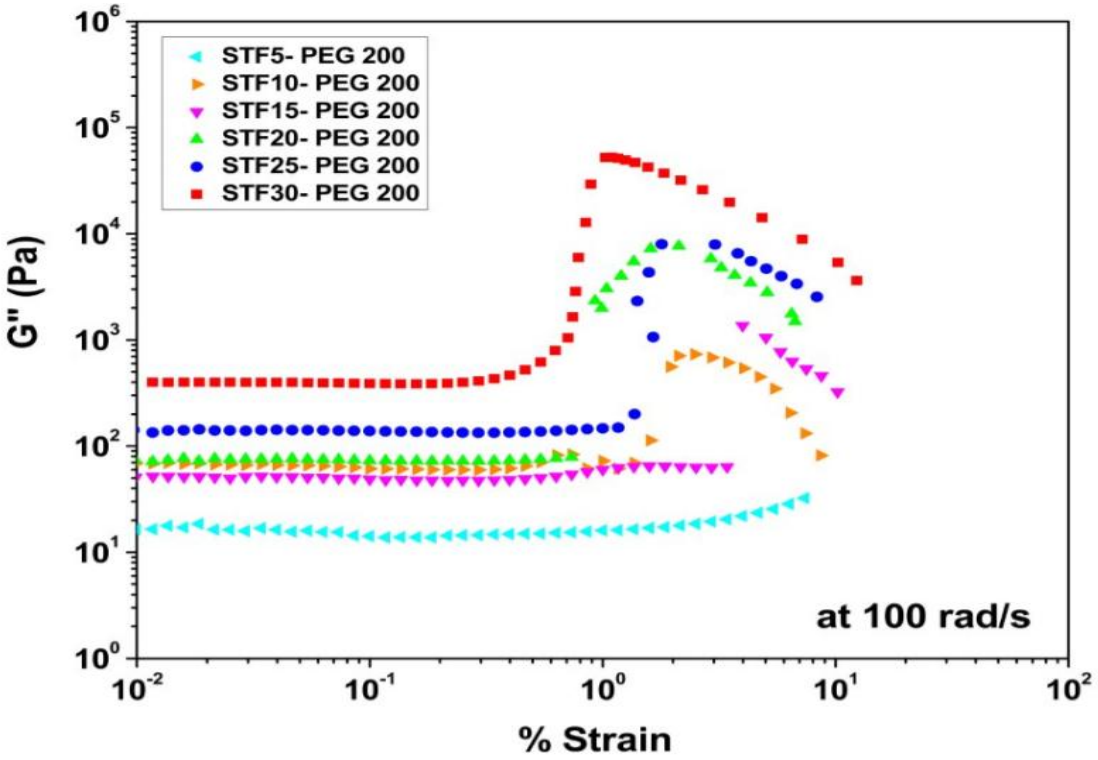

Figure 4.37. Elastic G' modulus curves of STF5 to STF30-PEG 200 as a function of angular frequency at 100 rad/s

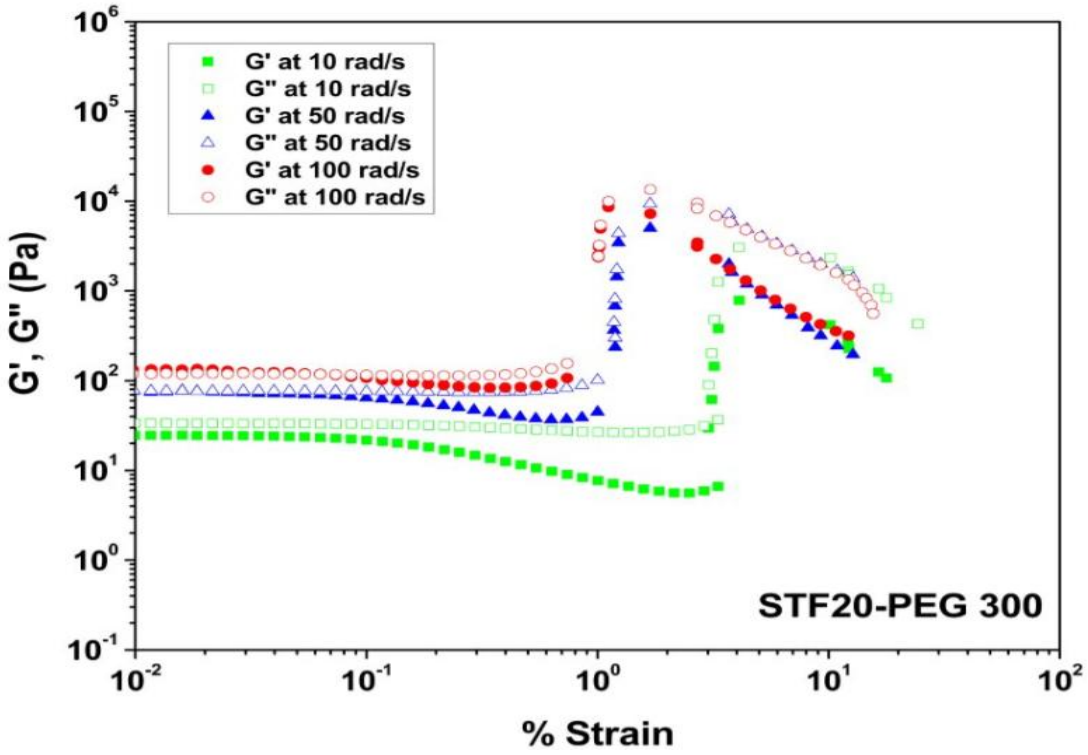

Figure 4.38. Elastic G' and viscous G" modulus curves of STF20-PEG 200 as a function of strain amplitude

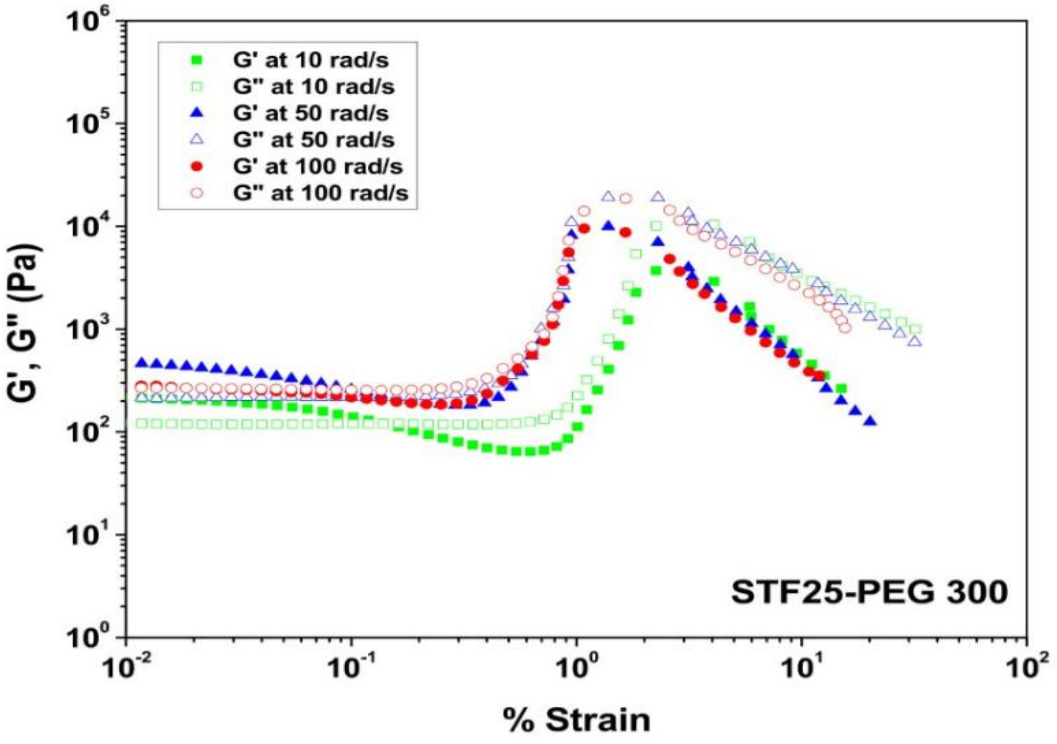

Figure 4.39. Elastic G' and viscous G" modulus curves of STF25-PEG 200 as a function of strain amplitude

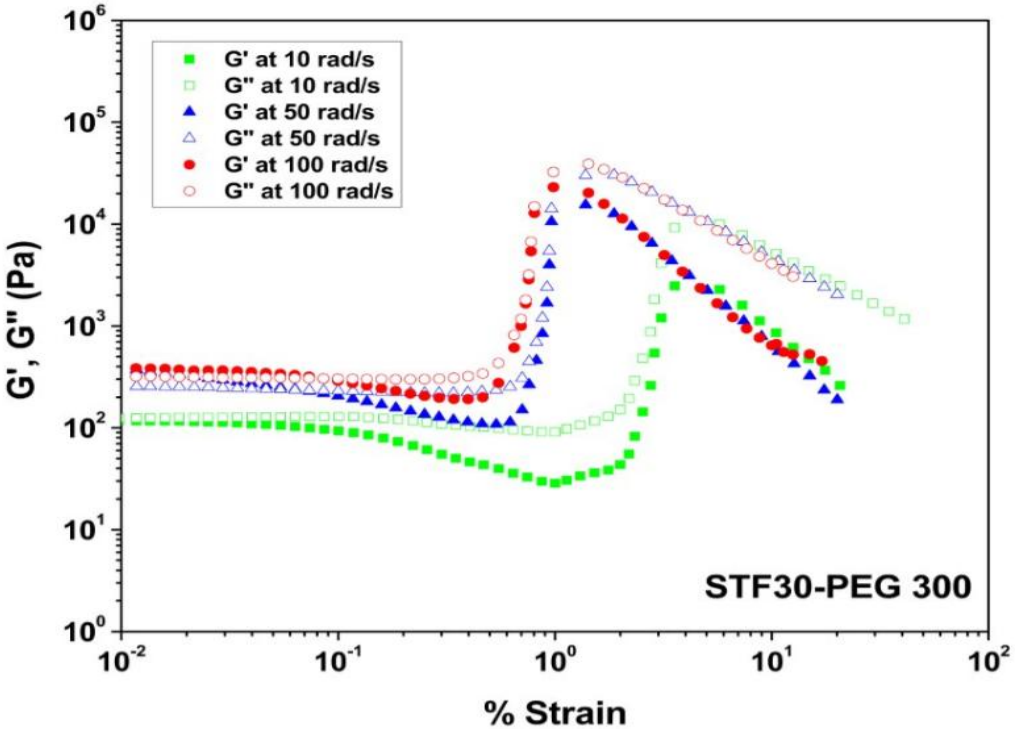

Figure 4.40. Elastic G' and viscous G" modulus curves of STF30-PEG 200 as a function of strain amplitude

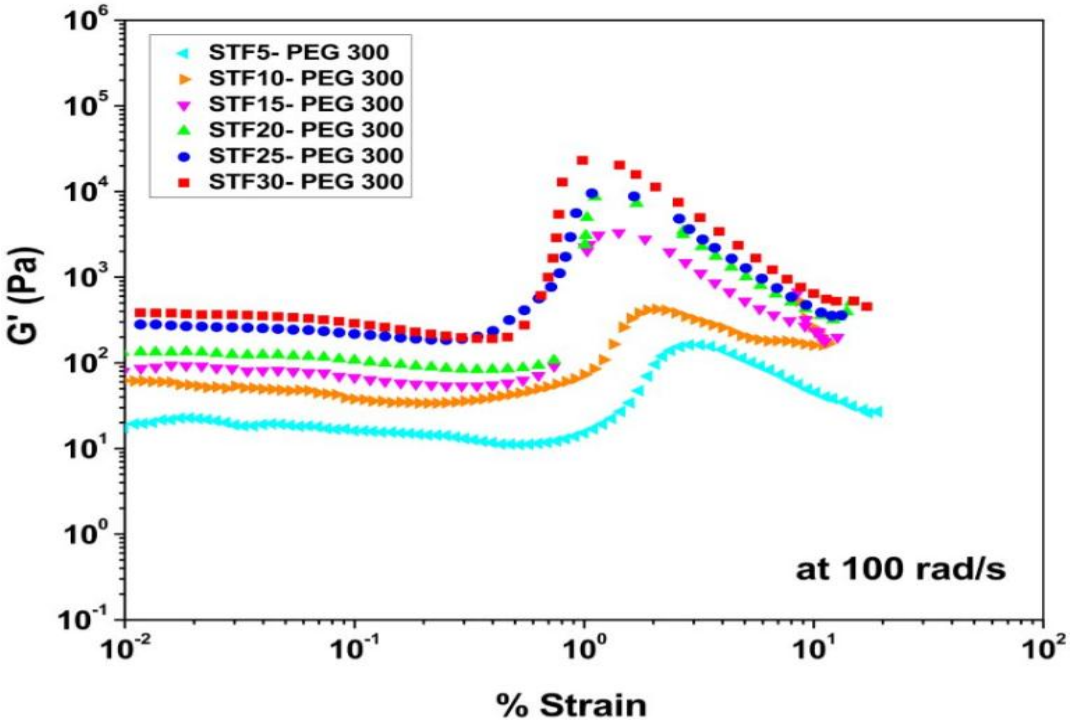

Figure 4.41. Elastic G' modulus curves of STF5 to STF30-PEG 300 as a function of angular frequency at 100 rad/s

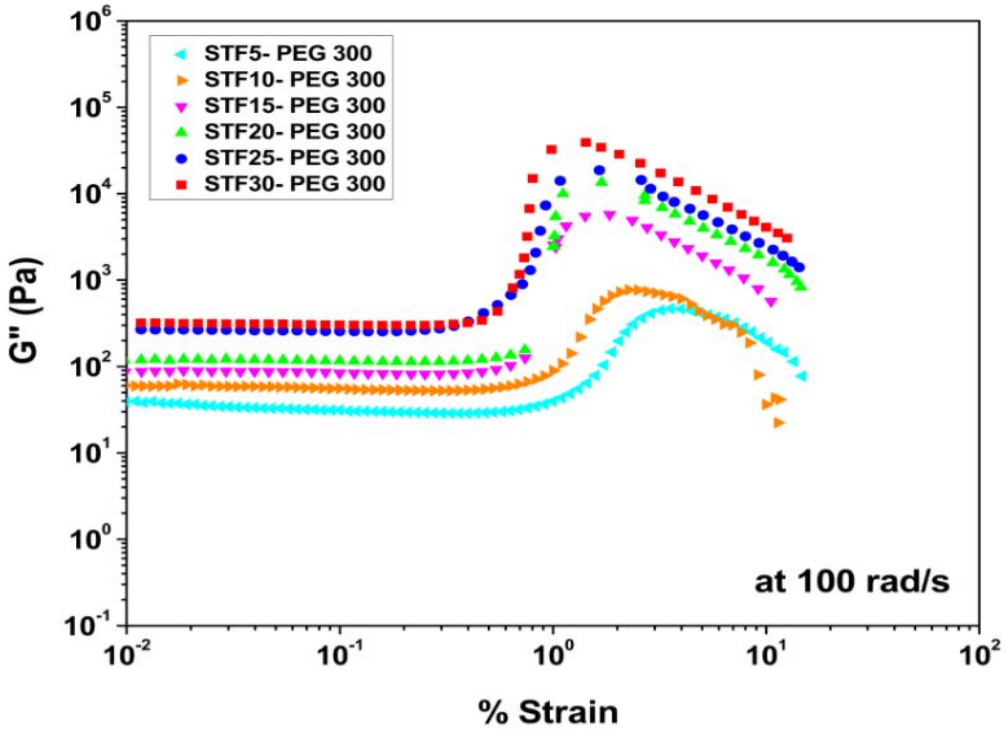

Figure 4.42. Elastic G" modulus curves of STF5 to STF30-PEG 300 as a function of angular frequency at 100 rad/s

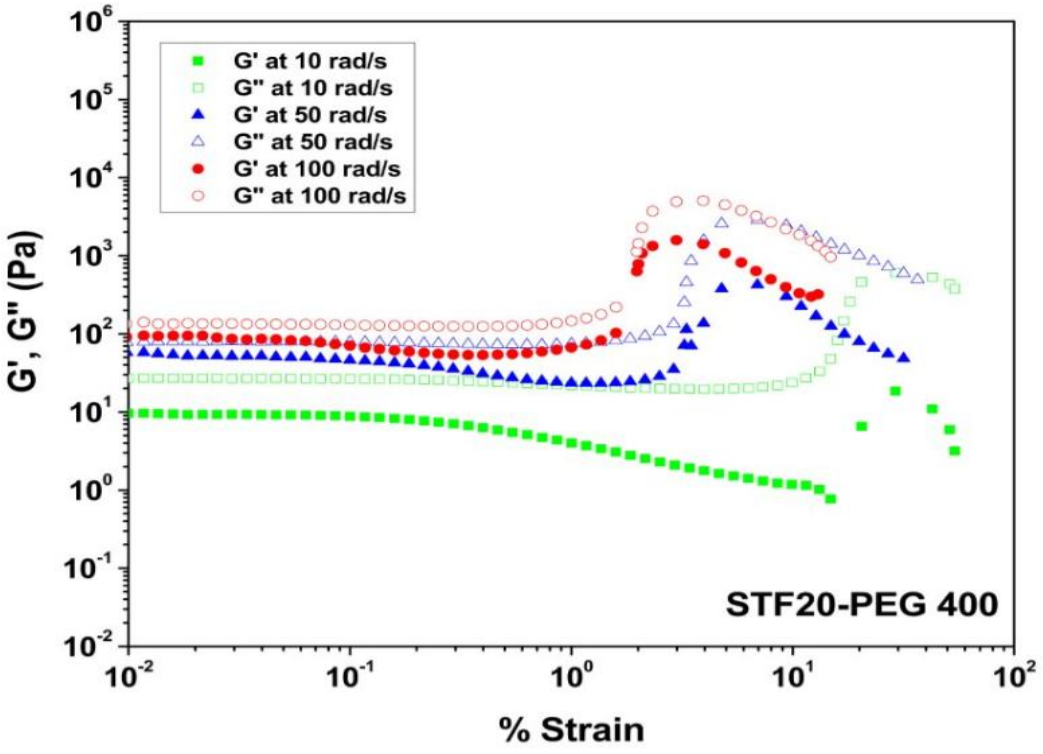

Figure 4.43. Elastic G' and viscous G" modulus curves of STF20-PEG 400 as a function of strain amplitude

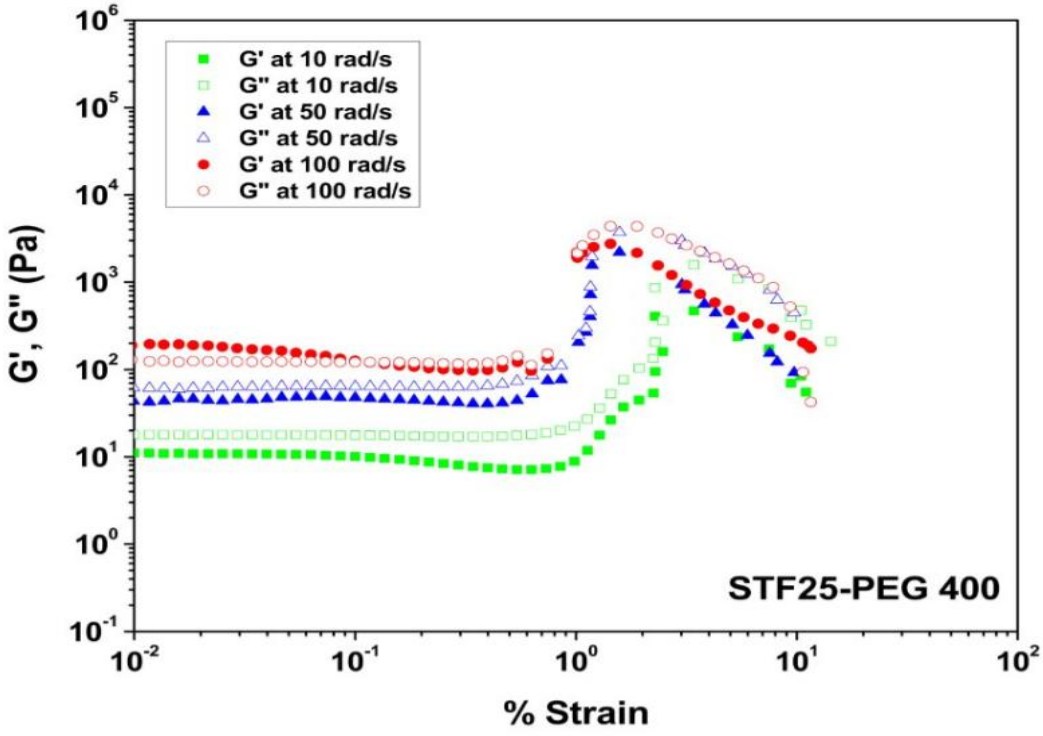

Figure 4.44. Elastic G' and viscous G" modulus curves of STF25-PEG 400 as a function of strain amplitude

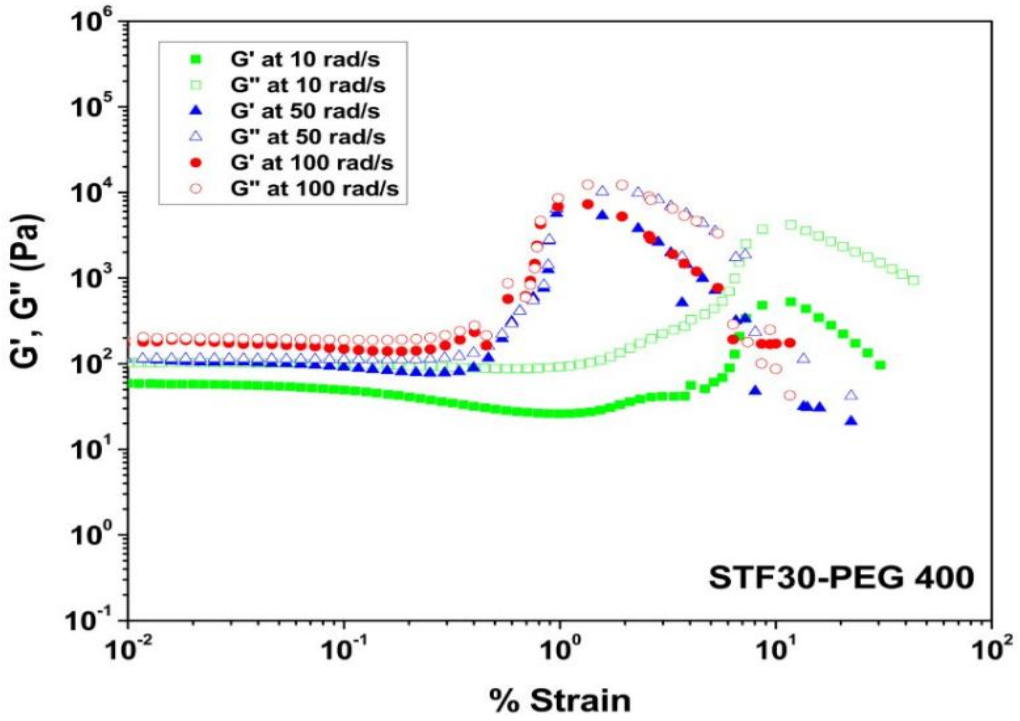

Figure 4.45. Elastic G' and viscous G" modulus curves of STF30-PEG 400 as a function of strain amplitude

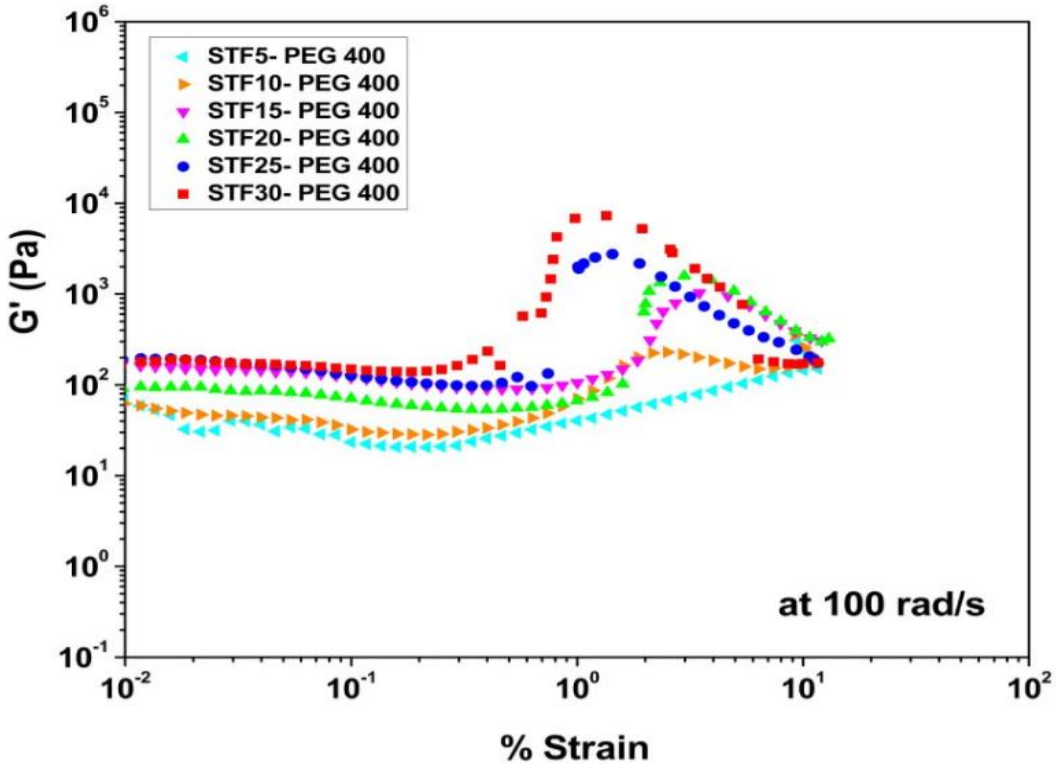

Figure 4.46. Elastic G' modulus curves of STF5 to STF30-PEG 400 as a function of angular frequency at 100 rad/s

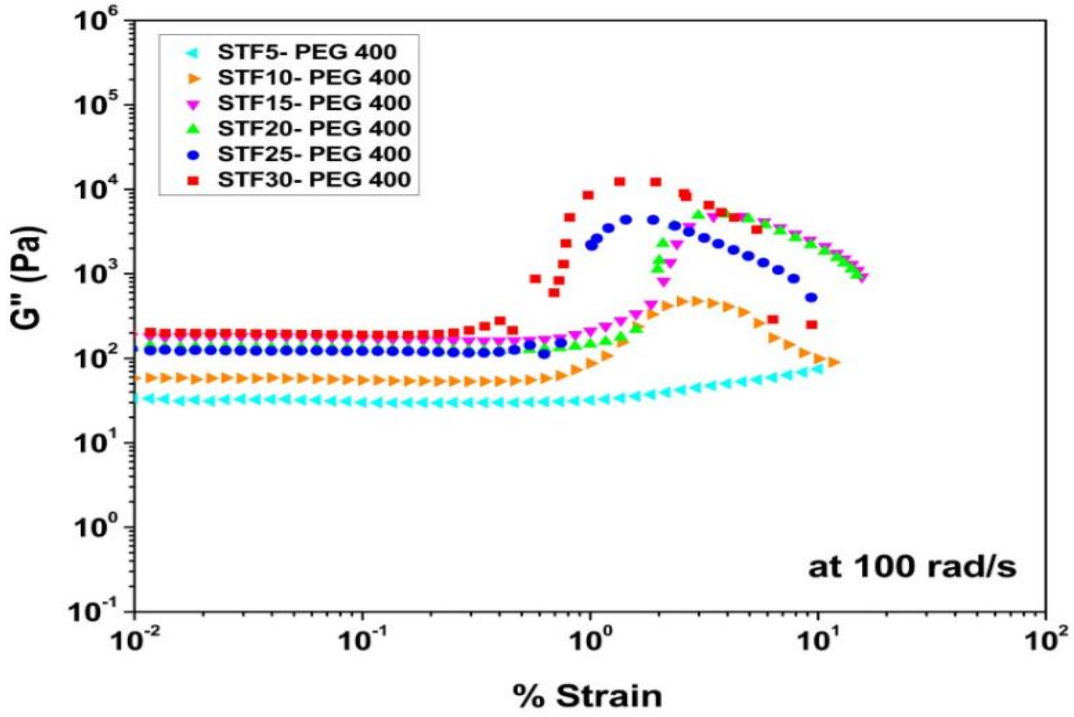

Figure 4.47. Elastic G" modulus curves of STF5 to STF30-PEG 400 as a function of angular frequency at 100 rad/s

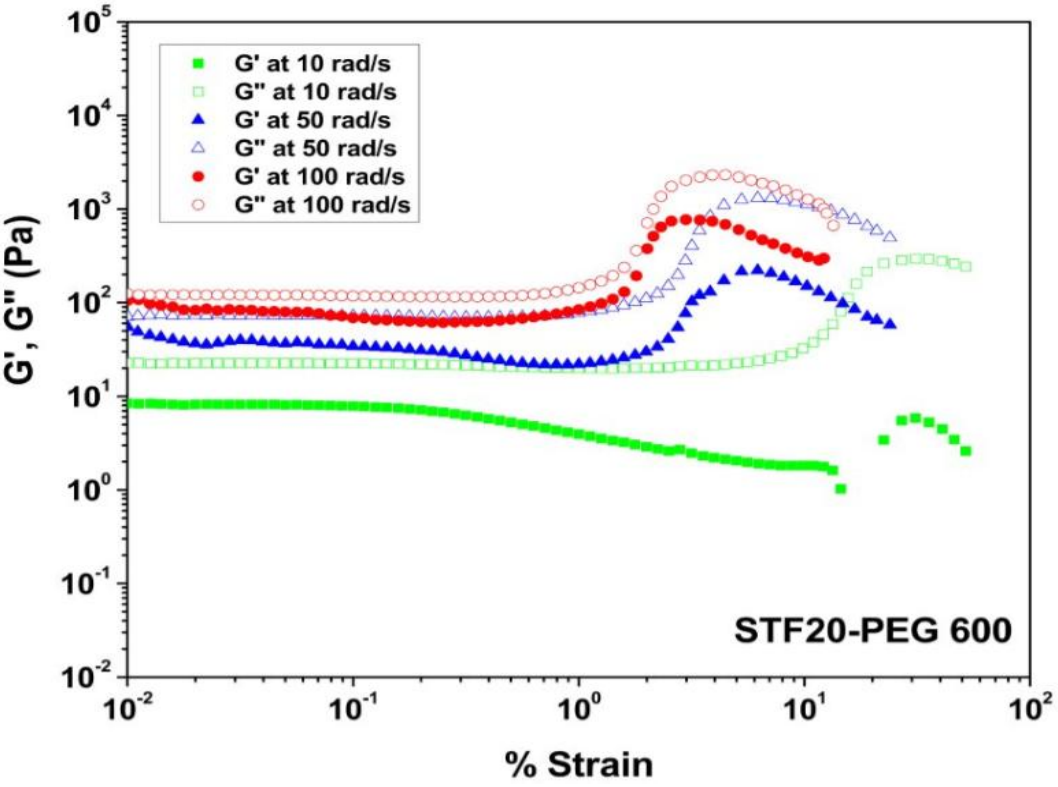

Figure 4.48. Elastic G' and viscous G" modulus curves of STF20-PEG 600 as a function of strain amplitude

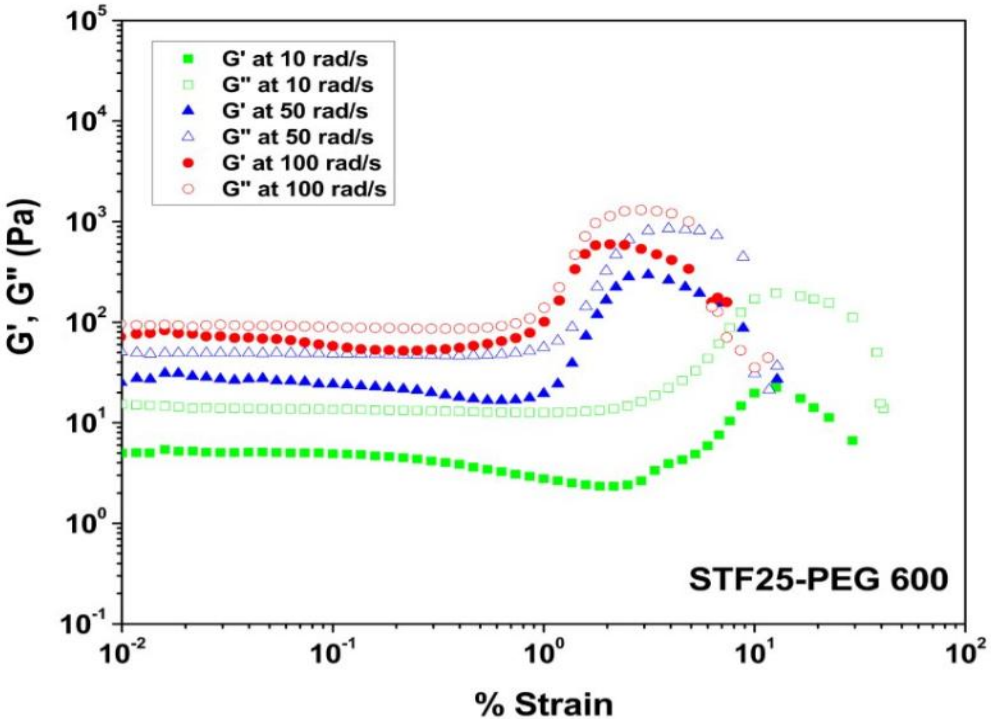

Figure 4.49. Elastic G' and viscous G" modulus curves of STF25-PEG 600 as a function of strain amplitude

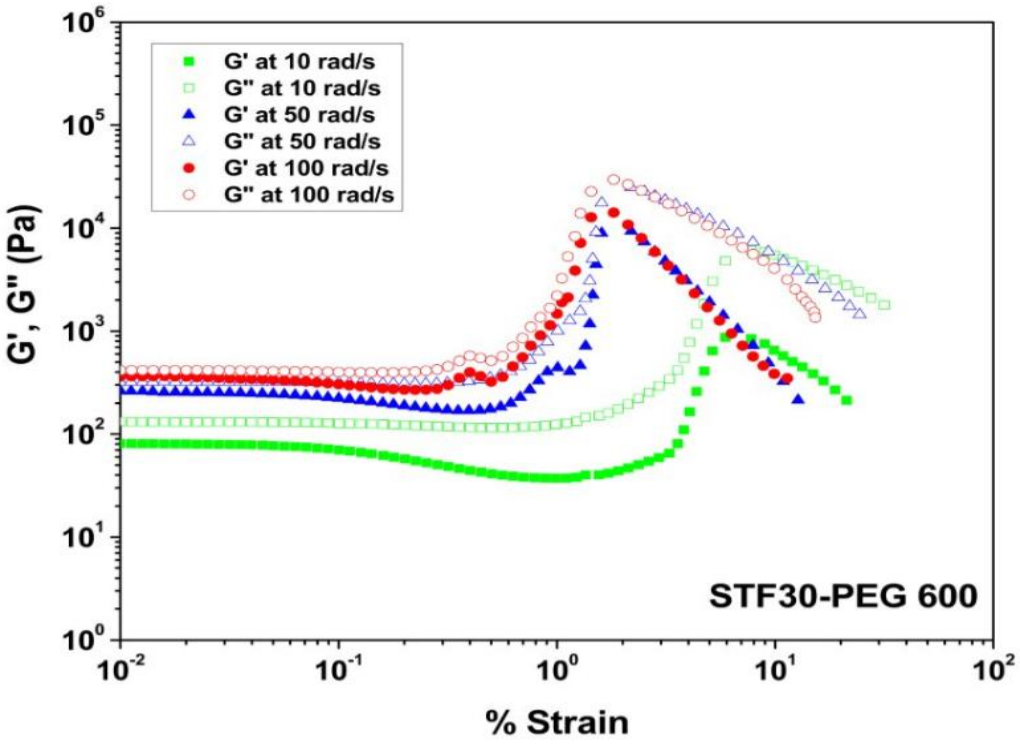

Figure 4.50. Elastic G' and viscous G" modulus curves of STF30-PEG 600 as a function of strain amplitude

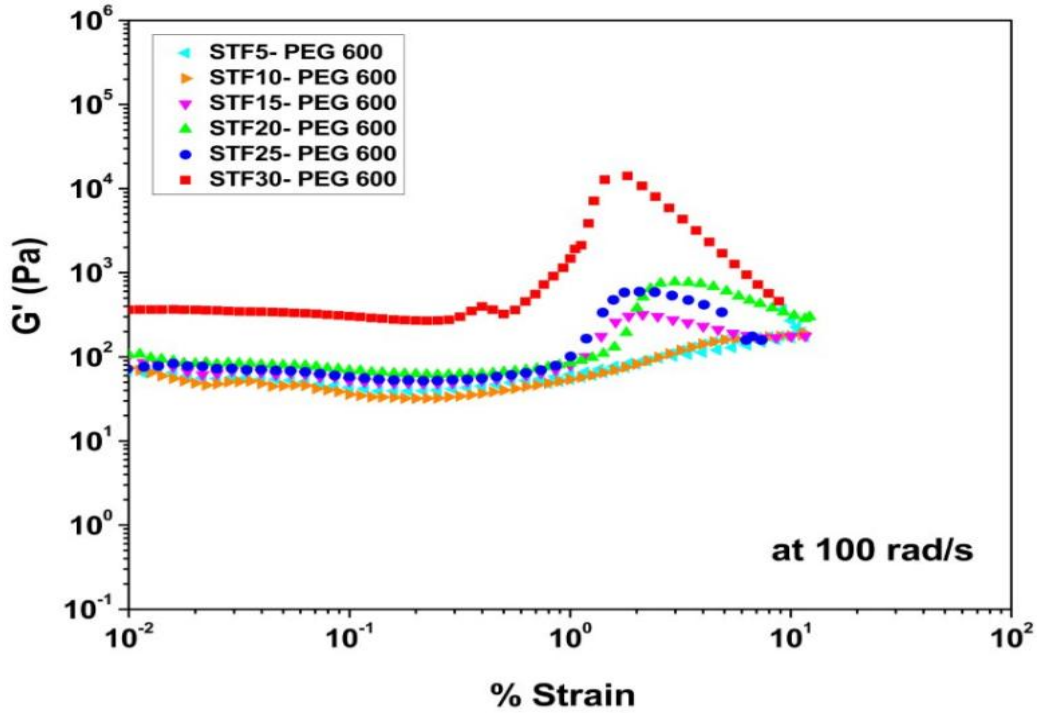

Figure 4.51. Elastic G' modulus curves of STF5 to STF30-PEG 600 as a function of angular frequency at 100 rad/s

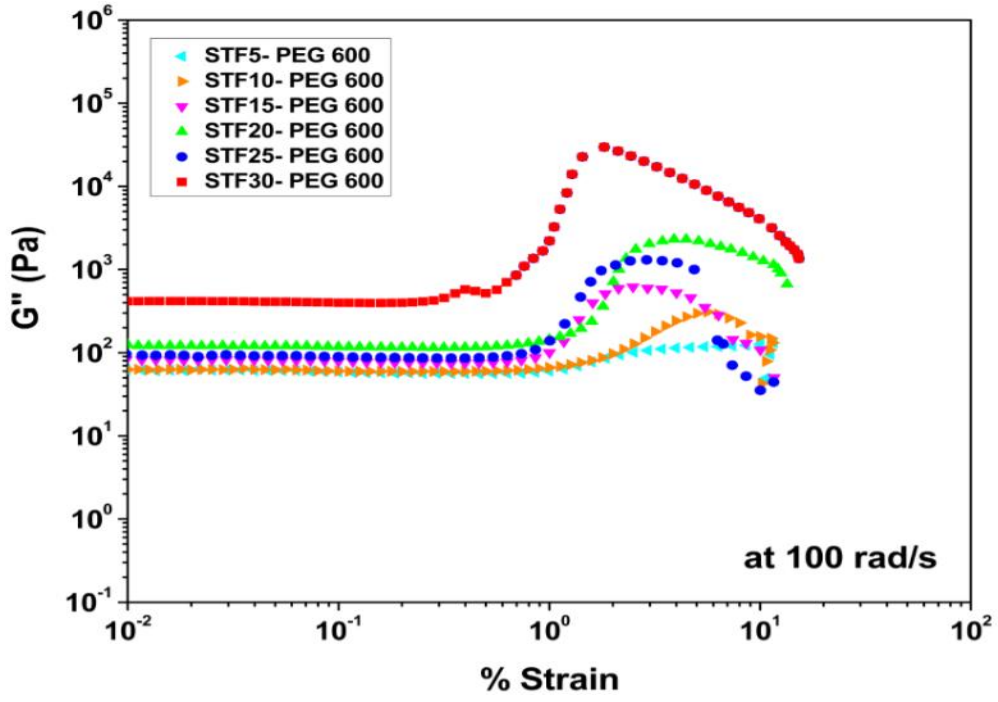

Figure 4.52. Viscous G" modulus curves of STF5 to STF30-PEG 600 as a function of angular frequency at 100 rad/s

4.3. Quasistatic Stab Test Results

Stab tests was performed with an engineering spike which was mounted the load cell of Schimadzu AGI Universal test machine with a rate of 500 mm/min through a penetration distance of 30 mm. The details of the test was expressed in the experimental part. Each of the targets were composed of 10 layers of aramid with the size of 20x20 cma nd the add-on amount of 15%. The aramid fabrics were impregnated with STF30-PEG 200, 300, 400 and 600 from which the best rheological properties were obtained. The STFs were diluted in ethyl alcohol before impregnation. The test results were compared with the sample consists of neat aramid fabrics. The add-on% was calculated as in equation below;

$$\text{Add} - \text{on}\% = \frac{\text{weight of the STF impregnated sample} - \text{weight of the neat sample}}{\text{weight of the STF impregnated sample}} \quad (4.1)$$

According to the Figure 4.53. aramid fabric/STF targets supports higher load than the neat fabrics. The best stab test result is obtained for aramid fabric/STF30-PEG 200 composite as 137 N whereas the neat fabrics supports 74.3 N. When the molecular weight of the medium fluid is increased, the loading resistance decreased gradually. All of the results and percent increase in the stab resistants of target specimens are given in Table 4.5.

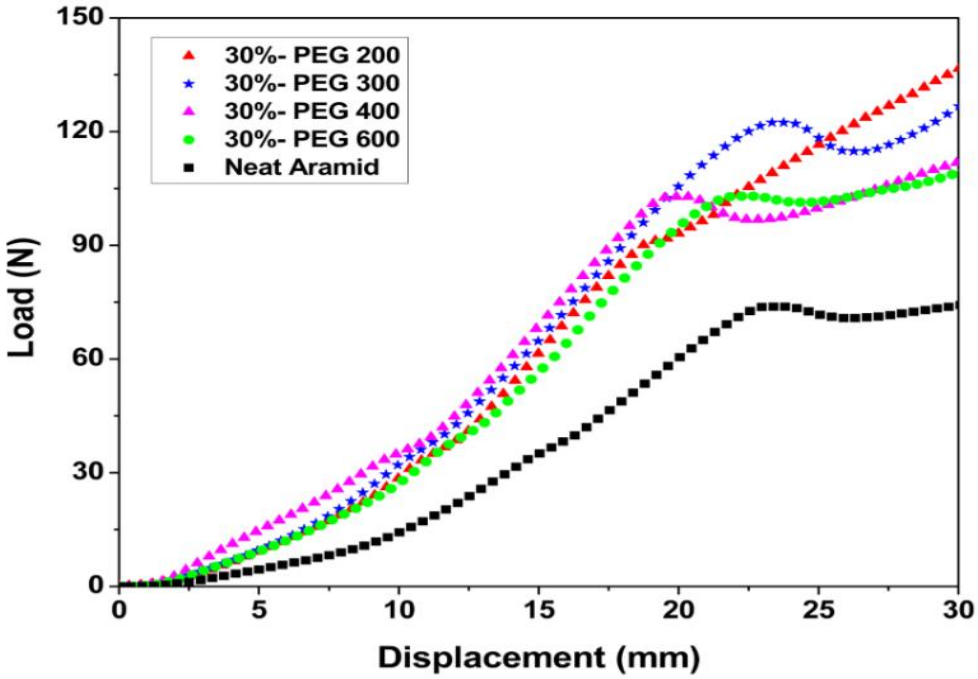

Figure 4.53. Load–displacement curves of neat and STF impregnated Kevlar targets for quasistatic stab testing

Table 4.5. Stab test results and specifications of the target specimens

Sample	Add-on (%)	Load (N)	Increase (%)
Neat Aramid	-	74.3	-
STF30-PEG 200/Aramid composite	15	137	84.4
STF30-PEG 300/Aramid composite	15	127	71
STF30-PEG 400/Aramid composite	15	114	53.4
STF30-PEG 600/Aramid composite	15	110	48

4.4. Flexibility Test Results

Flexibility measurements were performed for 10 layers of 200x200 mm sized neat and STF impregnated aramid fabrics. The edge of the sample which was vacuumed, connected with a wire to the head of the Schimadzu tensile test machine to measure the flexibility (Figure 4.54.). Tests were conducted by applying 6 N force. STF

impregnation decrease the flexibility of the aramid fabrics. Also, increasing the molecular weight of the medium fluid makes the specimens more stiff by decreasing the bending angle (Figure 4.55 and Table 4.6). The bending angle θ was calculated as given below;

$$\theta = \tan^{-1}\left(\frac{\text{measured height (mm)}}{100\ \text{mm}}\right) \tag{4.2}$$

The measurements were carried out from the half of the specimen size to bend the sample. Therefore, the denominator in equation 4.3 was taken as 100 mm.

Figure 4.54. Flexibility measurement method

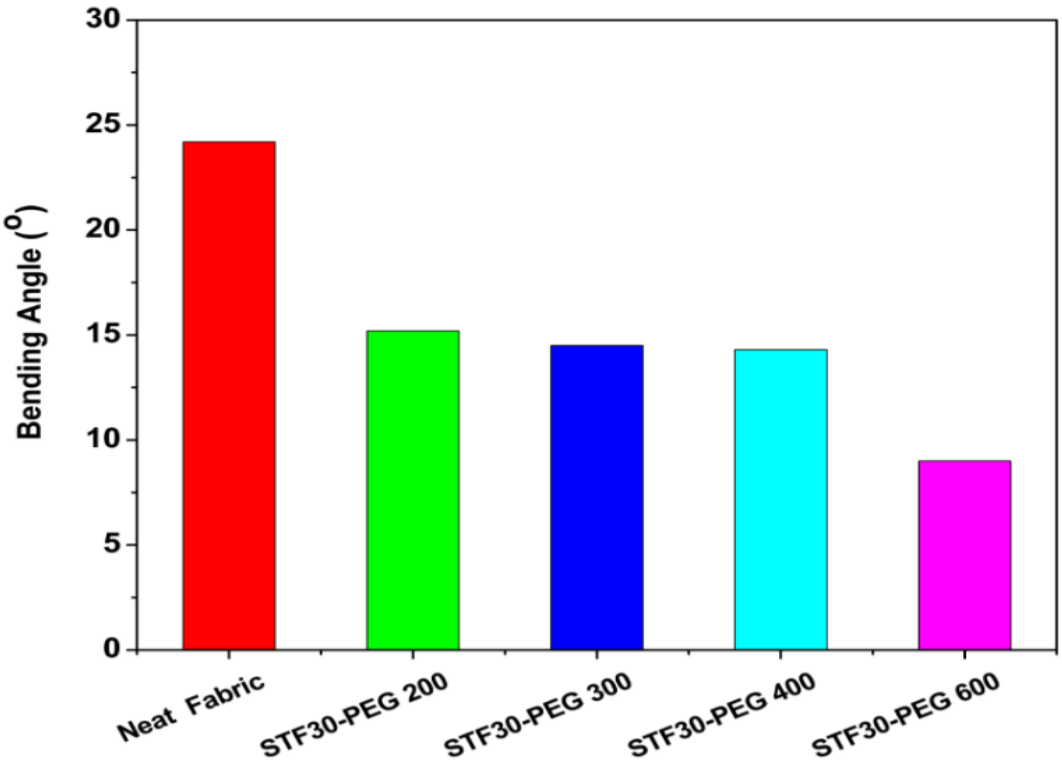

Figure 4.55. Bending angles of neat and STF impregnated fabrics

Table 4.6. Flexibility Test Results of the neat and aramid fabric composites

Sample	Number of Layers	Bending Angle (°)
Neat Aramid	10	24.2
STF30-PEG 200/Aramid fabric composite	10	15.2
STF30-PEG 300/Aramid fabric composite	10	14.5
STF30-PEG 400/Aramid fabric composite	10	14.3
STF30-PEG 600/Aramid fabric composite	10	9

4.5. Ballistic Test Results

Ballistic tests were carried out with different configurations of UHMWPE and Twaron fabric and PE laminae to provide enhanced ballistic protection. It was estimated that the complex structure of UHMWPE absorbs much more STF causing enhanced impact resistant. 60% fumed silica containing PEG 200 and STF30-PEG 300 were chosen based on the obtained ballistic pre-tests. Aramid fabrics were impregnated with 60% fumed silica- PEG 200 solution with the add-on amountS of 10, 15% whereas UHMWPE fabrics were soaked into STF30- PEG 300 solution which was prepared by the dispersion of the STF30-PEG 300 in ethyl alcohol with add-on% amount of 20. The rheological properties of 60% fumed silica- PEG 200 could not be measured, because at such high concentrations it can not be grinded with agate mortar. Tests were conducted with V_{50}. The configurations of the prepared targets are given in Table 4.7. The configurations were determined depending on the weight limits and number of layers which was determined by SSM.

Table 4.7. Configurations of STF/Fabric composites

Sample ID	**Configuration**
A	-15 layers neat aramid fabric
B	-15 layers STF impregnated aramid fabric (%60 SiO_2-PEG 200)
C	-17 layers STF impregnated aramid fabric (%60 SiO_2-PEG 200)
D	-10 layers PE laminae -7 layers UHMWPE fabric (STF30- PEG 300)
E	-10 layers PE laminae -4 layers aramid fabric (%60 SiO_2-PEG 200) -3 layers UHMWPE fabric (STF30- PEG 300)

According to the Table 4.8. addition of STF on to the aramid fabrics increased the V_{50} test results from 509.8 to 524.3 m/s. Also, increasing the number of aramid fabrics and amount of STF increased the ballistic limit to 610 m/s. The use of UHMWPE fabrics with PE laminae gave better result. However, the best result was obtained with the combination of PE laminae, UHMWPE and aramid fabrics. In this case, the measured value was 623 m/s. Figure 4.56. show the graphical illustration of these V_{50} test results.

Table 4.8. Ballistic test results of STF/Fabric composites

Sample ID	**Number of Layers**	**Add-on%**	**V_{50} (m/s)**
A	15	10	509.8
B	15	10	524.3
C	17	15	610
D	17	20	620
E	17	15 (for aramid fabric) 20 (for UHMWPE fabric)	623

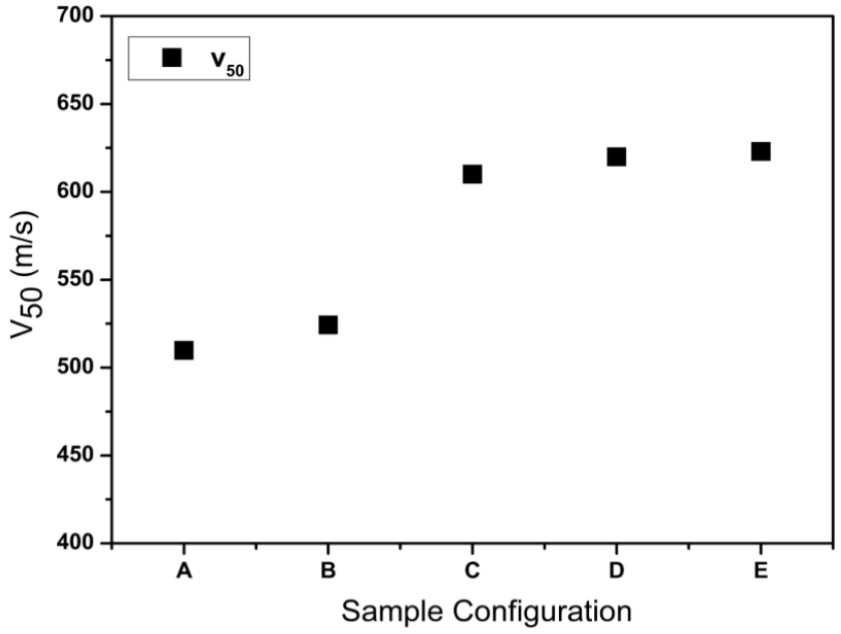

Figure 4.56. V_{50} test results of the ballistic test targets

The front and back view of the sample B before and sample D before and after the V_{50} test is seen in Figure 4.57., 4.58 and 4.59, respectively. Also, Figure 4.60 and 4.61 demonstrated that the UHMWPE fabrics are well coated with STF.

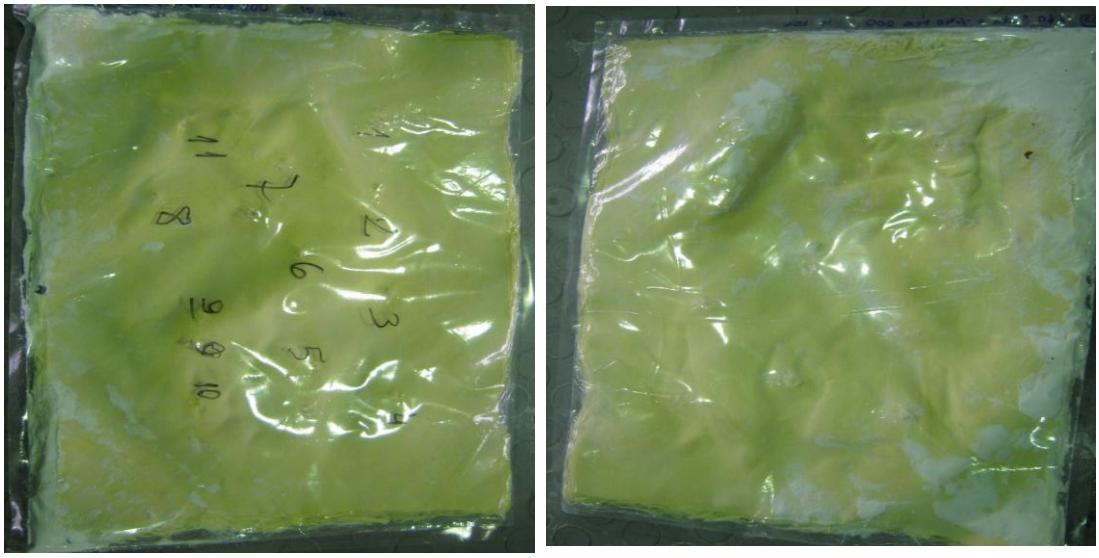

Figure 4.57. Appearance of sample B after V50 test (a) front view (b) back view

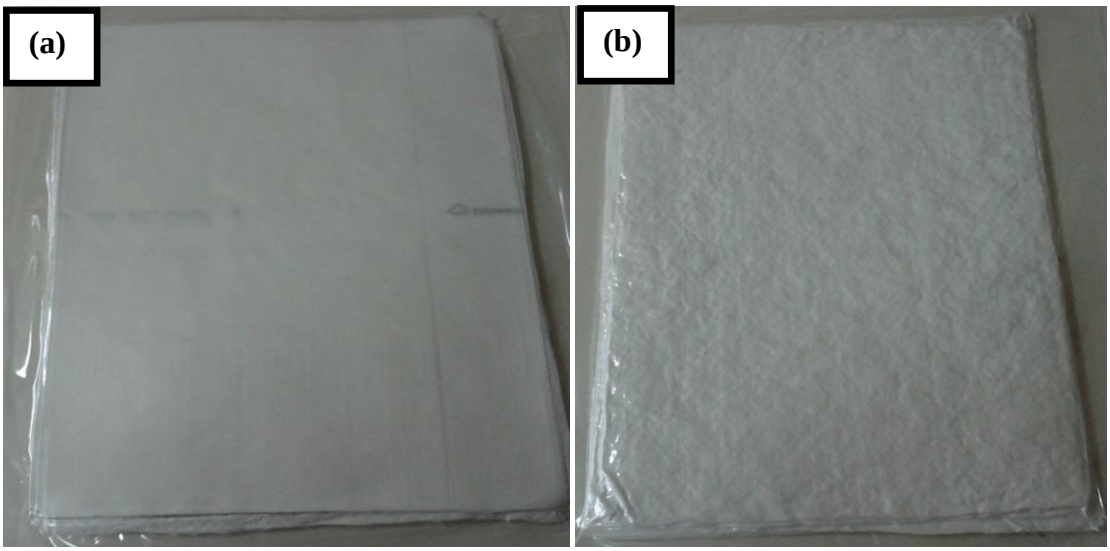

Figure 4.58. Appearance of sample D before V50 test (a) front view (b) back view

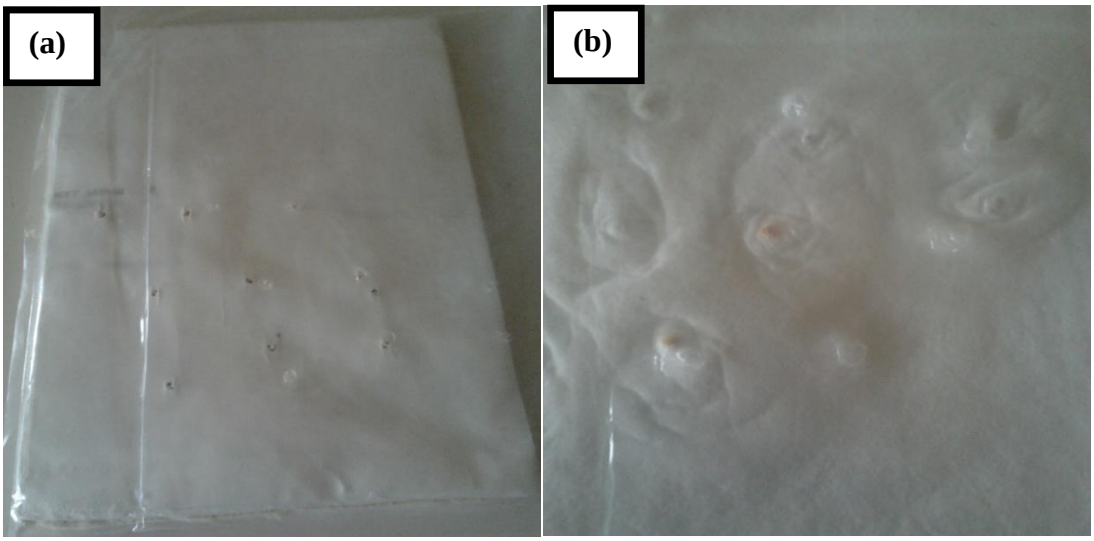

Figure 4.59. Appearance of sample D after V50 test (a) front view (b) back view

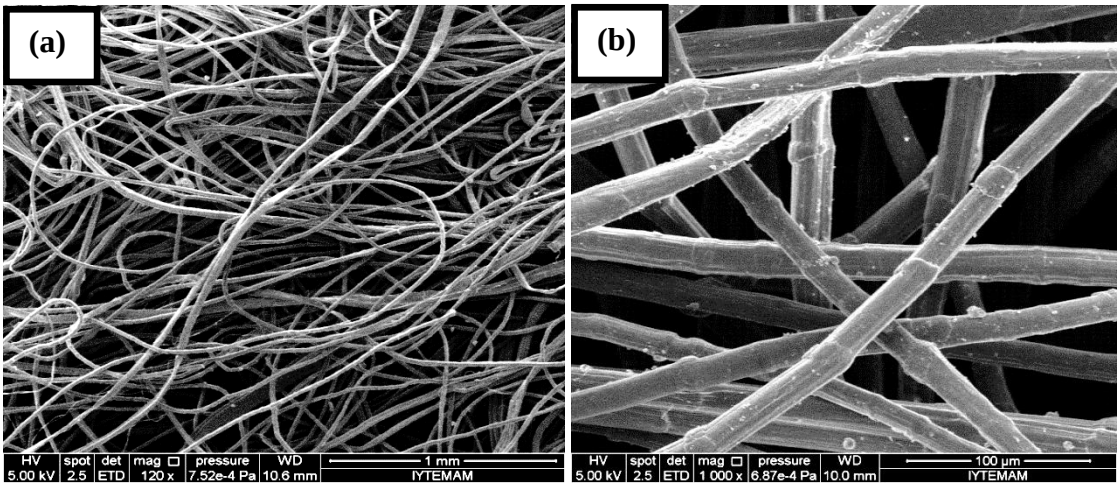

Figure 4.60. SEM images of neat UHMWPE fabric at different magnifications (a) 120x (b) 1000x

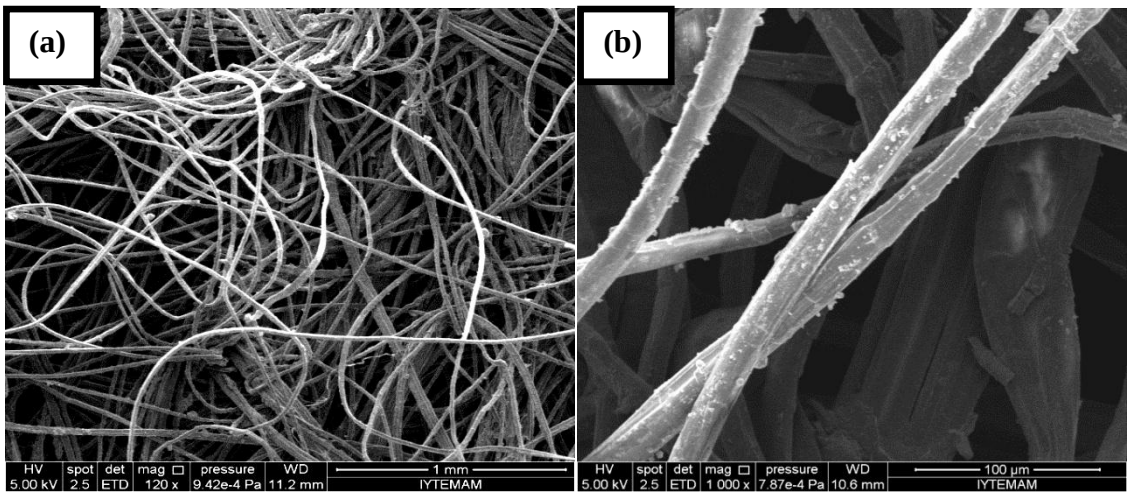

Figure 4.61. SEM images of STF30-PEG 300 impregnated UHMWPE fabric at different magnifications (a) 120x (b) 1000x

CHAPTER 5

CONCLUSIONS

In this study, colloidal dispersions of fumed silica nanoparticles in PEG were prepared to determine the changes in rheological properties with increasing fumed silica concentration and molecular weight of PEG. Also, the use of these STFs to enhance the impact resistant properties Twaron® aramid and UHMWPE fabrics for armor applications lies within the scope of this thesis.

Fumed silica nanoparticles were suspended in Newtonian PEG 200, PEG 300, PEG 400 and PEG 600 with increasing silica loading from 5 to 30 wt%. The characterization results showed that fumed silica that is used in this study is a polydisperse material which consists of branched-like aggregates. Also, they were succesfullyinteracted with polymeric medium and the loss of silica during the production process was negligible. Rheological properties of STFs were investigated by stress controlled rotational rheometer with steady-state and dynamic shear modes. In steady shear mode, all of the STFs exhibit a shear thickening property with strikingly increasing viscosity as shear stress and rate of shear are increased. The magnitude of the shear thickening enhanced while weight fraction of filling particles is increasing. It was observed that the viscosity jump in shear thickening region was steeper for STFs which have higher silica concentration and lower molecular weight of medium. The maximum viscosities were obtained for STF30s. So, the maximum viscoisty of STF30-PEG 200 was measured as 1622 Pa.s whereas it was found as 1241, 588.3, 350 Pa.s for STF30-PEG 300, 400 and 600, respectively. Also, the onset of shear thickening was generally observed earlier with increasing silica loading and decreasing PEG molecular weight. Unexpectedly, , the STF which first began to thicken with the applied shear force was STF30-PEG 300 with a shear rate of 11.1 s^{-1} The critical shear rates of STF30-PEG 200, 400 and 600were observed at 14.4, 30.4 and 57.4 $s^{-1,}$ respectively.

Dynamic shear measurements were conducted under sinusoidal oscillation in terms of frequency and strain sweep modes. In frequency sweep mode, behavior of elastic (G') and viscous (G") moduli values with varying frequency was measured in the range of 0.1-1000 rad/s by keeping % strain amplitude constant at 100, 500 and 1000%.

Both moduli varies strongly with angular frequency. For all of the STFs G" values was greater than G' about on one order of magnitude. Based on these results, it was concluded that the STFs are composed of nonflocculated discrete units. Furthermore, the moduli values exhibit a thickening effect at critical frequency. The magnitude of this thickening was increased with increasing strain amplitude. The critical frequency values undergo a reduction with increasing fumed silica concentration and strain amplitude.

Similarly, in strain sweep mode, angular frequency was held fixed at 10, 50 and 100 rad/s and both moduli values were observed at varying strain amplitude (between 0.1-100%). The graphs obtained under strain sweep mode resembles the steady shear rheological measurements showing strain thickening behavior. The amount of strain thickening was also enhanced by increasing silica concentration and angular frequency. The onset of the thickening was obtained at lower strain amplitudes with higher angular frequencies and concentration. All of the dynamic measurements reflect and verified the thickening propety of the STFs.

Stab test results showed that the STF impregnation enhanced the resistance of the aramid fabrics to spike impactor when compared to the neat fabrics. On the other hand, increasing the polymer molecular weight of the STFs which were used in the impregnation procedure decreased the stab resistivity of the fabrics. The sample of aramid fabric/STF30-PEG 200 composite supported the highest load with 137 N among the other STF impregnated aramid fabric composites while neat aramid fabrics were supporting 74.3 N load. This is equivalent to a 84.4% increase in stab resistivity of neat aramid fabrics. The loads which were supported by STF30-PEG 300, 400 and 600 impregnated fabrics were obtained as 127, 114, 110 N, respectively. Flexibility results also show the same behavior with stab test results, but reversely. STF impregnation decreased the bending angle of the samples as well as increasing molecular weight of the medium fluid. The bending angle of neat aramid fabrics was 24.2^{o} whereas it was measured as 15.2, 14.5, 14.3 and 9^{o} for STF30-PEG 200, 300, 400 and 600 with decreasing trend. This means that the higher the polymer molecular weight, the stiffer the composites.

Ballistic tests were performed for different configurations of aramid fabrics, PE laminae and UHMWPE fabrics in terms of V_{50}. According to the results the most effective configuration was found for the composite of 10 layers PE laminae-4 layers aramid fabric (%60 SiO_2-PEG 200)- 3 layers UHMWPE fabric (STF30- PEG 300) with

a 623 m/s V_{50} value. Therefore, it can be concluded that the use of STFs has the potential in armor applications.

REFERENCES

Cavallaro P.V., 'Soft Body Armor: An Overview of Materials, Manufacturing, Testing, and Ballistic Impact Dynamics', 1 August **2011,** NUWC-NPT Technical Report 12,057

Decker M.J. , Halbach C.J. , Nam C.H. , Wagner N.J. , Wetzel E.D.,' Stab resistance of shear thickening fluid (STF)-treated fabrics, **2007**,*Composites Science and Technology*, 67 (565–578).

Egres R.G. Jr., Lee Y.S., Kirkwood J.E., Kirkwood K.M., Wetzel E.D., Wagner N.J.,' "Liquid armor": Protective fabrics utilizing shear thickening fluids', October 26-27, **2004**, IFAI 4th Int. Conf. on Safety and Protective Fabrics, Pittsburgh, PA.

Barnes H. A., Hutton J. F., Walters K., ' An Introduction to Rheology', **1989**, Rheology Series 3, Elsevier.

Duvarcı Ö. Ç., 'Rheological Behavior Of Nanocrystalline/Submicron Ceramic Powder Dispersions',**2009**, PhD. Thesis, İzmir Institute of Technology.

Boersma W. H., Laven J., Stein H., 'Shear Thickening (Dilatancy) in Concentrated Dispersions', **1990**, AIChE Journal, 36(3) 321-332.

Carreau P.J., Lavoie P.A., Yziquel F., 'Rheological properties of concentrated suspensions',**1999**,Rheology Series, Volume 8, Pages 1299–1345.

Mewis J., Wagner N., 'Colloidal Suspension Rheology', Cambridge University Press, **2012**.

Wagner N.J., Brady J.F., 'Shear thickening in Colloidal Dispersions', American Institute of Physics, Physics Today, **2009**.

Barnes H.A., 'Shear-Thickening ("Dilatancy") in Suspensions of Nonaggregating Solid Particles Dispersed in Newtonian Liquids', **1989**, *Jon Wiley & Sons Inc., Journal of Rheology*, 33(2), 329-366.

Goodwin J. W. and Hughes R. W., 'Rheology for Chemists : An Introduction', Royal Society of Chemistry, **2007**.

Malkin A. Y., Isayev A. I., 'Rheology concenpts, methods and applications', Chem Tec. Pub, 2012, 2nd Edition.

Sochi T., 'Flow of Non-Newtonian Fluids in Porous Media', **2010**, Journal of Polymer Science: Part B: Polymer Physics, Vol. 48, 2437–2767.

Chhabbra R. P. and Richardson J. F. 'Non-Newtonian Flow and Applied Rheology: Engineering Applications', **2008**.

Erdoğan T., 'Development Of Liquid Armor Materials And Rheological Behavior of Shear Thickening Fluids (STFs)', **2011**,MSc. Thesis, Izmir Institute ofTechnology.

Lee Y. S., Wetzel E. D., Egres Jr. R. G., Wagner N. J., 'Advanced Body Armor Utilizing Shear Thickening Fluids', **2002**, 23rd Army Science Conference. Orlando, FL. December 2-5.

Tanner R. I., 'Engineering Rheology', **2002**, Oxford Engineering Science Series 52, 2nd Edition,

Galindo-Rosales F.J., Rubio-Hernandez F.J., Sevilla A., **2011**, 'An apparent viscosity function for shear thickening fluids', *J. Non-Newtonian Fluid Mech*.,166, 321–325.

Hoffman, R. L. 'Explanations for the cause of shear thickening in concentrated colloidal Suspensions', **1998,** *Inc. J. Rheol*., 42(1), January/February,111-123.

Raghavan S. R. and Khan S. A., 'Shear-Thickening Response Of Fumed Silica Suspensions Under Steady And Oscillatory Shear', **1997**, *Journal Of Colloid And Interface Science*,185, 57–67.

Hoffman, R. L. 'Discontinuous and Dilatant Viscosity Behavior in Concentrated Suspensions. I: Observations of a Flow Instability', *Transactions of The Society of The Rheology*, **1972**, 16:1 155-173.

Bossis G. And Brady J. F. ' The rheology of Brownian suspensions', **1989**, *Journal of Chemical Physics*, 91(3), 1866-1874.

Bender J., Wagner N. J., 'Reversible shear thickening in monodisperse and bidisperse colloidal dispersions', September/October **1996**, *J. Rheol.* 40(5).

Bettin G., 'High-Rate Deformations Behavior and Applications of Fluid Filled Reticulated Foams', **2007**, PhD. Thesis, .

Kang T. J.,Kim C. Y., Hong K. H., 'Rheological Behavior of Concentrated Silica Suspension and Its Application to Soft Armor', 1541, **2012**, *Journal of Applied Polymer Science*, Vol. 124, 1534-1541.

Kalman D. P., Schein J. B., Houghton J. M., Laufer C. H. N., Wetzel E. D., and N. J. Wagner, 'Polymer Dispersion Based Shear Thickening Fluid-Fabrics For Protective Applications', 3-7 June **2007**, *Proceedings of SAMPE 2007*, Baltimore, MD.

Wetzel Eric D., Lee Y. S., Egres R. G., Kirkwood K. M., Kirkwood J. E., and Wagner N. J., 'The Effect of Rheological Parameters on the Ballistic Properties of Shear Thickening Fluid (STF)–Kevlar Composites', NUMIFORM 2004. **June 13-172004**. Columbus, OH.

Zhang X Z, Li WH and Gong X L, 'The rheology of shear thickening fluid(STF) and

the dynamic performance ofan STF-filled damper', **2008**, *Smart Mateials and Strucures*,17,035027 (7pp).

Hassan T. A., Rangari V. K., Jeelani S., 'Sonochemical Synthesis and Rheological Properties Of Shear ThickeningSilica Dispersions',**2010**, *Ultrasonics Sonochemistry*,17, 947–952.

Genovese D. B., 'Shear rheology of hard-sphere, dispersed, and aggregated suspensions, and filler-matrix composites',**2012**,*Advances in Colloid and Interface Science,* 171–172, 1–16.

Hassan T. A., Rangari V. K., Jeelani S., 'Synthesis, processing and characterization of shear thickening fluid (STF) impregnated fabric composites', **2010**, *Materials Science and Engineering A,* 527, 2892–2899.

Rosen Brian A., Laufer Caroline H. Nam, Kalman Dennis P., Wetzel Eric D., and WagnerNorman J.," Multi-Threat Performance Of Kaolin-Based Shear Thickening Fluid (STF)-Treated Fabrics", **3-7 June 2007**, *Proceedings Of Sampe*, Baltimore, Md.

Crawford N. C., Popp L. B., Johns K. E., Caire L. M., Peterson B. N., LiberatoreM. W., Shear thickening of corn starch suspensions: Does concentration matter?', **2013**, *Journal of Colloid and Interface Science,* 396 83–89.

Lomakin E. V., Mossakovsky P. A., Bragov A. M., Lomunov A. K., Konstantinov A. Y., Kolotnikov M. E., Antonov F. K., Vakshtein M. S., 'Investigation of impact resistance of multilayered woven composite barrier impregnated with the shear thickening fluid', **2011**, Arch Appl Mech, 81:2007–2020.

Cabot Bulletin Sheet, **2008**, Cabot Corp.

Technical Bulletin Fine Particles, Aerosil® Fumed Silica for Solvent-Free Epoxy Resins TB27, Evonik Industries, **2009**.

Krishnamurthy L.N. And Wagner J. N. ,' Shear thickening in polymer stabilized colloidalDispersions', **November/December2005**, *J. Rheol.* 49(6), 1347-1360.

Pancera S.M., Itri R., Petri D.F.S., 'The effect of poly(ethylene glycol) on the activity, structural conformation and stability of yeast hexokinase', **2004**, *Progr Colloid Polym Sci* 128: 178-183.

Walker W.J., James S.R., 'Adsorption Behavior of Poly(ethylene glycol) at the Solid/Liquid Interface', **1999**, *J. Am. Ceram. Soc.,* 82 [3] 585–90.

Acartürk F., Ağabeyoğlu İ., Çelebi N., Değim T., Değim Z., Doğanay T., Takka S., Tırnaksız F., 'Modern Farmasötik Teknoloji', **2009**, *Türk Eczacılar Birliği Eczacılık Akademisi Yayını*.

Mezger Thomas G.,' The Rheology Handbook: For Users of Rotational and Oscillatory Rheometers', **2006**, *Vincentz Network,* 2nd Ed.

Han C. D., 'Rheology and Processing of Polymeric Materials, Volume 1: Polymer Rheology', **2007**, Oxford University Press.

Saito Y., Hirose Y., Otsubo Y., 'Shear-induced reversible gelation of nanoparticle suspensions flocculated by poly(ethylene oxide)', **2011**, *Colloids and Surfaces A: Physicochem. Eng. Aspects,* 384 40– 46.

Lee Y. S., Wagner N.J., 'Dynamic properties of shear thickening colloidal suspensions',**2003**, *Rheol Acta*, 42: 199–208.

Gopinath G., Zheng J.Q., Batra R.C., 'Effect of matrix on ballistic performance of soft body armor', **2012**, Composite Structures 94 2690–2696.

Liang SunL., Sheng Xiong D., Yun Xu C.,'Application of Shear Thickening Fluid in Ultra High Molecular Weight Polyethylene Fabric', **2013**, *J. Appl. Polym. Sci.,* DOI: 10.1002/APP.38844.

Dong Z., Manimala J. M. And Sun C. T., Mechanical Behavior of Silica Nanoparticle-Impregnated Kevlar Fabrics', **2010**, *Journal Of Mechanics Of Materials And Structures,* Vol. 5, No. 4.

Wetzel E. D., Wagner N. J., 'Novel Flexible Body ArmorUtilizing Shear Thickening Fluid (STF) Composites', **2003**, *14th International Conference on Composite Materials, San Diego, CA.*

Ballistic Resistance of Body Armor NIJ Standard-0115.00, **2000**, *National Institute of Justice*

Ballistic Resistance of Body Armor NIJ Standard-0101.04, **2000**, *National Institute of Justice*

V_{50} Ballisctic Test for Armor,MIL-STD-662F, **1997**, US. Department of Defense Test Method Standard

Raghavan S. R., Walls H. J., Khan S. A., 'Rheology of Silica Dispersions in Organic Liquids: New Evidence for Solvation Forces Distated by Hydrogen Bonding', **2000**, Langmuir, 16, 7920-7930.

Qui-mei W., Jian-ming R., Bai-yun H., Zhong-cheng Z., Jian-peng Z., 'Rheological Behavior of fumed silica suspension in polyethylene glycol', **2006**, *Journal CSUT*, Vol.13 No.1.

Boersma W. H. , Laven J.,. Stein H.N., 'Viscoelastic Properties of Concentrated Shear-Thickening Dispersions', **March 1, 1992**, *Journal of Colloid and lnterface Science,* Vol. 149, No. 1.